5

NON DESTRUCTIVE STRUCTURE EVALUATION:

AN APPLICATION OF SEISMIC SIGNAL ANALYSIS

by

Michel Kahan

Ingénieur des Ponts et Chaussées (1992)
Ingénieur diplômé de l'Ecole Polytechnique (1989)

Submitted to the Department of
Mechanical Engineering in Partial Fulfillment of
the Requirements for the Degree of

MASTER OF SCIENCE
in Mechanical Engineering
at the

Massachusetts Institute of Technology

February 1993

Signature of the Author_____
Department of Mechanical Engineering
September 10, 1992

Certified by_____
Professor Eduardo A.M. Kausel
Thesis Supervisor

_____
Professor Triantaphyllos Akylas
Thesis Reader

Accepted by_____
Professor Ain A. Sonin
Chairman, Departmental Graduate Committee

NON DESTRUCTIVE STRUCTURE EVALUATION: AN APPLICATION OF SEISMIC SIGNAL ANALYSIS

by

MICHEL KAHAN

Submitted to the Department of Mechanical Engineering
on September 10, 1992, in partial fulfillment of the requirements
for the Degree of Master in Science in Mechanical Engineering

ABSTRACT

Techniques of wave propagation in layered plates are used to evaluate the integrity and the material properties of the asphalt covered concrete deck of a bridge. Seismic waves are generated on the field by a point impact load, which is studied in detail, and surface motions are recorded at four stations forming a single line with the impact location.

In order to simplify the problem and to lay the ground for a field analysis, numerical simulations are carried out for an impact problem on an infinite layered plate and the surface displacements at the location of the four stations are processed in the time-frequency domain. Two major types of waves are isolated: waves that are multiply reflected in the thickness dimensions of the plate, primarily observable in the vicinity of the impact point (i.e. at the first two stations), and surface waves that are dominant at the two most remote stations.

The multiply reflected waves are used in an impact-echo method to measure the deck thickness and to detect possible delaminations. The numerical simulations yield very good results and, although the length of field recordings needs be extended, the field results are also promising.

Surface displacements at the two most remote stations, obtained by numerical simulations, are processed in the frequency domain to compute the dispersion curves of surface waves. Such dispersion curves are used to evaluate the elastic properties of the materials, in particular the shear wave velocities in the asphalt and in the concrete. This technique can be used to point out concrete in poor condition, however, the analysis shows stability problems.

Thesis Supervisor: Dr. Eduardo A.M Kausel
Title: Professor of Civil Engineering

To my family,
To my nephew and nieces,
and to all those who love them

Aknowledgements

First of all, I would like to thank my parents for trusting me and supporting my choices, whatever they happened to be. Not all of them were wise, and I am most grateful to my parents for not having mentioned those.

I would also like to thank the French Ministry of Foreign Affairs, that has granted me a scholarship of the 'Lavoisier' program, which has been of most helpful.

During the elaboration of this thesis, I have more than once benefited from the advice of Professor Eduardo Kausel and Professor Daniele Veneziano. I would like to express my gratitude to them for the time they have devoted to me. I would also like to thank Yi-Ping for sharing his research experience.

I would to thank Professor Akylas for accepting to read my thesis on behalf of the Department of Mechanical Engineering.

I would like to thank Paul Fisk and Dick Holt at Weston Geophysical, for sharing their practical experience and for supplying us with the experimental data that we have used in our research.

I definitely thank all my friends for their lovely society, for their enthusiasm, and their kindness that has made my stay in Boston a delightful period in my life. With a special thanks to Elizabeth for her cookies, and few other things...

Between the acting of a dreadful thing and the first motion
All the interim is like a phantasma or a hideous dream
[24]

Between the introduction and the conclusion
All the interim is left to your imagination
[6]

TABLE OF CONTENTS

CHAPTER I : INTRODUCTION

Outline

I- Statement of Problem

- I-1) Motivations for Non-Destructive-Testing techniques
- I-2) State of the art
- I-3) Engineering constraints and limitations
- I-4) Objectives

II- Statement of Solution

- II-1) Description of approach
- II-2) Technique used for data acquisition
- II-3) Sensors
- II-4) Preliminary interpretation

III- Development

- III-1) Initial impulse shape
- III-2) Understanding the problem: forward models
- III-3) Heuristic inverse techniques: Impact-Echo and Surface Wave methods

I- STATEMENT OF PROBLEM

I-1) Motivations for Non-Destructive-Testing techniques

The maintenace of concrete structures such as bridge decks or pavements requires that the civil engineer or the maintenance engineer be in possession of tools that enable him to scrutinize in depth the structure in such a way that he can identify and locate possible defects. Those structures suffer from degradations that are most of the time invisible from the surface. With a system that checks the physical state of the structure in depth it can be decided whether or not the user's safety is jeopardized, in which case proper maintenance can be carried out.

Several techniques exist to assess the condition of a concrete structure. The most reliable consists in taking a sample of the structure, by coring, and analyzing it. The major drawback of this destructive method, is that it cannot be carried out on a large scale without damaging too much the structure. By contrast, non destructive testing (NDT) methods scan the object but do not degrade it.

I-2) State of the art

This safety interest has aroused several non-destructive evaluation techniques among which we find radar, sonic, ultrasonic and seismic inspections. The choice of the best method to use depends primarily on the material to be tested, the information expected, and the experimental conditions on the field. Radar methods are efficient in detecting and delineating reinforcing steel bars and possible delaminations, as well as cracked and voided spots where moisture occurs. If radar examination works well for the inspection of layers close to the surface, a deeper penetration in the structure at lower frequencies must be traded off against a poorer resolution. Radar techniques are also inefficient to locate voids where water or moisture is absent.

Acoustics methods (i.e. seismic, sonic and ultrasonic) all work on a common principle. Waves emitted by transducers or impact generators, are transmitted through the concrete medium along complex paths, bounce back and forth on interfaces and boundaries until they are received by sensors at the surface. Again according to the materials and the shape of the structure, different frequencies must be used, and the system must be chosen accordingly. All these methods aim at determining the internal characteristics, such as the elastic properties, strengths of the materials, and help the

engineer to locate and evaluate cracks, delamination, voids and other possible deteriorations.

Seismic measurements have been intensively used in geophysics, in particular in the exploration for oil. As it has been so far very successful in that domain, we may want to extend the scope of those methods to the evaluation of concrete structures and pavements. The main advantage of seismic wave generation on other acoustic methods, is that it is easy to generate a fairly great amount of energy which penetrates deep in the structure and therefore allows the inspection of thick media. Besides, it is also quite easy to perform seismic impacts using a hammer or shooting a bullet onto the structure. The experimental setup is usually small and measurements can be done extremely fast on a large scale. This operational reliability compensates for a possible additional complexity in the processing of collected data or in the interpretation of the results.

Because of that additional complexity, the direct interpretation of seismic traces is very seldom straightforward, and the data must be processed quite intensively to convey clear information. In addition, since the experimental conditions are very seldom that of a laboratory, the seismic signal is usually mixed with noise and statistical analysis must often be carried out.

I-3) Engineering constraints and limitations

The maintenance engineer is most often concerned with the evaluation of a huge area, as of a highway an airport runway, or a bridge deck, and must therefore cope with a considerable amount of data. To be effective, an evaluation system should be able to operate in the field, in real time. This must be one of our major concerns and it will be the criterion to state whether the scanning system we want to achieve is operational or not. Clearly, there must is a compromise to find between an operational system and a complex analysis.

I-4) Objectives

In this thesis, our aim is to lay the ground for a methodology of seismic analysis in order to perform an in-place, non-destructive testing of concrete decks. We want to be able to process seismic recordings in order to characterize the depth, thickness and some specific properties (i.e. Young modulus, shear modulus...) of the concrete structure and above all, locate and identify delaminated, cracked or weak portions.

Our first step is to understand the physical problem of wave propagation in a structure such as a bridge deck. We, of course, refer to the literature, and we also make use of numerical simulations. The main difficulty is to simplify the analysis, so that it can actually be operational. For that purpose, we reduce the complex problem of wave propagation in a deck, to simpler ones, where only few propagation modes exist and are well identified. Evidently, those simpler models are valid in certain areas in space, and at certain moments in time, and we need to define those conditions properly.

II- STATEMENT OF SOLUTION

II-1) Description of approach

Our approach can be decomposed in two steps: in order to have a good understanding of the physical problem, we first develop models, that we name forward models, and find out where they are applicable. Then, starting analyses carried out according to those models, we conceive inverse algorithms that process the field or simulated data in order to reveal properties of the structure or of the materials.

The forward models aspire to describe the propagation of waves in concrete structures of different geometries and material characteristics. Very few analytical solutions exist and therefore this part is generally performed with finite element codes. In our case, for simplicity reasons (justifications are given in chapter III), we model the bridge deck as an infinite layered plate. In the simulations, we account for the presence of defects by varying the thicknesses or the elastic properties of the sublayers which constitute the plate.

Based on the forward models, the inverse schemes draw information from the signal collected on the field, to yield certain characteristics of the structure. Namely, for each wave propagation mode that we study through a forward model, we design an algorithm for the inverse problem. Since we wish that the numerical analysis be operational on the field, a major constrain for us, is to produce an algorithm that can be executed in real time.

II-2) Technique used for data acquisition

All seismic wave measurements are performed by Weston NDT[1] with the WesCET system. The latter consist in an impact generator (a BB gun) and four sensors aligned on a row that record vertical stress at the surface. The gun shoots a copper bullet almost vertically towards the asphalt at a speed of 360 ft/s (110 m/s). The sensors are placed respectively at 1" (2.54cm), 7" (17.8cm), 19" (48.3cm), 31" (78.7cm) as shown in Figure 1.1. They are attached to four wheels (four per wheel) so that as the device rolls on the pavement, a row the sensors comes in contact with the asphalt every foot (30.5cm). The contact between the deck and sensor is improved by a fluid that is injected in between, shortly before the gun is triggered. This system thus accounts for surface irregularities.

The BB gun shoots a copper bullet at a speed of 110 m/s that bounces back on the deck surface. This problem is studied in detail in chapter II in which we derive the contact time of the impact, and the shape of the contact force. The sensors are piezo electric systems that transform vertical stress into voltage. Each sensor is connected to a multiplexed 12 bit A/D converter that has a resolution of 5 millivolts. The converter is activated by a 1 MHz clock and since the four channels are multiplexed, the sampling rate for each channel is 250 kHz, leading to a Nyquist frequency of 125 MHz, which is more than enough for our problem, as we prove it in chapter III. The data are recorded by a desktop computer in a van at the site.

The first station, 1" away from the impact location, is mainly used by Weston NDT as a trigger channel to detect the arrival of a surface impulse and start the recording on all four channels. Triggering occurs when this first channel exceeds 50 millivolts. To account for the travel time of the Rayleigh wave that is actually detected, 50 microseconds of flat signal are added at the beginning of each channel. The first three channels are recorded digitally over a period of 500 microseconds (125 samples) and the fourth channel over a longer period of 750 microseconds (188 samples).

[1] Weston NDT, P.O. Box 550, Lyons Street, Westboro, MA 01581-05550

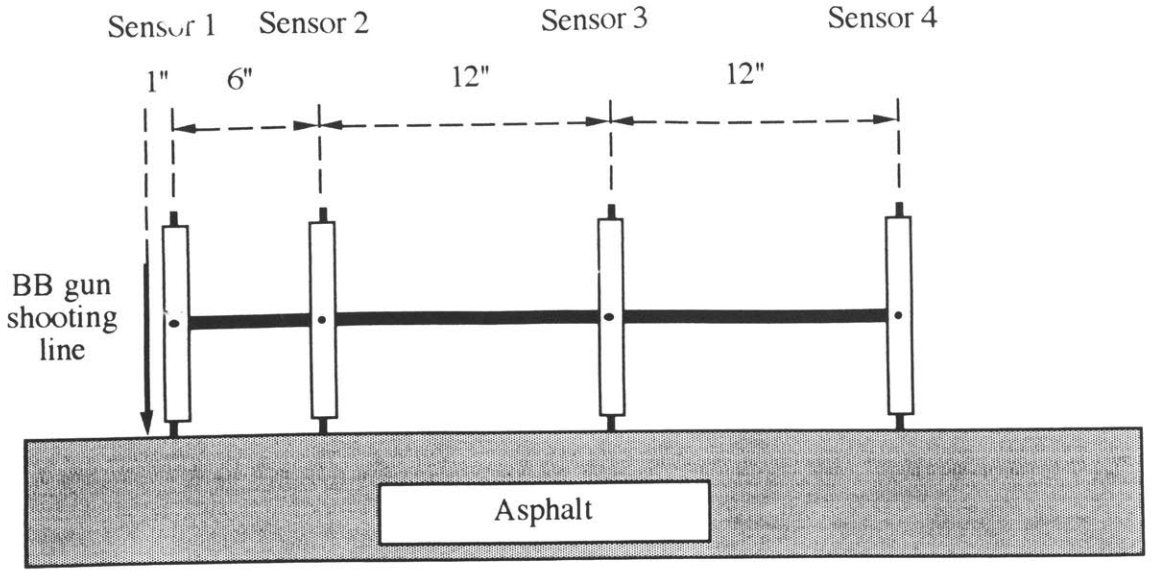

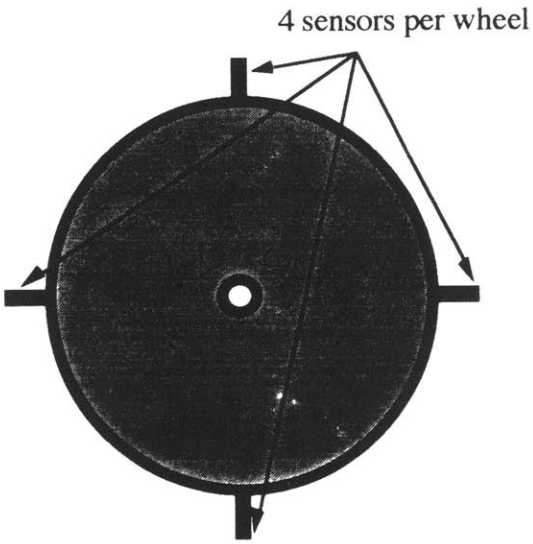

Figure 1.1: Recording device

The whole recording system is operated by a single man on a large scale (it scrutinizes a bridge deck or a road at a rate of 5,000 square feet, i.e. 460 square meters per hour). This fast pace explains why we are so concerned with an automatic and real time analysis of the data. The machine rolls on the bridge deck in between two supporting beams, as shown in Figure 1.2, in such a way that it is always on the concrete slab only.

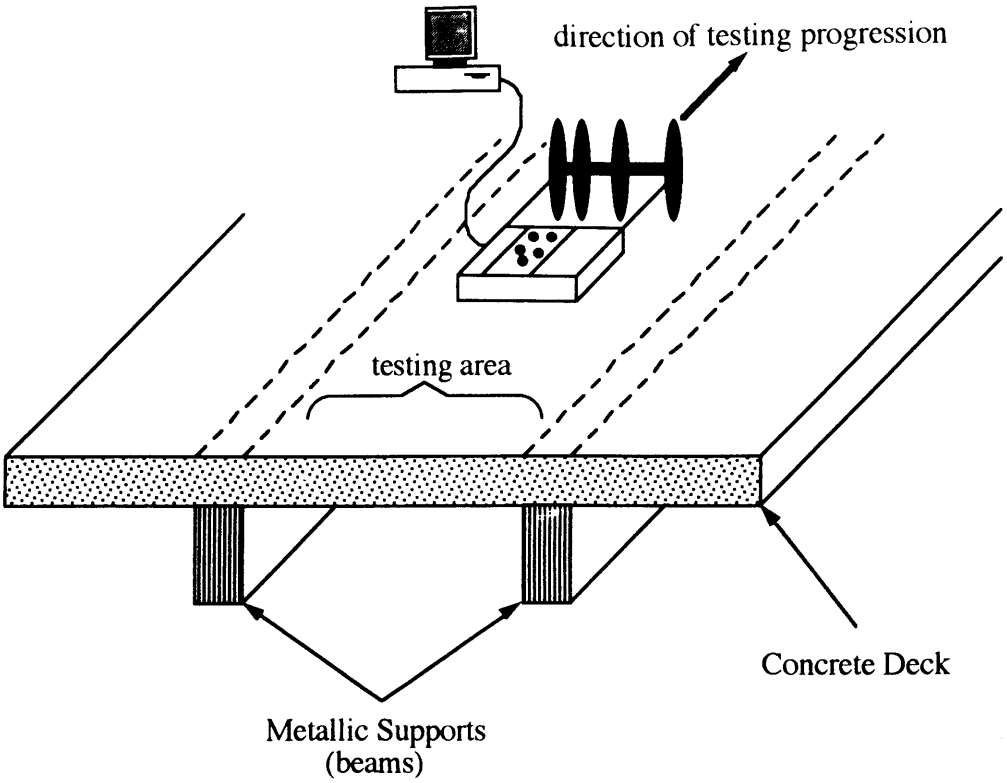

Figure 1.2: Testing area on a concrete deck bridge

II-3) Sensors

The sensor used by Weston NDT, is a piezo electric device that is primarily designed for underwater acoustics. In the way it is mounted, it measures the pressure at its surface in contact with the deck surface. In the numerical simulations that we carry out, the output is the surface motion at the location of the sensors, in terms of displacements, velocities or accelerations. To compare it with the field data, we need to relate the contact pressure of the coupled system deck-sensor with one of the surface motion quantities. In appendix A, we show that the relation between the contact pressure and the surface motion in terms of displacements and its derivatives, depends essentially on the way the sensor is attached to the supporting wheel. We come to the conclusion, that with the actual setting, the recordings are proportional to accelerations. However, this connection can be changed easily, and the recordings can be made proportional to displacements. Therefore, there are no particular constraint on the variable of analysis, and we must use, the one that yields the more structural information. We show for that purpose, in chapter III, that displacement is the richest quantity in terms of structural information.

II-4) Preliminary interpretation

We present here briefly, how the engineers at Weston NDT, interpret the data collected in the field. Figure 1.3 shows a set of field data recorded on a bridge deck. The vertical axis displays the horizontal distance on the bridge deck in feet. The recordings at the four stations are shown one after the other on the horizontal axis. The compression and Rayleigh waves arrival times are marked manually (P and R) at station 3 and 4. With these graphs, P and S wave velocities can be computed. Other elastic characteristics are also inferred from those velocities.

A weak zone is marked in Figure 1.3, which corresponds to a sudden change in the global aspect of the signal. The engineers at Weston NDT interpret this sudden change as a deterioration of the structure.

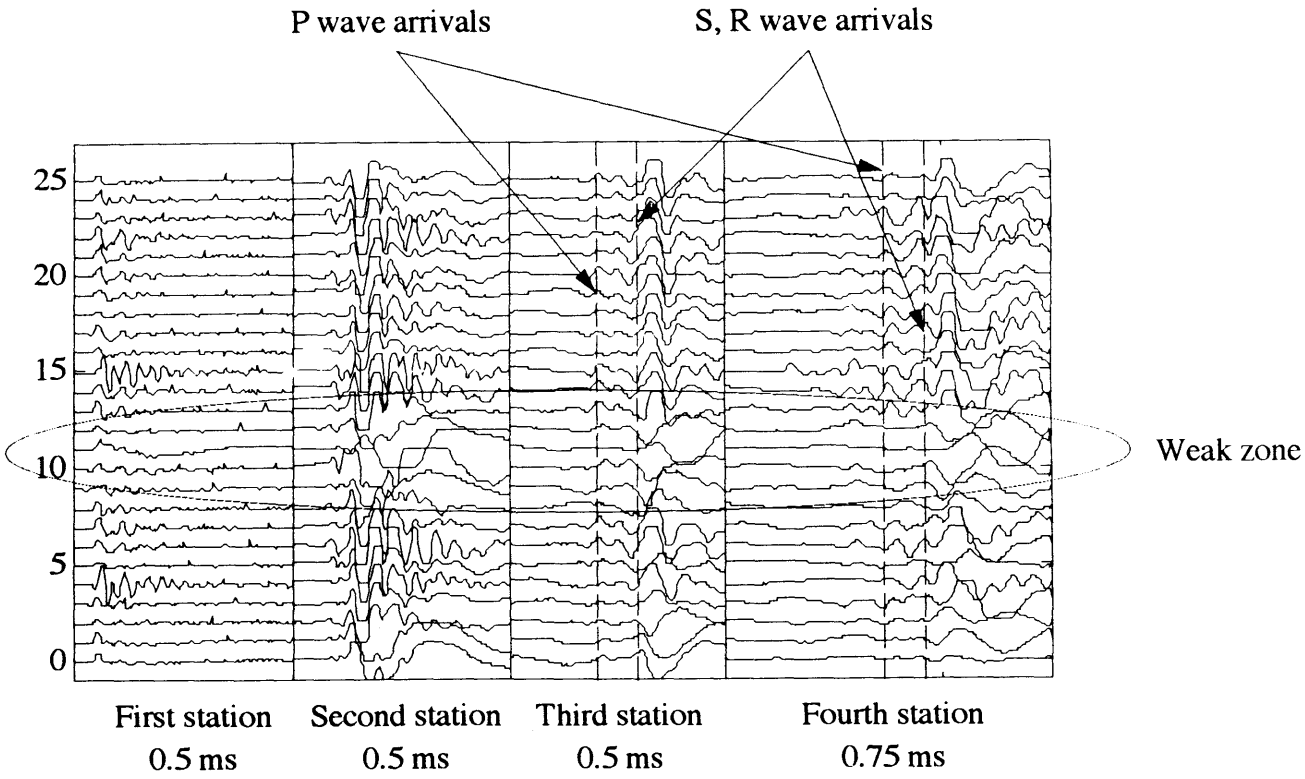

Figure 1.3: Field recordings

III- DEVELOPMENT

III-1) Initial impulse shape

Our first concern is to understand in detail, wave propagation phenomena in a layered (concrete and asphalt) plate subject to an bullet impact. In chapter II, we study the initial step of the mechanical problem, i.e. the impact of a cooper bullet on an asphalt layer. Our main purpose in doing so, is to compute the duration of the impact and the shape of the contact force versus time. Indeed, this kind of information is extremely useful to determine the frequency component of the collision force and hence, of the propagating waves in the deck. For that purpose, we review in chapter II, the Hertz theory for contact problems. In particular, we apply Timoshenko's analytical solution of the impact of two elastic spheres to our case. We also compare the analytical results with those of a finite element code.

III-2) Understanding the problem: forward models

Having obtained the initial impulse shape, we can proceed in the analysis of wave propagation in a bridge deck. The objective of chapter III is first to delineate the area where certain waves are observable in order to sketch a strategy for an analysis. Thus, we review the characteristics of body waves and surface waves, first in a half space and eventually in an infinite plate. We especially account for geometric attenuation of those waves in order to decide where they should be studied in practice.

To be more specific, we introduce numerical simulations based on a layered plate model. We process the results, namely surface displacements at the locations of the true stations, in the time and in the frequency domain. We develop a local Fourier transform that enables us to locate the arrival times of different waves.

In particular, we separate the study of body and surface waves by reserving the data of stations 1 and 2 to the analysis of multiply reflected compression waves (see chapter IV) and the results of station 3 and 4 to the analysis of surface waves (see chapter V).

III-3) Heuristic inverse techniques: Impact-Echo and Surface Wave methods

The next step is to design a methodology to analyze field data. Body waves, essentially compression waves, are addressed to in the Impact-Echo method in chapter

IV. The idea behind this technique is to locate, in the frequency domain, multiply reflected P waves that bounce back and forth across the thickness of the plate, but do not propagate horizontally. We first adopt a heuristic approach that looks at ray paths in a layered (concrete and asphalt) plate. Although it gives quite good results, in particular for the measurement of the total plate thickness, it does not take into account all the coupling effects between the asphalt and the concrete layers. Therefore, we also study the exact solution for a two-layer plate. In each case, we build up an algorithm for the inverse problem that consists in finding the main geometric characteristics, primarily the thickness of the deck.

In chapter V, we focus more on the elastic properties of the materials than on the geometry of the structure. Namely, we compute by different means, the surface wave velocity. We then relate it to the average elastic moduli, so as to obtain an estimate of the condition of the structural materials. The inverse algorithm consists here, in comparing the velocities derived from the numerical analysis, with the exact analytical solution.

CHAPTER II :IMPACT PROBLEM

Outline

I- Introduction and scope of work

II- Mathematical model

III- Discretization

IV- Numerical Solution and comparison with analytical solutions

V- Conclusion

I- INTRODUCTION AND SCOPE OF WORK

In this chapter we establish the reaction of a soft asphalt layer to the impact of a spherical copper bullet. The results of this analysis, in particular, the values of the force applied by the bullet onto the layer will be used as an initial wavelet data in further studies of wave propagation in the concrete deck with a thin asphalt layer on top. Our aim is primarily to compute the contact time and the shape of the reaction of the asphalt layer.

To this purpose, we compare the result of a finite element model with an analytical solution based on Hertz contact theory and developed by Timoshenko and Goodier [26]. In order to validate the use of the finite element model, we first test it on a simpler model, namely the impact of a copper bullet on a rigid surface, and then we will extend the model to the impact on the asphalt layer.

II- MATHEMATICAL MODEL

II-1) Derivation

In [15], Timoshenko and Goodier derived equations for the contact force and deformations associated with the impact of two elastic spheres of radii R_1 and R_2 approaching with initial velocities V_1 and V_2 parallel to their center line. In our particular case, one of the spheres is a copper bullet of radius R_2=2mm, and the other has an infinite radius ($K_1=\infty$) to represent either a flat rigid surface (in which case E_1 is infinite) or a soft asphalt layer (E_1 finite).

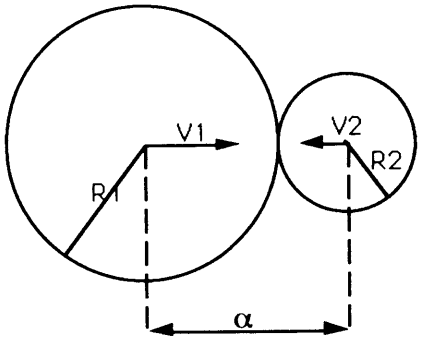

Figure 2.1: Timoshenko and Goodier's impact of two spheres

Timoshenko assumed that all materials remain linearly elastic, and that the radius of contact the surface is very small in comparison to the radii of the spheres.

Therefore, our finite element model also deals with linearly elastic materials. We will look for any discrepancies between the finite element results and the mathematical model, to check if the radius of the contact surface reaches the order of magnitude of R_2.

We will only consider a one dimensional problem, the centers of gravity of the spheres moving on a single common line.

Timoshenko derived the following: as soon as the spheres come to contact, they develop compressive forces, the resultant of which is labeled P (positive). Their velocities V_1 and V_2 vary according to equation (2-1)

$$m_1\frac{dV_1}{dt} = -P \qquad m_2\frac{dV_2}{dt} = -P \tag{2-1}$$

where m_1 and m_2 are the masses of spheres 1 and 2. Define α to be the distance one sphere approaches the other due to local compression, then

$$\dot{\alpha} = V_1 + V_2 \qquad \ddot{\alpha} = -P\frac{m_1 + m_2}{m_1 m_2} \tag{2-2}$$

Now using the notations

$$n_1 = \frac{m_1 + m_2}{m_1 m_2} \qquad n = \sqrt{\frac{16}{9\pi^2}\frac{R_1 R_2}{(R_1 + R_2)(k_1 + k_2)^2}} \tag{2-3}$$

where

$$k_i = \frac{1-\nu_i^2}{\pi E_i} \quad i=1,2$$

E_i and ν_i being, respectively, the Young's modulus and Poisson's ratio of the two materials, the equation of motion becomes

$$\ddot{\alpha} = -\,n.\,n_1\alpha^{3/2} \tag{2-4}$$

Integrating once, we obtain the velocity of approach

$$\dot{\alpha}^2 = v_0^2 - \frac{4}{5}nn_1\alpha^{5/2} \tag{2-5}$$

where v_0 is the initial approach velocity. In particular, we find the distance of approach when the compression is maximum to be

$$\alpha_1 = \left(\frac{5}{4}\frac{v_0^2}{nn_1}\right)^{2/5} \tag{2-6}$$

The equations above can be integrated numerically and the results in the two particular cases that we have chosen will be compared to the finite element results later in this chapter.

One interesting value is the contact time, $t_{contact}$, which can be reduced to

$$t_{contact} = 2.94\,\frac{\alpha_1}{v_0} \tag{2-7}$$

	Copper Bullet	Asphalt
Young's Modulus	1.92E+11 Pa	8.04E+09 Pa
Poisson's ratio	0.33	0.33
density	8900 kg/m3	2100 kg/m3
P-wave velocity	5,660 m/s	2,382 m/s
impact on:	a rigid layer	a soft asphalt layer
contact time (microseconds)	4.42	15.97
maximum approach/R1	8.2%	29.9%

NB: R_2=2mm and V_0=110m/s

Table 2.1: Material characteristics

II-2) Numerical values

As stated above, the radius of the second sphere is extended to infinity in order to represent a flat surface. Hence, α becomes the approaching distance of the center of gravity of the spherical bullet to its target surface (either the rigid surface or the asphalt layer). The material characteristics are given in Table 2.1.

III- FINITE ELEMENT MODEL

III-1) Preliminary remarks

We can have an approximation of the first oscillatory mode of the bullet, saying that at the moment of impact, the projectile can roughly be seen as a rod of length 4mm fixed on one side and free at the other end, whose lowest natural frequency is c/4L = 353 kHz. We need to compare this value with the frequency components of the impact force (more or less half a sinusoid of 4 microsecond duration) whose spectrum is important around 1/8μs=125 kHz. We then expect the bullet to behave in a quasi-static fashion. It is even more the case when we consider the impact on an asphalt layer 1/32μ=31 kHz.

In this latter case, during the 16 microsecond impact, compression waves propagate in the asphalt layer with a phase velocity of 2,382m/s corresponding to a maximum distance of 38mm at the end of the impact. We therefore have to account for possible reflections on the boundaries of our finite element model.

III-2) Integration method and discretization

The problems studied here are fundamentally non-linear because of the contact condition. Therefore, only direct integration methods work. We used an implicit direct integration, namely the Trapezoidal Rule which is unconditionally stable. That allowed us to obtain results with a reasonable time step, i.e.: 0.25 microseconds for the impact on a rigid surface and 4 microseconds for the impact on an asphalt layer.

The mesh of the copper bullet is more refined around the contact area as shown in Figure 2.2, to ensure greater precision. The numerical results also show the importance of a fine mesh in the asphalt layer in the region of contact.

Since the model is completely symmetrical about the Z axis, both problems are dealt with axisymmetrically. The contact is frictionless as in the mathematical model.

IV-NUMERICAL RESULTS

IV-1) Impact on a rigid surface

All the following numerical results were obtained using the ADINA finite element code (of ADINA R&D) on the MIT CRAY X-MP.

Figure 2.3 shows the deformation of the bullet during the first part of the impact. At time t=0 the bullet hits the rigid surface with an initial velocity of 110 m/s. The calculations, i.e. the implicit direct integrations, were carried out with a time step of 0.25 microseconds.

Figure 2.4 shows the displacement at the center of the copper bullet and the corresponding contact force, as planned by Timoshenko's model and as computed by ADINA. We can see that the curves of the analytical solution and of the finite element solution are extremely well correlated.

We infer from this that this finite element mesh gives very satisfactory results as far as the copper bullet is concerned.

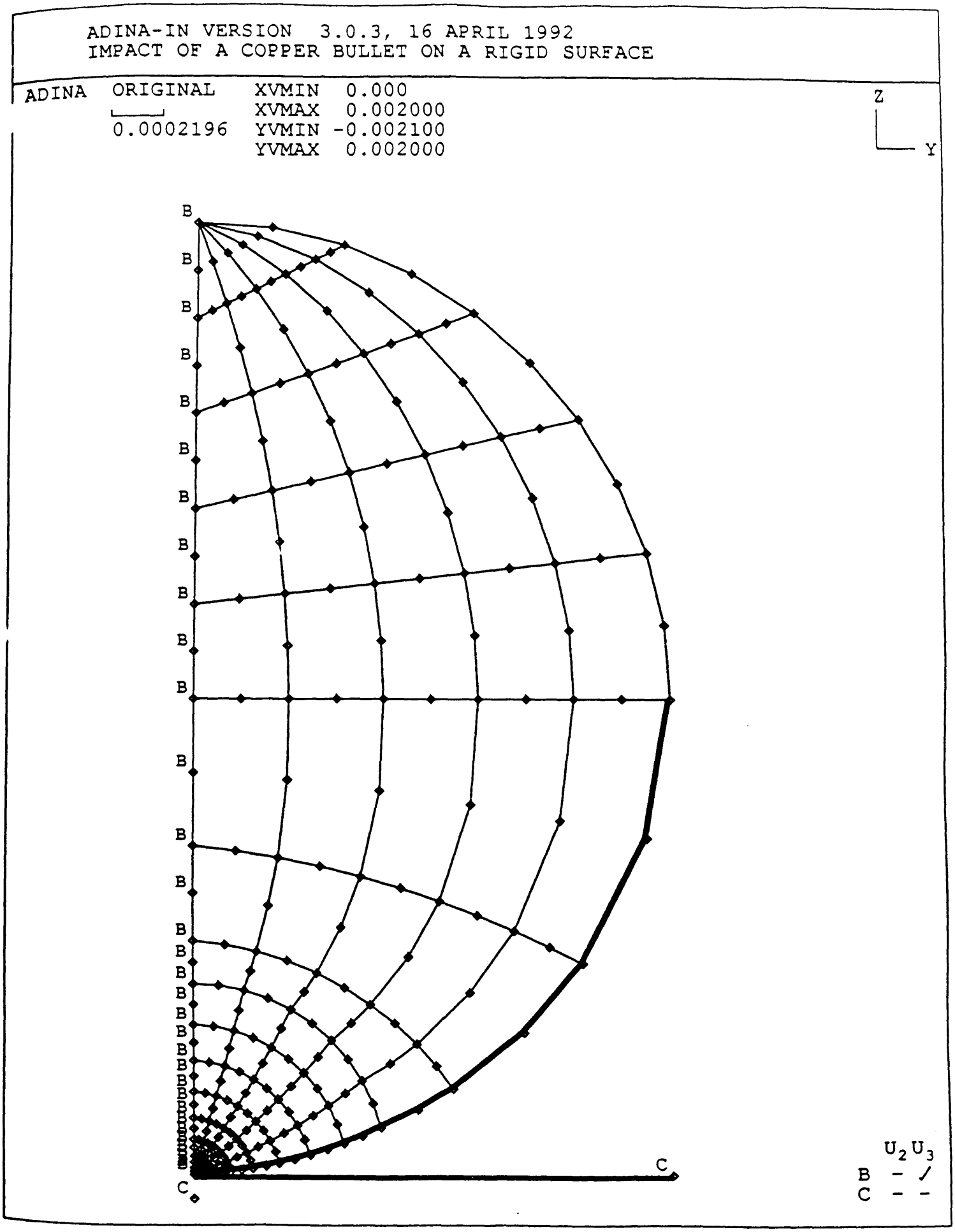

Figure 2.2: Copper Bullet Mesh

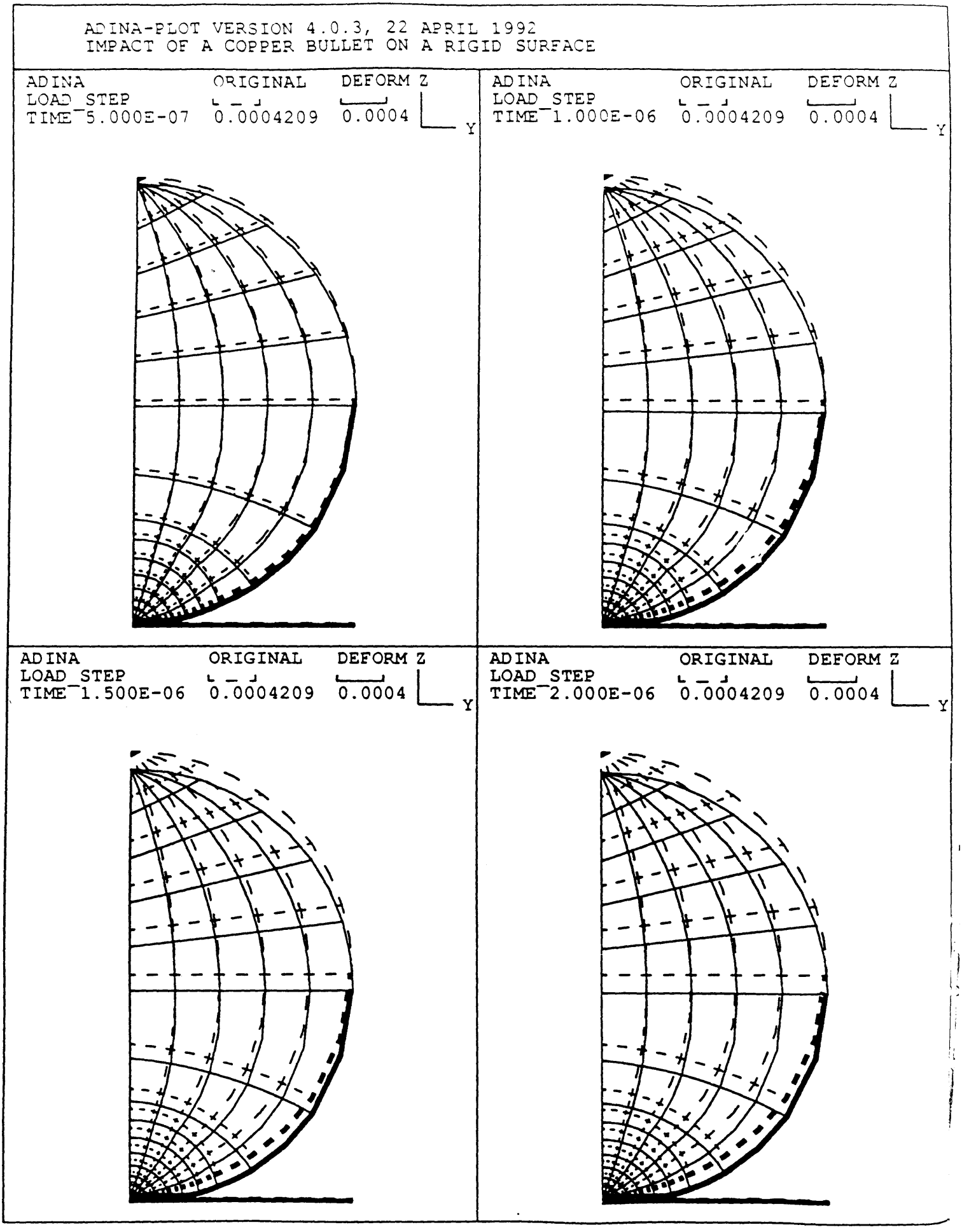

Figure 2.3: Deformation of the copper bullet : impact on a rigid surface

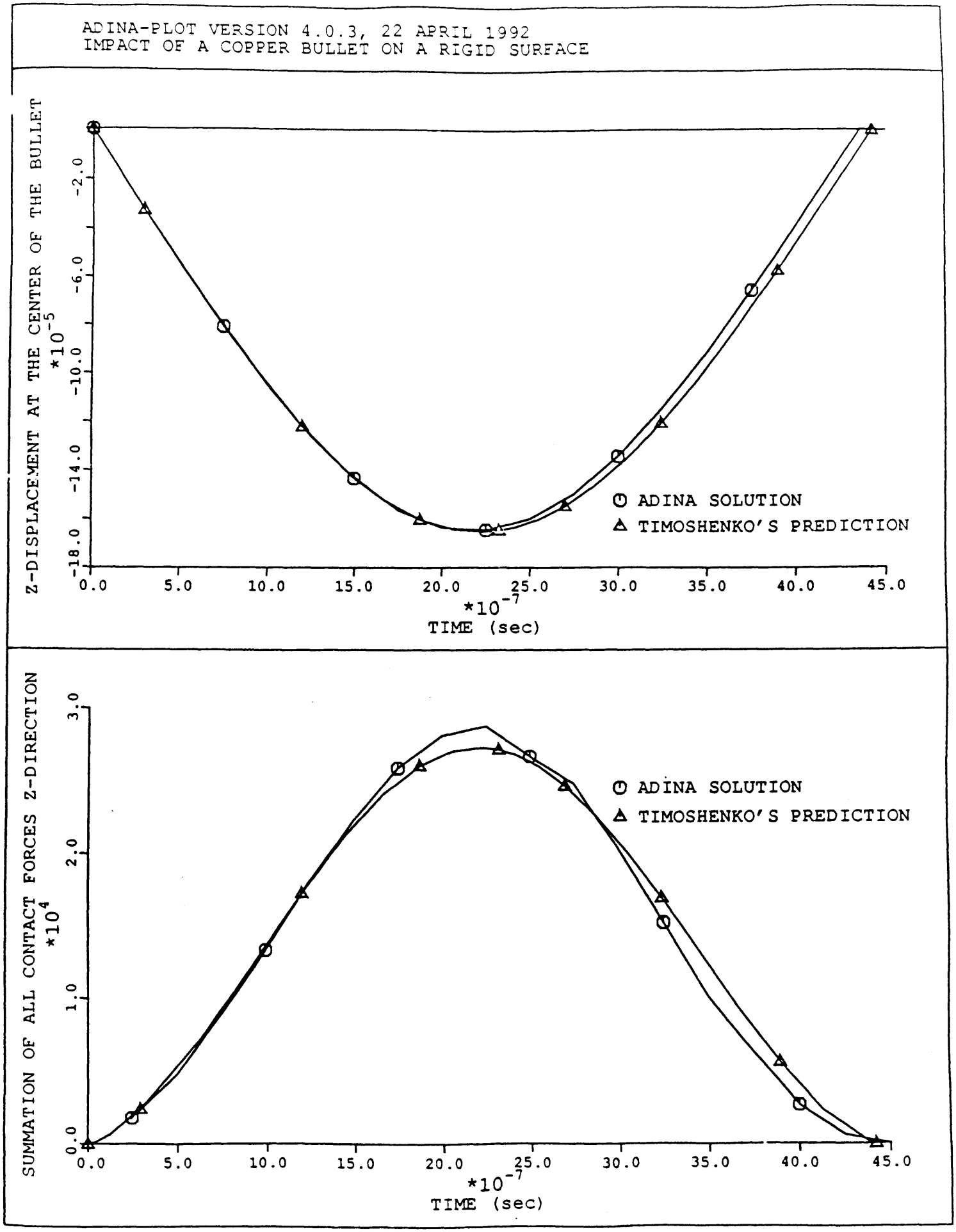

Figure 2.4: Impact on a rigid surface: finite element and analytical solution

IV-2) Impact on a soft asphalt layer

The initial conditions are the same as in the previous section. The bullet mesh is also identical, but several meshes were used to represent the asphalt layer and we will now evaluate the results.

We must remember that copper is by far stiffer than asphalt. Therefore the increase in the duration of contact when we shift from the rigid target surface to the soft one is of course due to the relative flexibility of the asphalt layer. Now, Timoshenko's model is based on a second sphere with infinite radius. Hence in the mathematical model, there are no boundaries and the asphalt layer should be an infinite half space.

We have thus introduced artificial boundaries in our finite element mesh, namely a totally fixed boundary at the bottom of the layer, a free boundary on the right handside, and a gliding boundary in the Z direction along the Z axis to comply with the axisymmetric requirements.

In our direct integration analysis, these spurious boundaries will cause troubles in the finite element solution and will drag it away from the analytical solution, if and only if, propagating waves coming from the impact zone in the asphalt have enough time to bounce back on the these boundaries and create reactions that do not actually exist.

The fastest among the waves are the compression ones (P-wave) whose phase velocity in the asphalt is 2382 m/s. Since the impact duration is approximately 16 microseconds, we end up with plane waves that will have traveled 38 mm.

We will compare two meshes for the asphalt layer that are represented in the YZ plane by squares of 10mm (mesh a) and 40mm (mesh b) side dimension respectively.

Figure 2.5 shows the deformations for mesh (a) and Figure 2.6 shows the displacement of the bullet center and the contact force as functions of time. We notice that Timoshenko's analytical solution and our finite element solution do not match that well any longer. This can be due to different reasons: the boundary problem that we have mentioned above, the time step of integration which is only 4 microseconds (we had trouble with the contact condition with a shorter time step) and eventually as we hinted at the beginning of this chapter, the radius of the contact surface is this time much closer in magnitude to the radius of the copper bullet.

We can get rid of the boundary problem by extending the finite element domain of the asphalt layer. For this purpose we used mesh (b), but the results shown in Figure 2.7 and Figure 2.8 were not improved by this modification. The careful reader has noticed that we have used a finer mesh near the impact zone. This was motivated by the

very poor results obtained with a regular grid. We conclude from these results that the boundaries are not the important issue in the discrepancy that we find between the finite element and the analytical solutions.

V- CONCLUSION

Out of the two finite element problems that we have examined, the impact of a spherical copper bullet on a rigid surface follows extremely well the analytical solution established by Timoshenko. However, we found more discrepancies when the impact of the bullet is performed on a soft asphalt layer; a likely reason is that the mathematical model may not have been satisfied that well, in particular because the radius of the contact surface was close to the radius of the impacting sphere.

Further work can, of course, be done on this particular subject, considering non-linear behavior of materials, especially for the asphalt, and taking into account local plasticities that may occur around the contact zone; this, however, goes beyond the scope of this thesis. In the following chapters, we shall assume that the shape of the force obeys Timoshenko's model and that the contact time is 16 microseconds.

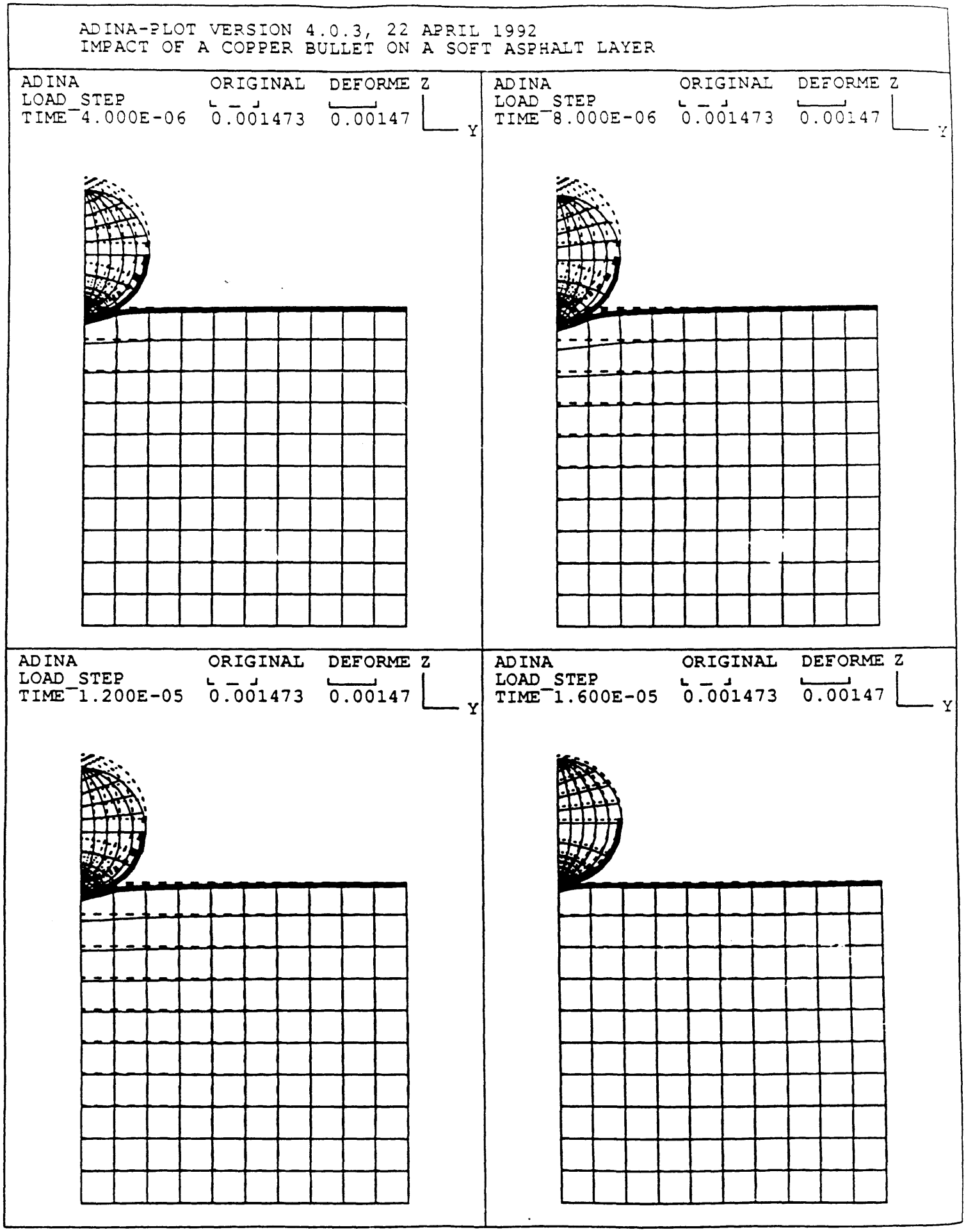

Figure 2.5: Mesh (a)

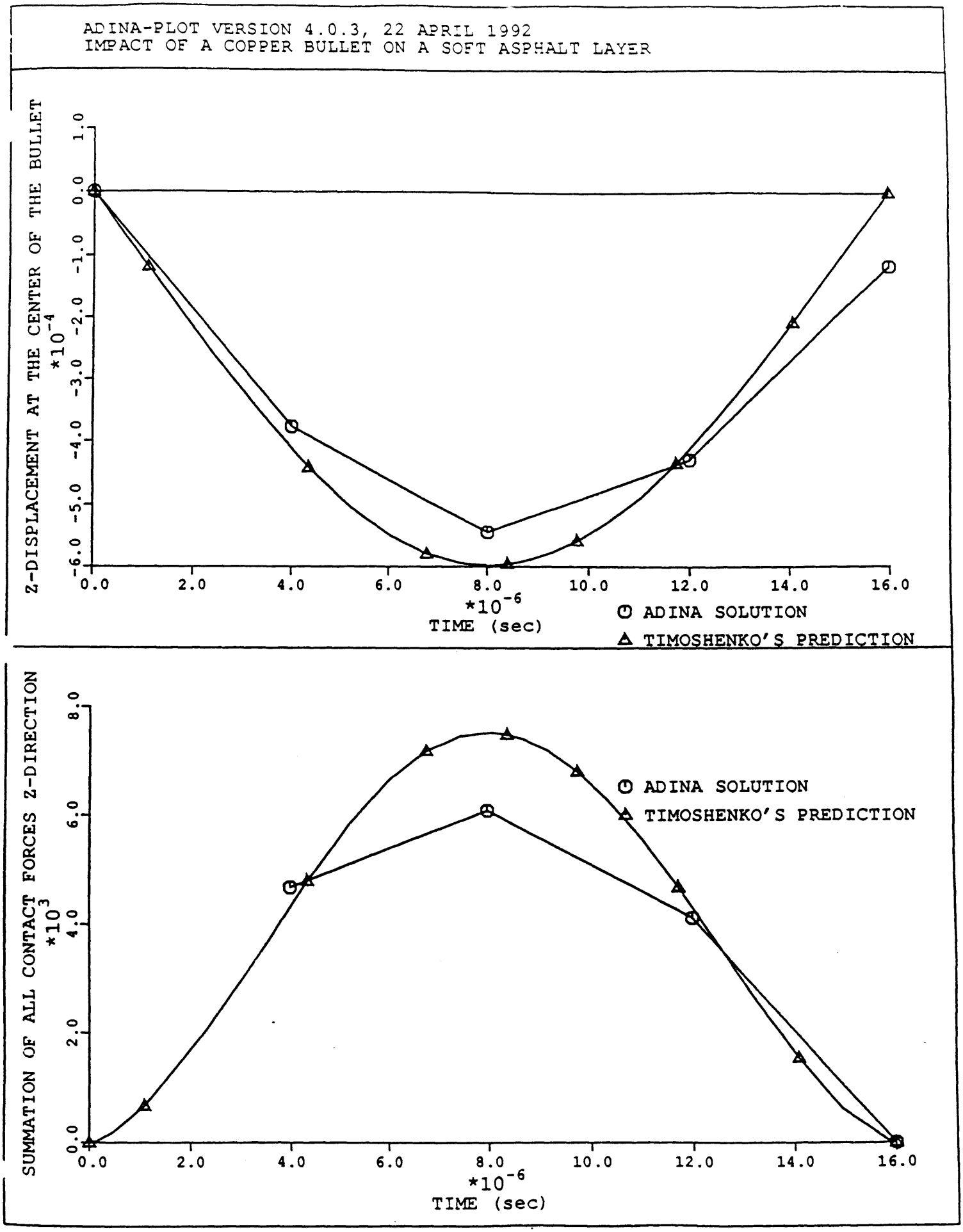

Figure 2.6: Mesh(a)

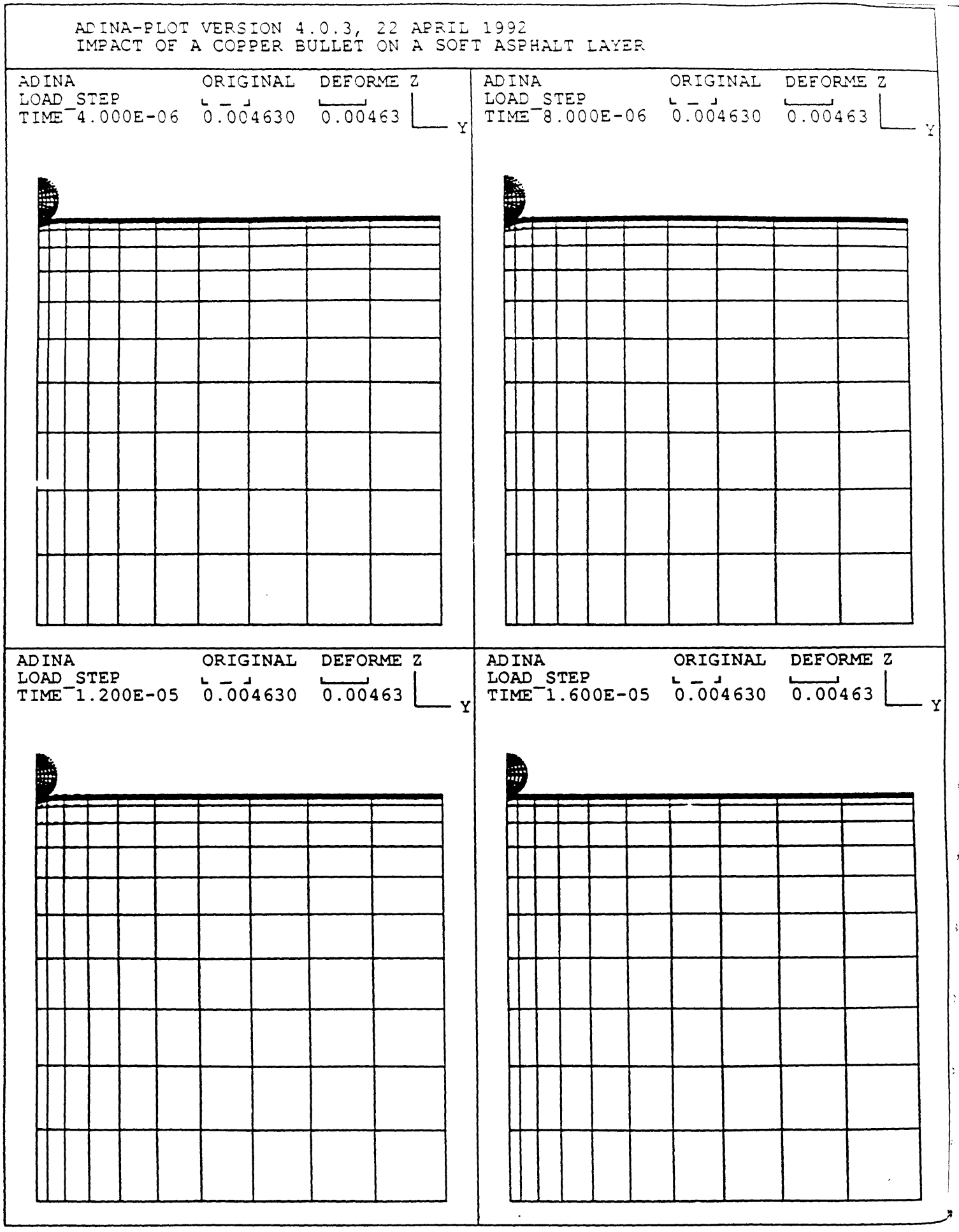

Figure 2.7: Mesh (b)

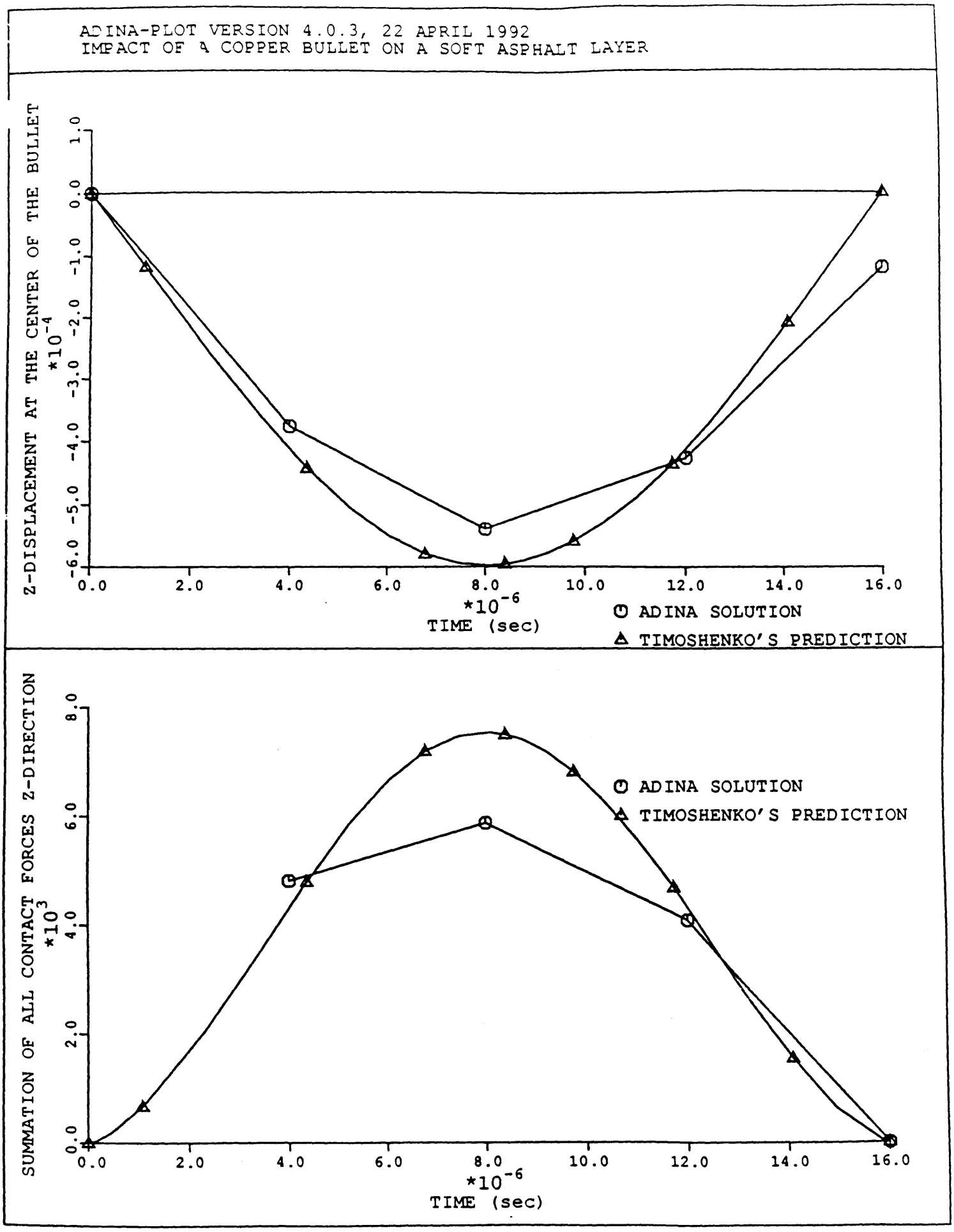

Figure 2.8: Mesh (b)

CHAPTER III: FORWARD MODELS FOR PLATES

Outline

I- Propagating waves in a homogeneous plate

- I-1) Characteristics of the problem
- I-2) Body waves
- I-3) Surface waves
- I-4) Far field behavior
- I-5) Finite Element Analysis

II- Modeling and simulation

- II-1) Two layer plate: asphalt covered concrete deck
- II-2) Parameters
- II-3) Simulations for an infinite plate

III- Strategy for the analysis

- III-1) Simulation and field data
- III-2) Local Fourier Transform. Location of the structural information
- III-3) Variable of analysis
- III-4) Impact-Echo method for close field and Surface Wave analysis for far field.

I- PROPAGATING WAVES IN A HOMOGENEOUS PLATE

I-1) Characteristics of the problem

As mentioned in chapter I, we are fundamentally interested in the response of a horizontal layered plate to an almost vertical impact of a copper bullet as described in chapter II. Hence, all the following models are axially symmetric and the vertical load is regarded as perfectly vertical. Besides, we assume all layers to be made of homogeneous elastic materials. At that point, we have two major options: we can either consider the deck to be a medium in which waves radiate from the impact point or we can see it as a structure supported by beams and columns that will oscillate according to a plate theory. The two approaches differ fundamentally and must be applied according to experimental situations. In our case the support conditions are not perfectly known and they would complicate the study dramatically if they were to be taken into consideration. Therefore, our approach will systematically be that of wave propagation in a layered medium. To avoid undesirable reflections from the supports we only consider infinite plates in the simulations, making sure that our field recordings are short enough not to contain waves that may have bounced back at the supports. In the energy range of the experiments, displacements strains and stresses remains small.

As mentioned in [17], a point impact on the surface of a solid plate, sees the plate in the first stages, as a half space, and produces two types of waves: body waves, among which we find compression (P) and shear (S) waves that propagate along spherical fronts as shown in Figure 3.1; and surface (R) waves that propagate along a cylindrical front on the free surface of the plate. In addition to theses waves, we also find low amplitude head waves, whose front extend from the intersection of the P wave spherical front with the free surface to a tangent point on the surface front of the S wave.

To have an idea of the importance of each of them, we refer to Miller and Pursey [8] who gave the following distribution of energy among the three main types for a vertically acting source at the surface of a uniform half space:

Wave Type	Percent of Total Energy
Surface (Rayleigh)	67%
Shear	26%
Compression	7%

Table 3.1: Distribution of wave energy
generated by a vertical source on a uniform half space

However, it must be understood that this distribution is not uniform in every direction; therefore, more details concerning the spatial distribution is given in the following paragraphs.

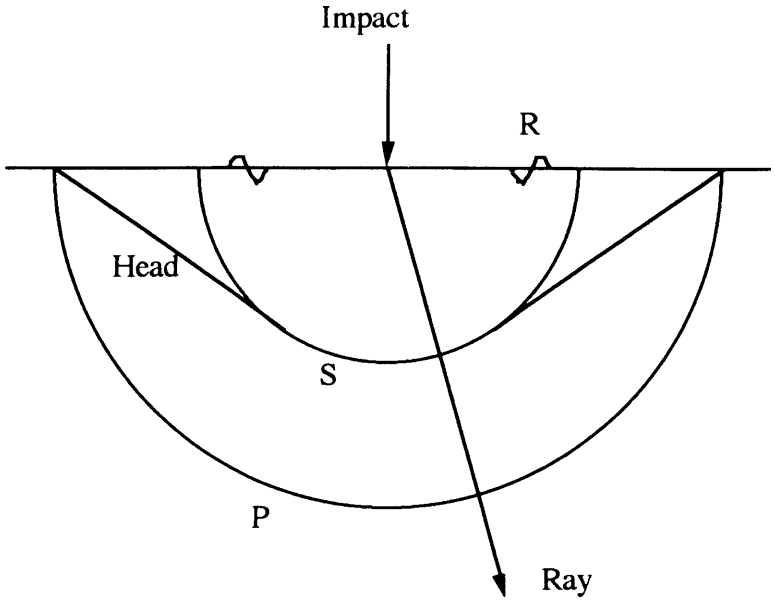

Figure 3.1: Wave fronts produced by a point impact at the surface of a half space

I-2) Body waves

Compression (P) waves and shear (S) waves both propagate along spherical fronts but generate different particle movements. P waves generate displacements parallel to the direction of propagation and S waves are characterized by perpendicular motion with respect to that direction. Among the shear waves we distinguish SV (vertical shear) waves and SH (horizontal shear) waves for which the displacements are polarized in a vertical and horizontal plane, respectively. In our horizontally layered plate model, SV and P waves are coupled whereas SH waves remain uncoupled. In addition, if the loading is strictly vertical, as it is assumed to be, SH waves do not exist at all.

Compression and shear waves travel at different speeds. The ratio of their phase velocities C_P and C_S in an elastic homogeneous medium depends only on Poisson's ratio ν as given in equation 3-1:

$$\frac{C_P}{C_S} = \sqrt{\frac{2(1-\nu)}{1-2\nu}} \tag{3-1}$$

For example, with a typical concrete Poisson's ratio of 0.20, the S wave travels at approximately 61% of the P wave speed. In addition, P and S wave velocities are related to the different moduli characteristic of the elastic material as follows:

$$C_P^2 = \frac{\lambda + 2\mu}{\rho} = \frac{E(1-\nu)}{\rho(1+\nu)(1-2\nu)} = c_0^2 \frac{1-\nu}{(1+\nu)(1-2\nu)} \tag{3-2}$$

$$C_S^2 = \frac{\mu}{\rho} = \frac{G}{\rho} = \frac{E}{2\rho(1+\nu)} = c_0^2 \frac{1}{2(1+\nu)} \tag{3-3}$$

$$c_0^2 = \frac{E}{\rho} \tag{3-4}$$

where we define

E	:	Young's Modulus
G	:	Shear Modulus
ν	:	Poisson's ratio
λ,μ	:	Lamé coefficients
ρ	:	mass density
c_0	:	rod compression wave velocity

As we mentioned earlier, the distribution of energy carried by the different waves is not homogeneous in space and depends highly on the loading conditions. In Figure 3.2, taken from [17], the distribution of particle amplitude displacements is shown for a vertical harmonic excitation. In case of a short vertical impact, i.e. a broad band signal, the distribution of displacements would be a superposition of patterns similar to this one.

We infer from this that just below the impact location, P waves predominate over S waves. This fact will be intensively used in the impact-echo method described later on. However, as rays deviates away from that vertical line, displacements are increasingly due to a complex mixing of P and S waves.

In a layered plate, body waves reflect at free boundaries and are also partially transmitted or reflected at internal interfaces between adjacent layers. We will discuss the parameters for the internal reflections in chapter IV along with the impact-echo method. Let us point out, however, that unless the incident P wave ray is perpendicular to the boundary or interface, it will give birth to both reflected P and S waves. The same is true for incident S waves. Therefore it will be difficult to handle reflections of body waves unless they propagate approximately along a vertical line below the impact point.

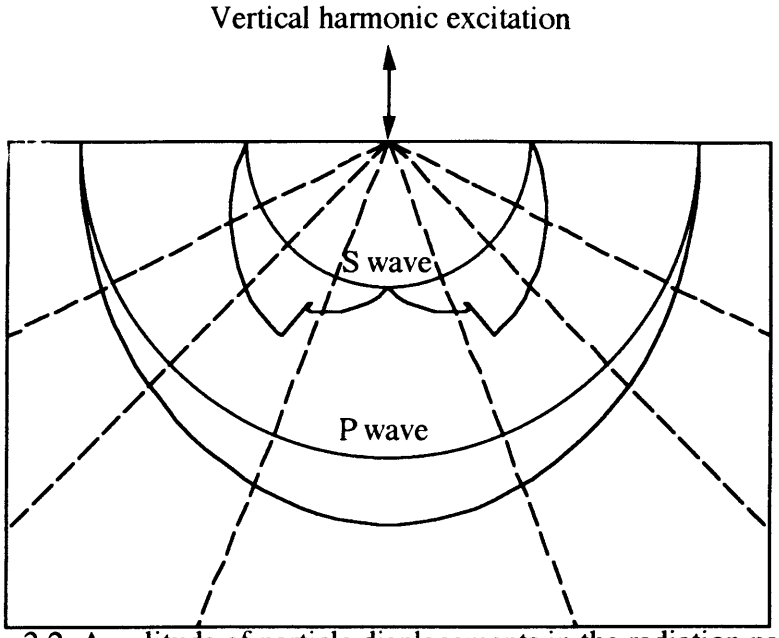

Figure 3.2: Amplitude of particle displacements in the radiation pattern produced by a vertical harmonic point source. From [17]

I-3) Surface waves

Although it is more common to talk of surface waves in the case of an infinite half space, we will also consider here surface waves that have a wavelength shorter than the plate thickness. Among many different kinds of surface waves, two particular types are usually predominant: Rayleigh waves and Love waves. Particle displacements in the latter, are confined to a horizontal plane and are perpendicular to the direction of propagation. Since our problem is purely axisymmetric and the loading is assumed to be perfectly vertical, those waves should not be present. Rayleigh waves, by contrast,

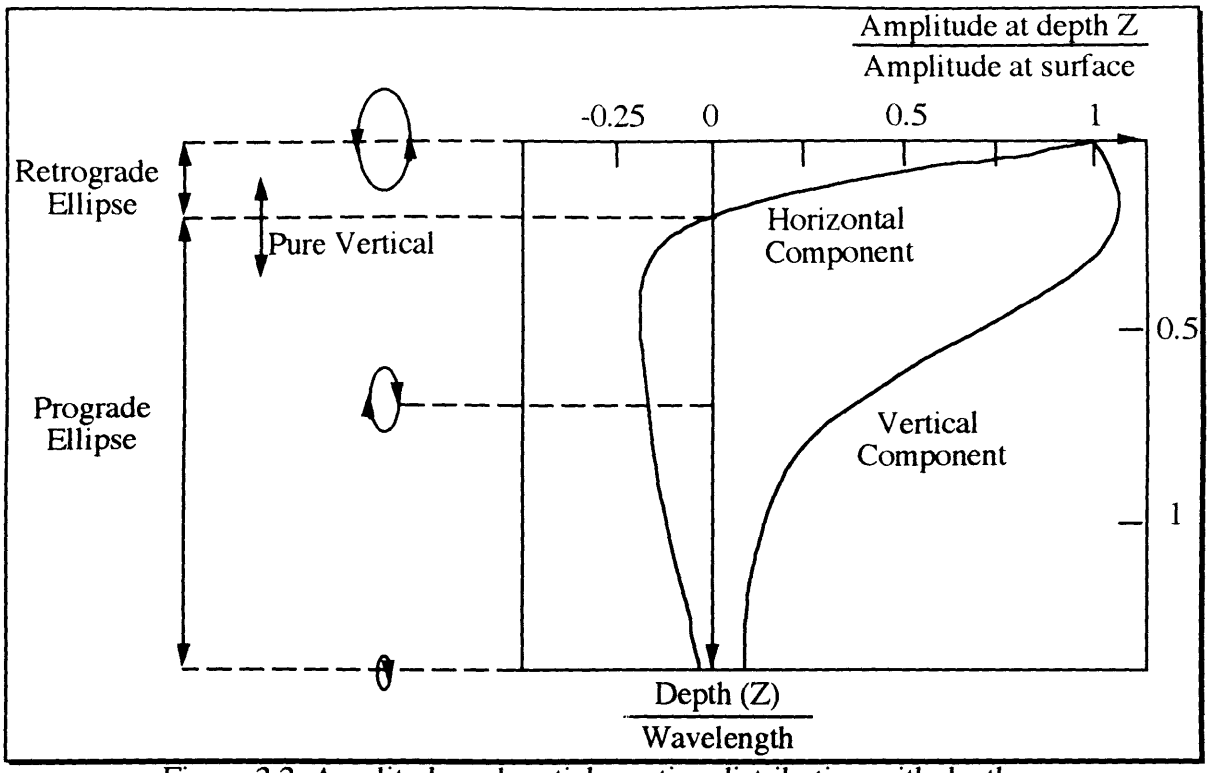

Figure 3.3: Amplitude and particle motion distribution with depth for Rayleigh waves. From [9]

generate particle motion in vertical planes and associate vertical and horizontal components. The combined movement is a retrograde ellipse close to the surface and, as depth increases, gradually changes first into a vertical line segment and eventually to a prograde ellipse as shown in Figure 3.3 taken from [9]. It is important to note that it only makes sense to consider Rayleigh waves whose wavelength is smaller than the thickness of the studied plate, since longer waves interfere with the lower free boundary.

The Rayleigh wave should be fully observed with our experimental conditions as soon as they actually develop, that is approximately at a distance of one wavelength from the impact point. They travel at a speed C_R very close to 90% of the shear wave velocity C_S. The ratio of the Rayleigh wave velocity over the shear wave velocity varies a little according to Poisson's ratio ν as shown in Table 3.2 taken from [1] for a uniform half space.

ν	C_R/C_S
0	0.862
0.25	0.919
0.333	0.932
0.5	0.955

Table 3.2: Velocity of Rayleigh wave for various Poisson's ratio

I-4) Far field behavior

Body waves travel faster than surface waves and are then the first to be recorded by remote sensors. However, as shown in [8] and [9] for instance, body waves amplitudes decay in proportion to r^{-1} along the their spherical front and in proportion to r^{-2} at the surface of the elastic half space, where r is the distance to the source. Surface waves amplitudes decrease only in proportion to $r^{-0.5}$. Hence, at the surface, compression and shear waves attenuate much faster than Rayleigh waves because of that geometrical damping. Assuming that all waves have an amplitude of 1 at the first station (1" from the impact point), the relative amplitudes of the first arrived body waves and of the Rayleigh waves at the following receivers are as presented in Table 3.3.

Station	1	2	3	4
r	1"	7"	19"	31"
amplitude of body waves	100%	2.04%	0.28%	0.10%
amplitude of surface waves	100%	37.80%	22.94%	17.96%

Table 3.3: Geometric attenuation of body and surface waves

I-5) Finite Element Analysis

Following directly the analysis carried out in chapter II, the finite element code ADINA was used again to visualize the early stage of wave propagation in the asphalt covered concrete deck.

Figure 3.4 shows the early stage displacements, 100 microseconds after the beginning of the 16 microsecond impact for an all concrete deck (that is without asphalt cover). Figure 3.5 indicates the vertical stress distribution. From the element shape we can actually see that the first (P) wave front corresponds to a compression of the elements whereas the following front brings shear deformation. The reflected compression wave is also clearly visible with its negative amplitude (white trace expanding upward from the bottom layer). However the major displacements on the top free boundary are caused by the surface wave (whose elliptic motion can be observed). The reflected compression wave also generates vertical displacements on the lower free boundary and will reach the upper surface later on.

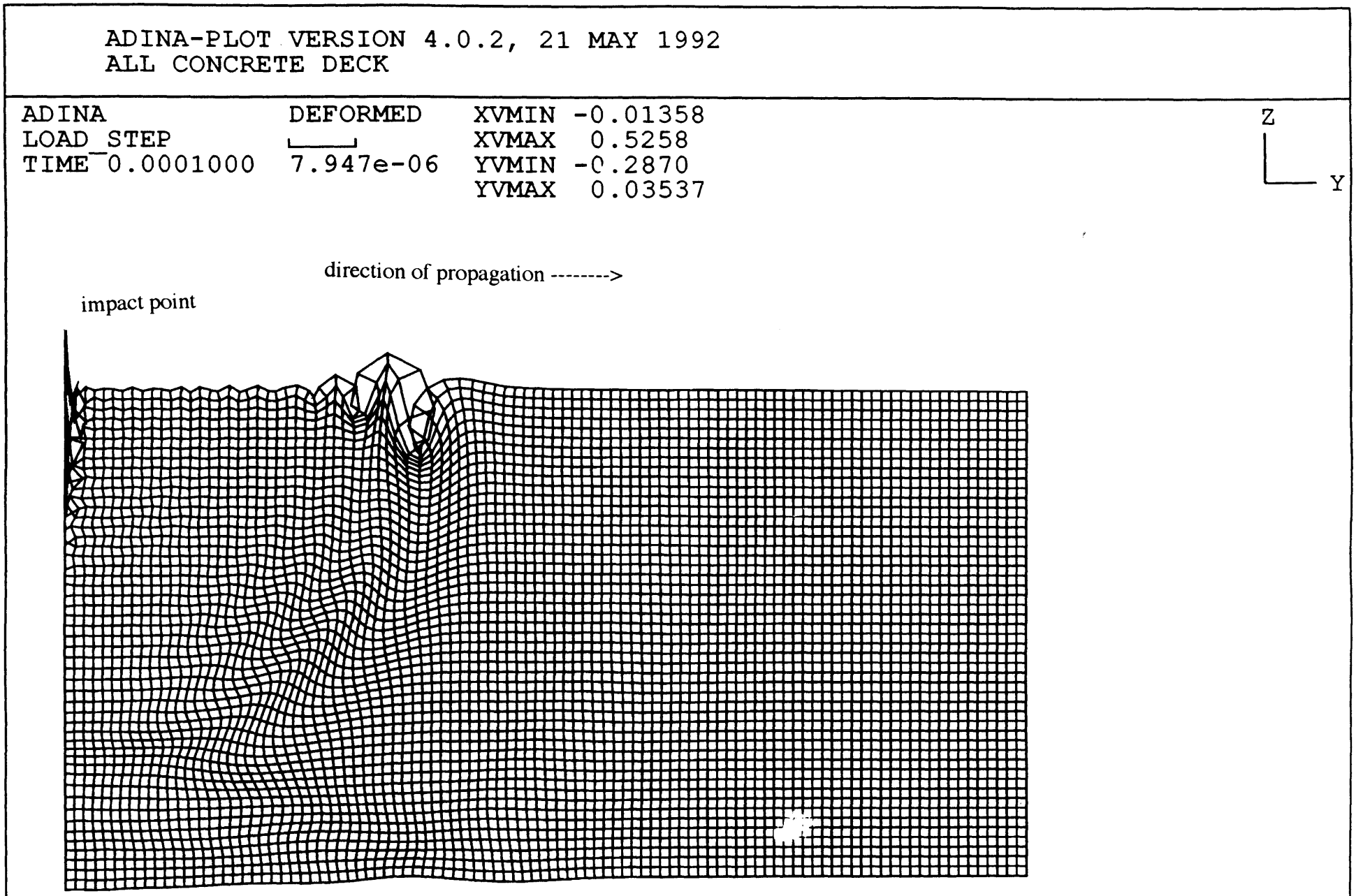

Figure 3.4: Early stage propagation: displacements

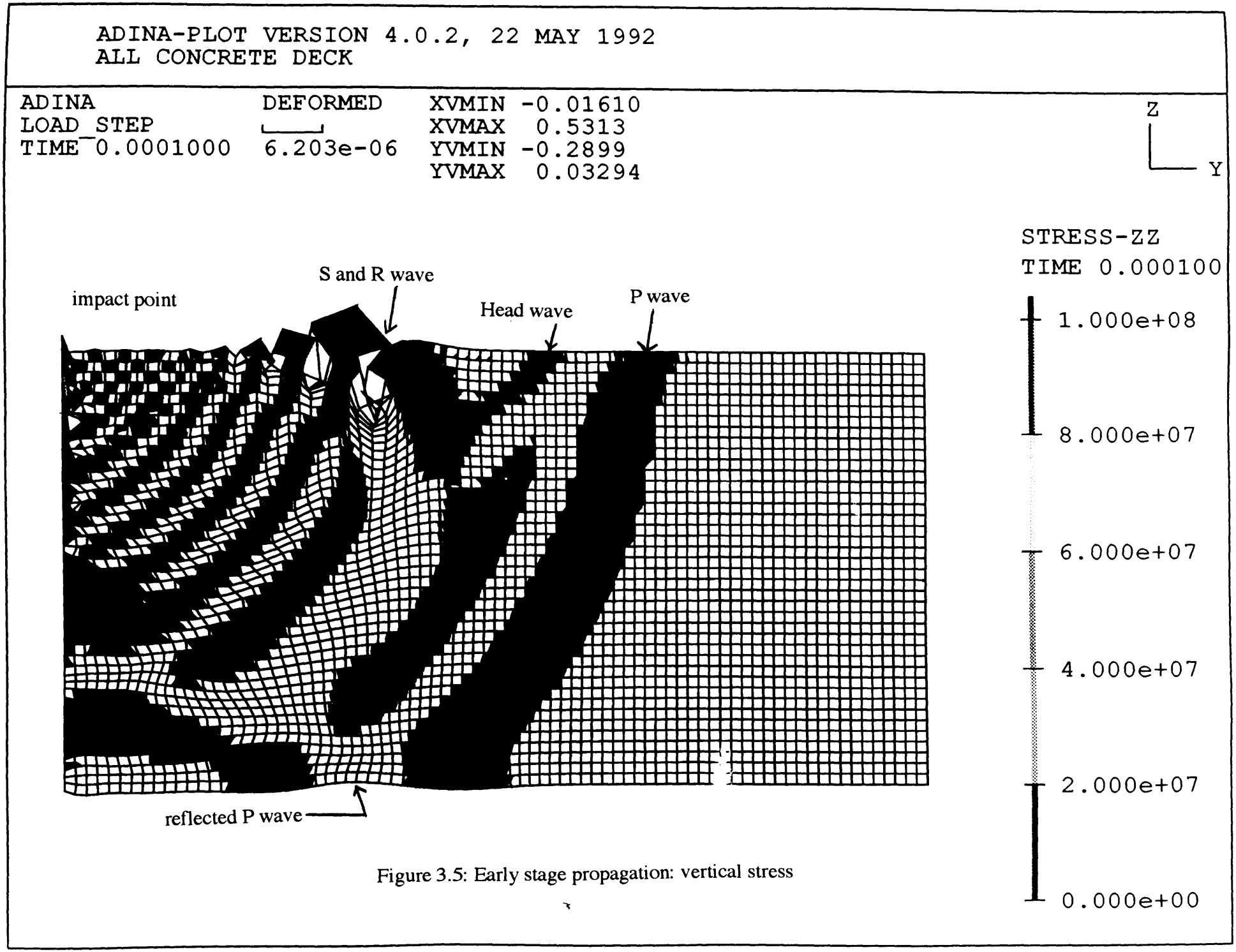

Figure 3.5: Early stage propagation: vertical stress

II- MODELING AND SIMULATION

II-1) Two layer plate: asphalt covered concrete deck

In order to understand the wave propagation problems in a concrete deck similar to those we wish to evaluate, we now carry out numerical simulations and process the results at surface points corresponding to the actual sensors. The idea behind this is to estimate the efficiency of several data analysis methods on noise free numerical data before we implement them to process field data.

The typical experimental object we are testing is a concrete deck between 8 and 10 inches covered with a thinner (1.5 to 2 inches) asphalt layer on top. In addition to this, there are reinforcement bars embedded in the concrete layer, both horizontal and vertical, the vertical being usually of a much smaller diameter. In terms of defect, we are primarily interested in detecting horizontal delamination, in particular adjacent to the horizontal rebar layer. Therefore all major components are or can be modeled to a very good approximation as horizontal layers. For the sake of simplicity we disregard the steel reinforcement . We end up eventually with a two layer model: a top asphalt layer generally of constant thickness and a concrete layer whose thickness depends on the possible presence of horizontal delamination.

The FORTRAN code PUNCH developed by Professor E. Kausel that we use for simulations is based on a layered medium model and is therefore very appropriate for our study. The program is built on a Haskell-Thompson transfer matrix technique (the theoretical background can be found in [7]). Each macro layer is discretized into thin sublayers within which displacements are assumed to vary linearly. All computations are carried out in the frequency-wave number domain. The impact source is simulated as a point load on the upper surface having a temporal variation in the shape of a Hanning window, very close to the shape found in chapter II. Convolved with the unit pulse response, it gave us the desired results in the form of displacements, velocities and accelerations at the location of the real sensors as defined in chapter I: 1" (station 1), 7" (station 2), 19" (station 3), 31" (station 4) from the impact point.

II-2) Parameters

A few parameters had to be adjusted to run the simulations, among which we find the number of sublayers, the range of frequencies to be computed, and the material characteristics.

The simulation was performed on an Gateway PC 386 machine, limited in the number of possible sublayers for storage reasons. However, since concrete and asphalt become very heterogeneous for waves of very short wavelength (less than an inch), too refined a discretization in sublayers would not really have been a realistic representation. Eventually, it turned out that sublayers half an inch thick (1.27cm) gave us quite good results and could be dealt with in our computer.

In the field recordings, the sample period is 4 microseconds corresponding to a sampling rate of 250 kHz and a Nyquist frequency of 125 kHz. However, a preliminary analysis of the field data showed that frequencies excited by the impact hardly exceeded 50 kHz. The simulation widely covered that range since computations were carried out for every frequency from 100 Hz to 102,400 Hz at 100 Hz intervals.

Eventually, typical material characteristics taken in the literature were used in the simulation and are summarized below in Table 3.4.

	asphalt layer	concrete layer
mass density	2100 kg/m^3	2200 kg/m^3
shear wave velocity	1200 m/s	2400 m/s
Poisson's ratio	0.33	0.20
damping	2%	1%

Table 3.4: Material characteristics for the simulations

II-3) Simulations for an infinite plate

With all parameters set as mentioned above, we ran a simulation for a 16μs impact on a two layer infinite plate: 10" (25.4 cm) of concrete covered with 2" (5 cm) of asphalt. The displacements at all four stations are presented in Figure 3.6. The arrival times for the direct body waves are also mentioned for stations 2, 3 and 4. The letters P and S designate respectively the arrival of the direct compression wave and the direct shear wave. The subscripts 'a' and 'c' stand for asphalt and concrete and designate whether the wave had traveled in the asphalt layer or in the concrete layer. Let us mention here

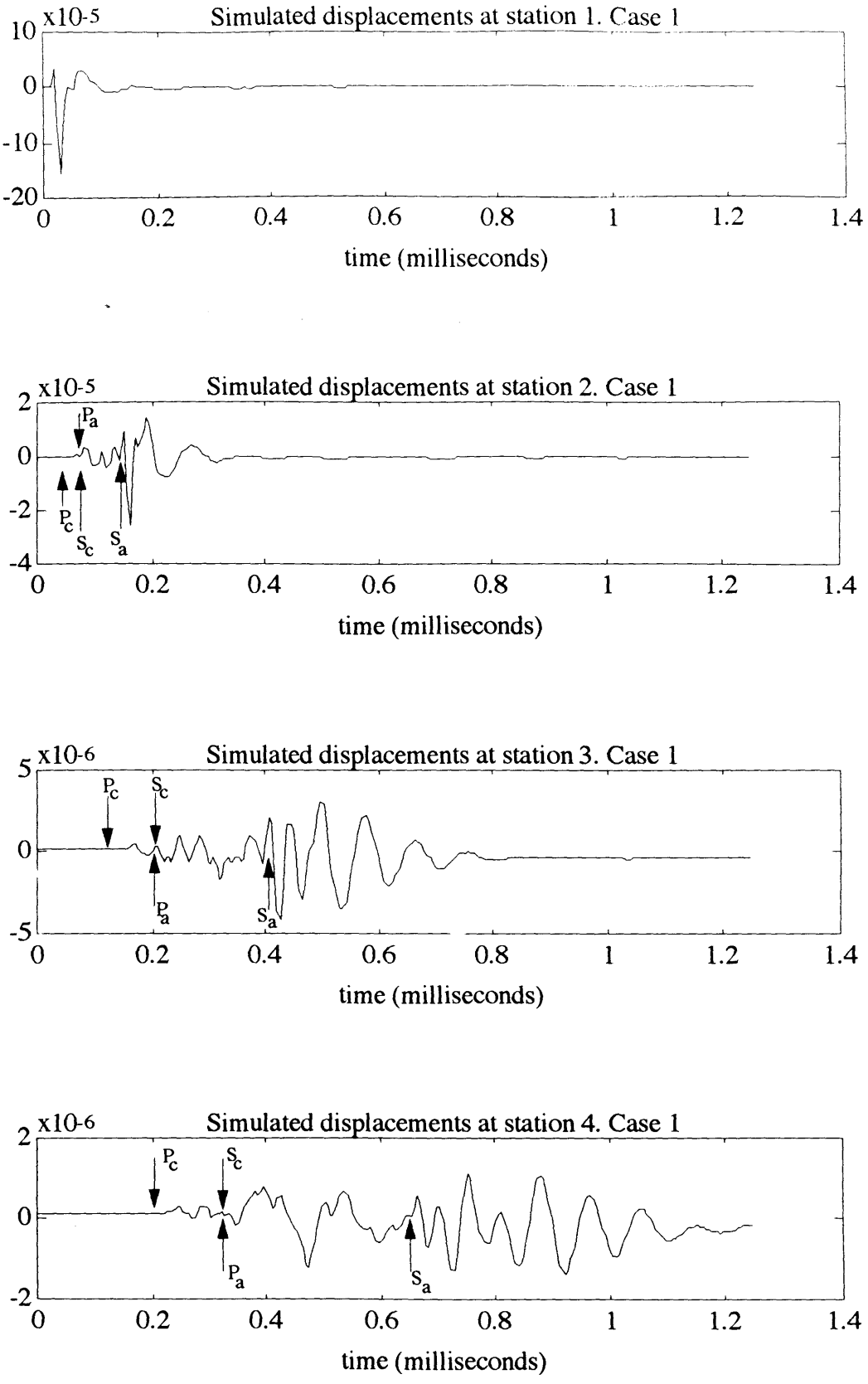

Figure 3.6: Displacements at all four stations for a 16μs impact on a 12" deck (2" of asphalt, 10" of concrete)

that Rayleigh waves follow closely the shear waves . More details will be given in chapter V.

Also, we must account for some discrepancies between the location of the arrow pointing at the arrival time of the P_C wave (computed as if it had traveled only in the concrete layer) and the first wiggle characteristic of its presence, visible shortly after. In effect, the ray path first crosses the asphalt layer, is refracted in the concrete layer just below the interface and eventually crosses again the asphalt back to the surface. The travel time is therefore slightly longer than indicated.

We did not mark the arrival times for the trace reproducing the displacements at station 1 for reasons of clarity. However, the jolt evidently indicates the passing of the surface wave.

For station 1 and 2, it seems that most of the signal energy is contained in the surface wave. However, if we clip the early part of the signal and zoom in on the tail, we observe (see Figure 3.7) oscillations that follow the passing of the Rayleigh wave. We will show in chapter IV, that those oscillations are primarily due to multiply reflected P waves. It is thus interesting to mention that an important part (in terms of information) of the signal lies after the arrival of the surface wave an might be difficult to detect because its amplitude is usually relatively small.

III- STRATEGY FOR THE ANALYSIS

III-1) Simulation and field data

The early study of the field data supplied by Weston NDT did not show too well the expected structural information primarily because the recorded traces were too short. Those were essentially intended to allow the detection of arrival times of several types of waves. In such a short time, structural modes hardly have time to develop. By contrast, our simulation results are not only noise free (with the exception of numerical noise), but can also be extended arbitrarily in time. In addition to this, we can also choose the variable we wish to study, that is displacement, velocity or acceleration and select the one that contains the most accurate information. Most of the time, it turned out that displacements were less sensitive to numerical noise and showed structural frequencies (i.e. the relatively low frequencies) best.

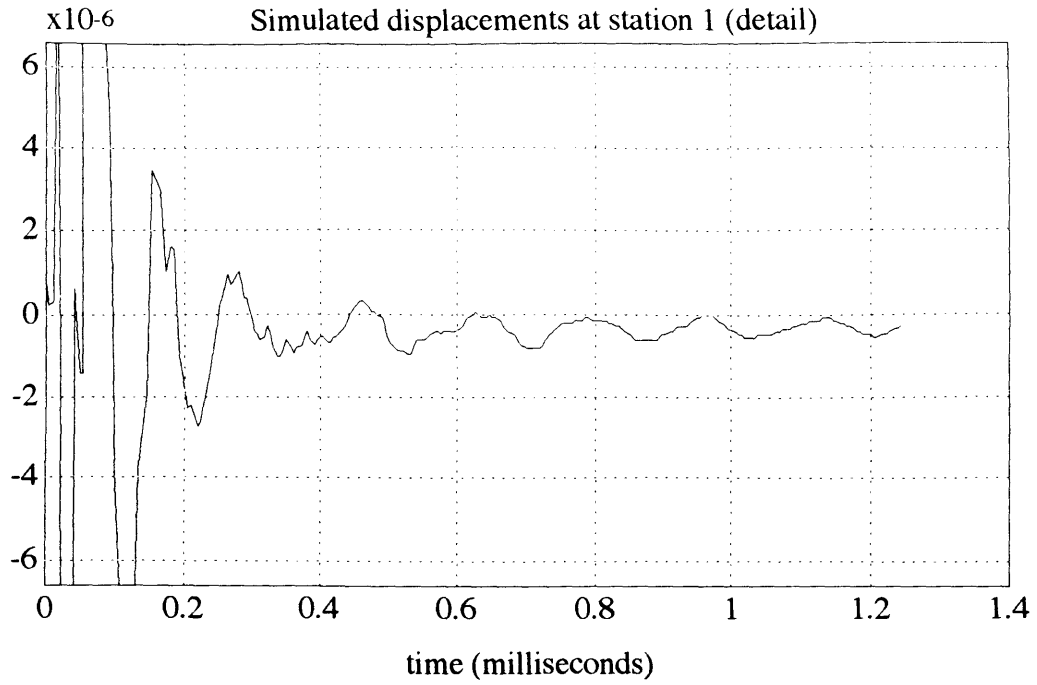

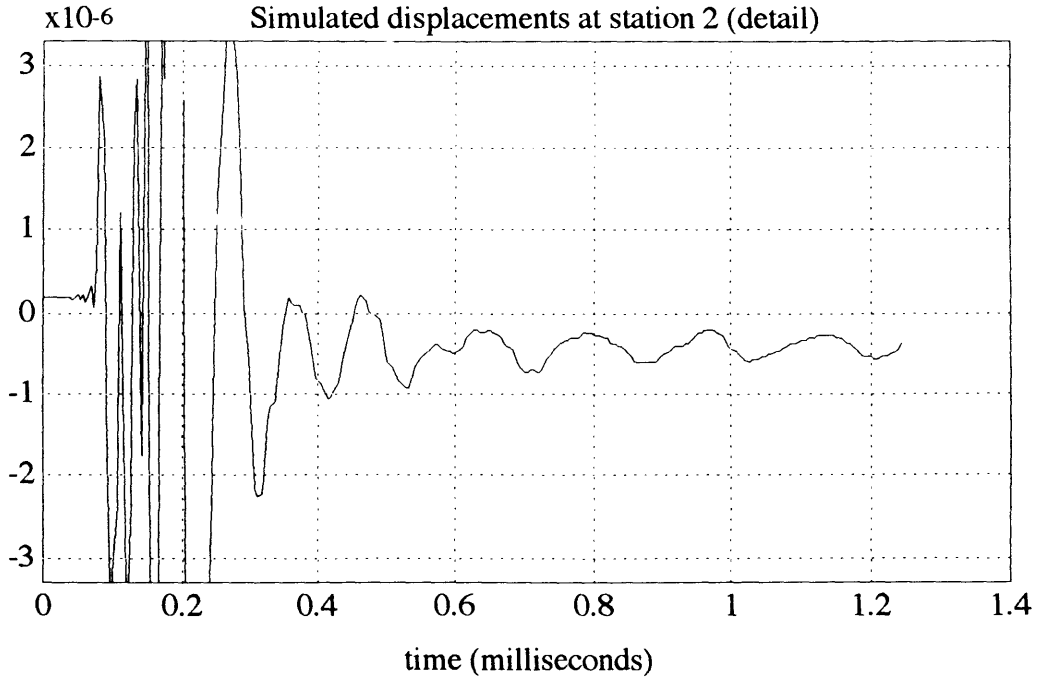

Figure 3.7: Displacements at station 1 & 2 (detail) for a 16μs impact on a 12" deck (2" of asphalt, 10" of concrete)

We concentrated our main effort on the measurement of the deck thickness and the detection of possible delamination. To that purpose we simulated the propagation of waves in decks of different heights (with a maximum of 12" for the whole deck including the asphalt layer). We also studied the influence of compression and shear wave velocities. The simulation were performed either on homogeneous concrete decks or, to comply with the most usual experimental situation, with an asphalt cover on top. In order to simplify, the asphalt layer thickness remained constant and equal to 2 inches (5cm) throughout all simulations.

The characteristics of the cases that we study hereafter are summarized in table 3.5

	asphalt layer thickness	concrete layer thickness	impact time
case 1	2" (5cm)	10" (25.4cm)	16μs
case 2	2" (5cm)	8" (20.3cm)	16μs
case 3	2" (5cm)	3" (7.6cm)	50μs

Table 3.5: Simulated cases

III-2) Local Fourier Transform. Location of the structural information

The difficulty with a transient signal such as a pulse traveling along infinitely many paths in a wave guide (here an infinite plate) is of two kinds. First, there are no structural modes in the sense we usually give to finite structures. However, reverberations and multiple reflections give birth to something similar, but, and here lies the second major problem, it takes a while before they actually develop and become detectable.

The impact, a short impulse, excites a wide band of frequencies, some corresponding to structural resonant or propagating modes (we will come back more precisely to that notion in chapter IV) that die out, supposedly, long after other frequencies.

Typically we have found that the essential part of the signal is contained in the first 2.5 milliseconds, for all sensors. After that limit, the signal is so attenuated, that it did not make any sense to look for any information in it. Hence, from now on, we refer to the *complete signal* as the first 2.5 milliseconds. Taking its Fourier Transform at station 1 for instance, shows that most frequencies are excited up to the cut-off frequency of the impact. This is depicted in Figure 3.8 along with the original signal in the time domain in the case of a 16 microsecond impact on a 12" deck (2" of asphalt and 10" of concrete). It

is clear, looking at both the trace versus time and the Fourier spectrum, that the broad range of frequencies is controlled by the large early pulse in the time domain, and that all subsequent oscillations are masked, too small to produce any significant peak in the frequency domain. This result is consistent if we perform the same global Fourier analysis on other stations and moreover, there are no detectable changes if we shift to thinner decks. We conclude that the global Fourier analysis turns out to be inefficient in revealing structural information. It is controlled primarily by the impact pulse that can only be used as mentioned in [17] to estimate the impact time.

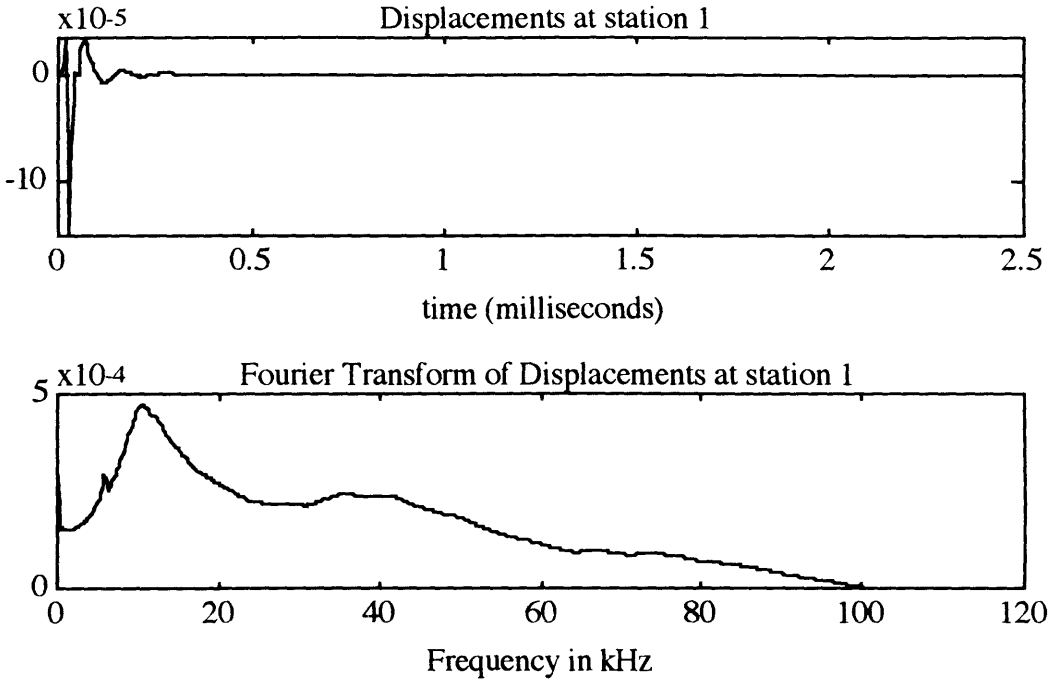

Figure 3.8: Displacements and Fourier Transform on the whole signal

If we look at the tail of a particular signal, after the passing of the large pulse that turns out to be primarily a surface wave, we can actually see oscillations of a much smaller amplitude, but that seem to have a consistent frequency component. This induced us to perform a *local Fourier analysis* that would characterize major frequencies of the signal and their dependence on time. A classical way to do it (see [12] for instance) is to multiply the signal by a window centered in the desired area we wish to study and then take a Fourier transform. The window width is a compromise between the resolution in frequency (that requires a large window) and the localization in time (that calls for a sharp window). To visualize the variation of the frequency content in time, we then slide the window along the time axis.

The window that gave the best results, because of its regularity and its very sharp image in the frequency domain was borrowed from I.Daubechies (see[2]) and is defined as follows:

$$g(t) = t_0^{-1/2} \begin{cases} \sin\left[\frac{\pi}{2}\nu\left(\frac{\pi + \omega_0 t}{2\pi - \omega_0 t_0}\right)\right] & \text{if} \quad -\frac{\pi}{\omega_0} \le t \le \frac{\pi}{\omega_0} - t_0 \\ 1 & \text{if} \quad \frac{\pi}{\omega_0} - t_0 \le t \le -\frac{\pi}{\omega_0} + t_0 \\ \sin\left[\frac{\pi}{2}\nu\left(\frac{\pi - \omega_0 t}{2\pi - \omega_0 t_0}\right)\right] & \text{if} \quad -\frac{\pi}{\omega_0} + t_0 \le t \le \frac{\pi}{\omega_0} \\ 0 & \text{otherwise} \end{cases} \tag{3.5}$$

where

$$\nu(x) = \begin{cases} 0 & , \quad x \le 0 \\ \sin^2\left(\frac{\pi}{2}x\right) & , \quad 0 \le x \le 1 \\ 1 & , \quad 1 \le x \end{cases} \tag{3.6}$$

in which ω_0 and t_0 must be chosen so that

$$\pi < \omega_0 t_0 < 2\pi \tag{3.7}$$

In theory, we can reconstruct the original signal if we shift that window by amounts of nt_0, where n is an integer. The sliding window is then

$$g_n(t) = g(t - nt_0) \tag{3.8}$$

However, since we are only interested in the analysis of the signal and not its reconstruction, we can shift the 'mother window' g(t) by smaller amounts in order to obtain a clearer picture.

We choose $f_0=\omega_0/2\pi=2000$ Hz and $t_0=250$ microseconds so that the sliding window is 500 microseconds long. The mother window is shown on Figure 3.9 and the analysis program written in MATLAB language is reproduced in appendix B. The window is progressively shifted in time by amounts of $t_0/2=125$ microseconds, and applied to the signal, i.e. in this case displacements. Note that we first adjusted the displacement curve so as to remove the rigid body component and then multiplied by the window. On that intermediary result, we take a Fast Fourier Transforms and for each shifted window, we plot the amplitude of the frequency spectrum. Thus we obtain a set of

amplitudes on a time-frequency grid, representative of the spectral component at various moments. We call that representation a windowed Fourier transform, or a local Fourier transform to stress the time dependency of the spectral analysis. Figure 3.10 shows the three dimensional result for the windowed Fourier transform of displacements at station 1 and 2, for case 1 (see Table 3.5). To compensate for attenuation with time, the Fourier spectrum of each individual windowed signal, is normalized with respect to the maximum spectral amplitude in this very window. Thus spectral amplitudes are represented here only by their relative importance with respect to the maximum at a specific time. In addition, only frequencies up to 25 kHz are represented here, because, as shown in chapter IV, they contain most of the structural information.

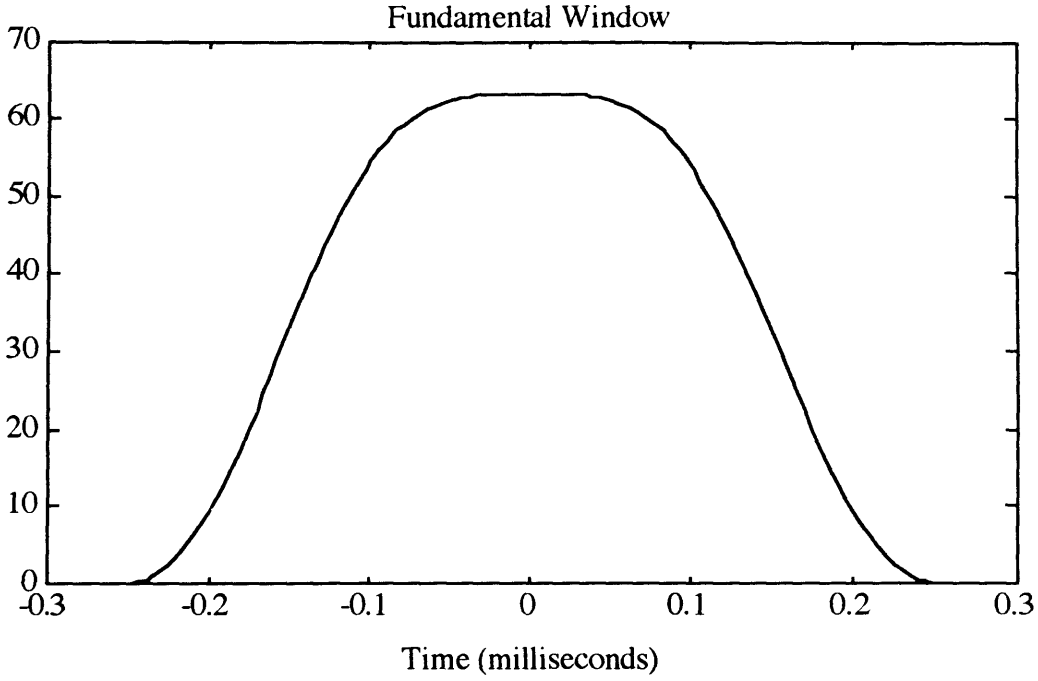

Figure 3.9: Basic window for local Fourier analysis

The three dimensional picture of Figure 3.10 shows that after a while, a particular frequency seems to become dominant. To be more specific, we also show a contour representation of the same information in Figure 3.11. Let us note, here, that later times are artificially amplified with our normalization. Yet, the recording of displacements at station 1 exhibits a major peak at approximately 6 kHz after a time lag of 0.4 milliseconds which seems to persist all the way through 2.5 milliseconds. At station 2, this peak appears later on (around 0.6 milliseconds). We observe a similar behavior in Figure 3.12 in which local Fourier transform are represented for station 3 and

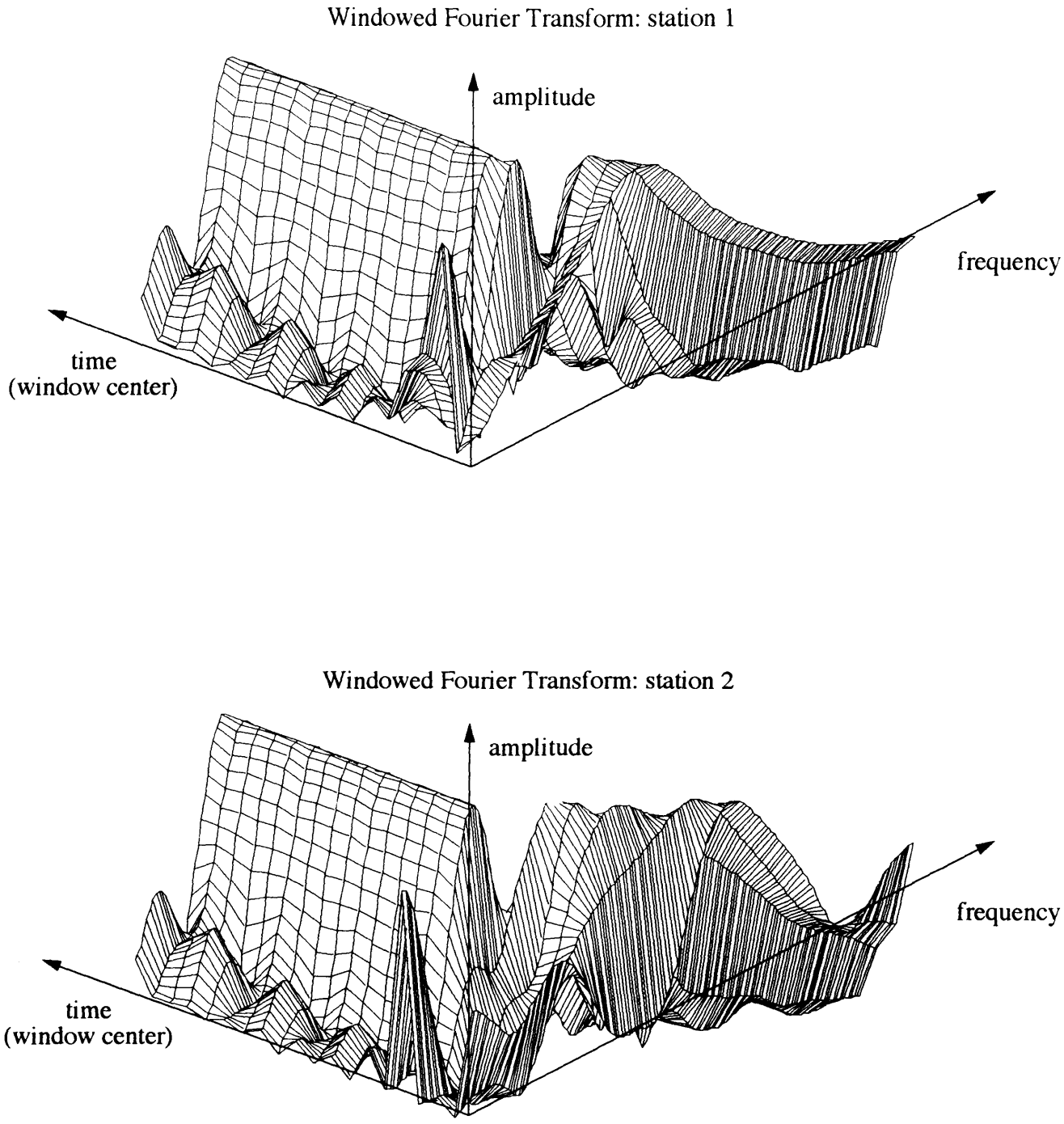

Figure 3.10: Windowed Fourier Transform (amplitudes)
case 1: 10" concrete deck, 2" asphalt cover
station 1 & station 2

station 4. Again a major persistent peak appears at the vicinity of 6 kHz after a longer time delay: 1.1 millisecond at station 3 and 1.4 millisecond at station 4. In chapter IV, we will interpret this peak as a resonant frequency of multiply reflected P waves that bounce back and forth on the free boundaries. The resonant frequency will turn out to be characteristic of the deck thickness. We will also account for the delay before those modes actually develop or are detectable. In particular, we can see in Figure 3.12 that another mode develops before the resonant mode: it is signaled with a full line arrow and its main frequency changes with time. In other words, different frequencies travel at different velocities: its a dispersive mode. To be more specific, high frequencies travel slower than low frequencies and this will proved to be characteristic of surface waves in a concrete deck covered with an asphalt layer. We notice that Rayleigh waves hardly develop before a distance of one wavelength (of the order of the concrete deck height) and therefore cannot be observed at station 1 or station 2. However, once they are present at station 3 and 4, their importance overcome that of the multiply reflected P waves and we need to wait until surface waves have completely passed by before we can actually detect the resonant mode.

The previous line of interpretation needs now to faced with changes in the characteristics of the deck. Case 2 and 3 (see table 3.5) give us that opportunity. As for a comparison, Figure 3.13 presents the local Fourier analysis at station 1 for both cases. We can clearly detect a shift towards higher frequencies in case 2 (up to 7 kHz) corresponding to slightly thinner concrete deck, and a dramatic shift (up to 12 kHz) in case 3 that models an 'infinite delamination' with a very thin concrete deck (3" only).

We must be careful in analyzing the contour plot of that last local Fourier transform. Once we multiply the displacement trace with the window, we take a Fast Fourier Transform of the result on a number of points large enough so that the frequency step is approximately 200 Hz. However, we have defined the window in (3.5) and (3.7) so that $f_0=\omega_0/2\pi=2000$ Hz would be the smallest significant frequency. Hence, the peak in the vicinity of 2 kHz in case 3 of Figure 3.13 is nothing else but the fundamental frequency f_0 and has no structural meaning.

III-3) Variable of analysis

A question rises naturally, whether we should focus more on displacements, velocities or accelerations. As we have seen in chapter I (see also appendix A), we can easily change the experimental setting, so as to record either displacements or accelerations on the field. Simulations of both displacements and accelerations at the four

stations show us that the frequency spectra of displacements contains much more information on the structure than that of accelerations. A good reason for this, which will be developed in chapter IV, is that the structural information lies in the low range of frequency (0 to 12 kHz) that is amplified by displacements, whereas accelerations emphasize high frequencies.

Therefore, we concentrate in the following, on surface displacements, with the idea that the experimental setting can be changed so as to record displacements as well.

III-4) Impact-Echo method for close field and Surface Wave analysis for far field.

Out of the first analysis of the simulations that we have been running on infinite plates, we draw two lines of conclusion. First resonant frequencies appear clearly after a while in particular in the close field, at station 1 and station 2 (1" and 7" from the impact point). Those peak frequencies seem obviously related to the geometry, in particular the thickness of the plate. It induces us to use the recordings at the first two stations to detect resonant modes. This is described in the literature as the Impact-Echo method and will be addressed to in chapter IV.

Station 3 and 4, in the far field did not seem propitious for that kind of analysis: the resonant frequency came too late and are most probably so attenuated that a practical analysis on the field would be meaningless. However, we mentioned that we could locate a surface wave in the early time of recording. Its dispersive characteristic will be used in chapter V to obtain information on the propagating medium. This is referred to as a spectral analysis of surface waves.

Our strategy for the analysis of both simulated displacements and field data now consists in reserving mainly station 1 and 2 to the detection of structural resonances via the Impact-Echo method, and stations 3 and 4 to study surface waves.

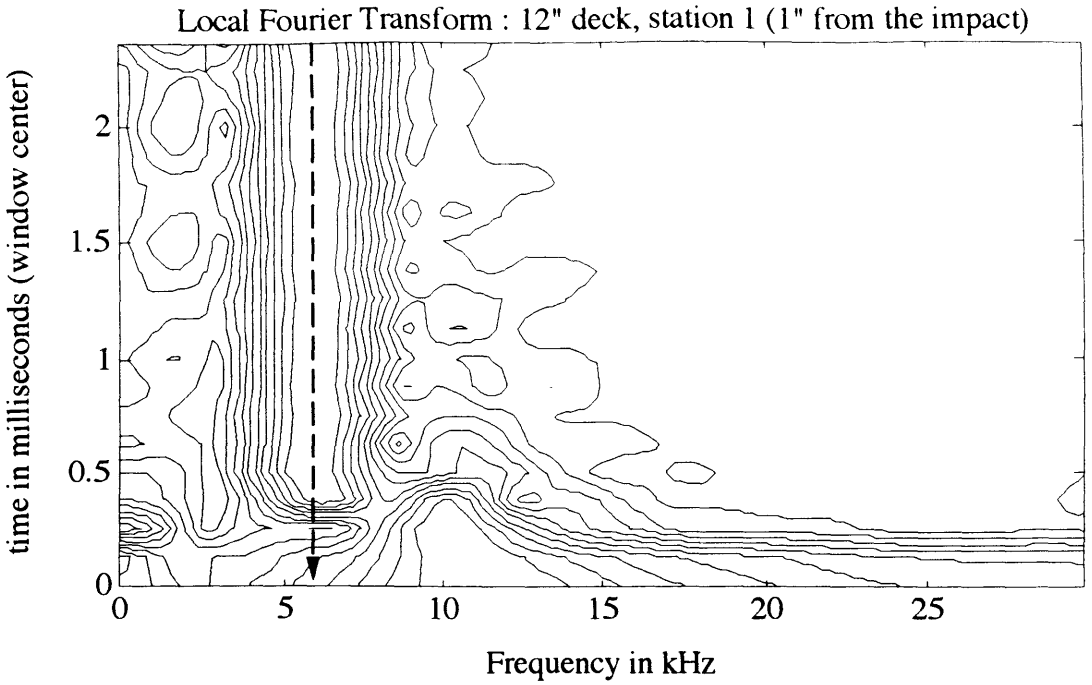

Multiply reflected P waves ------>

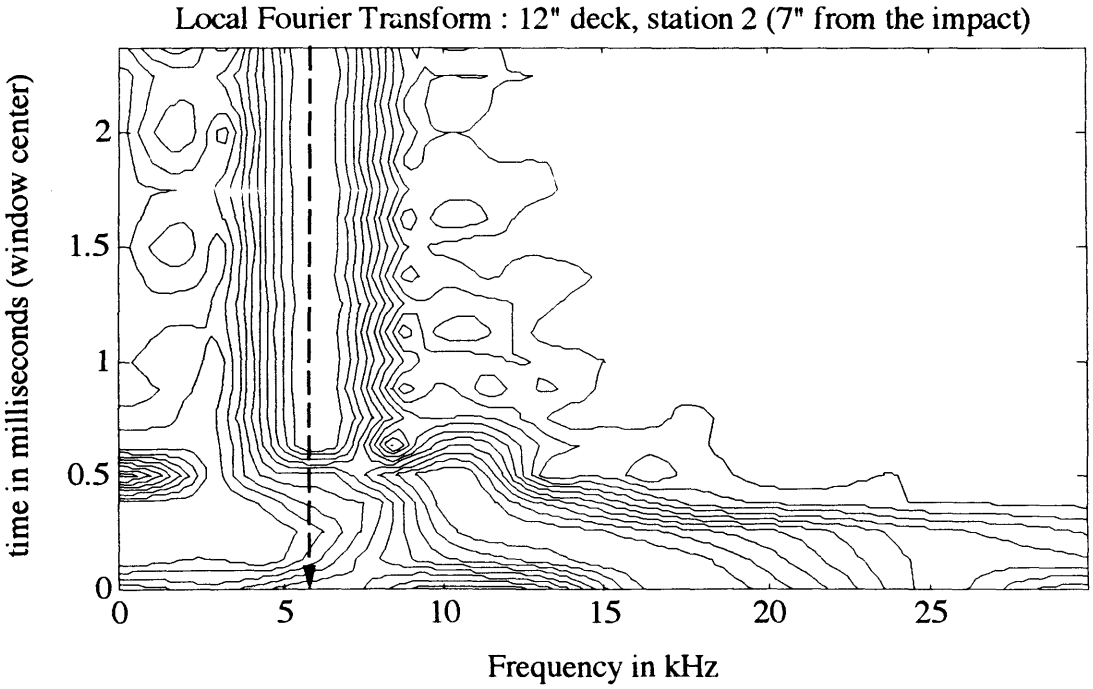

Figure 3.11: Windowed Fourier Transform at station 1 & 2
case1: 10" concrete deck, 2" asphalt cover

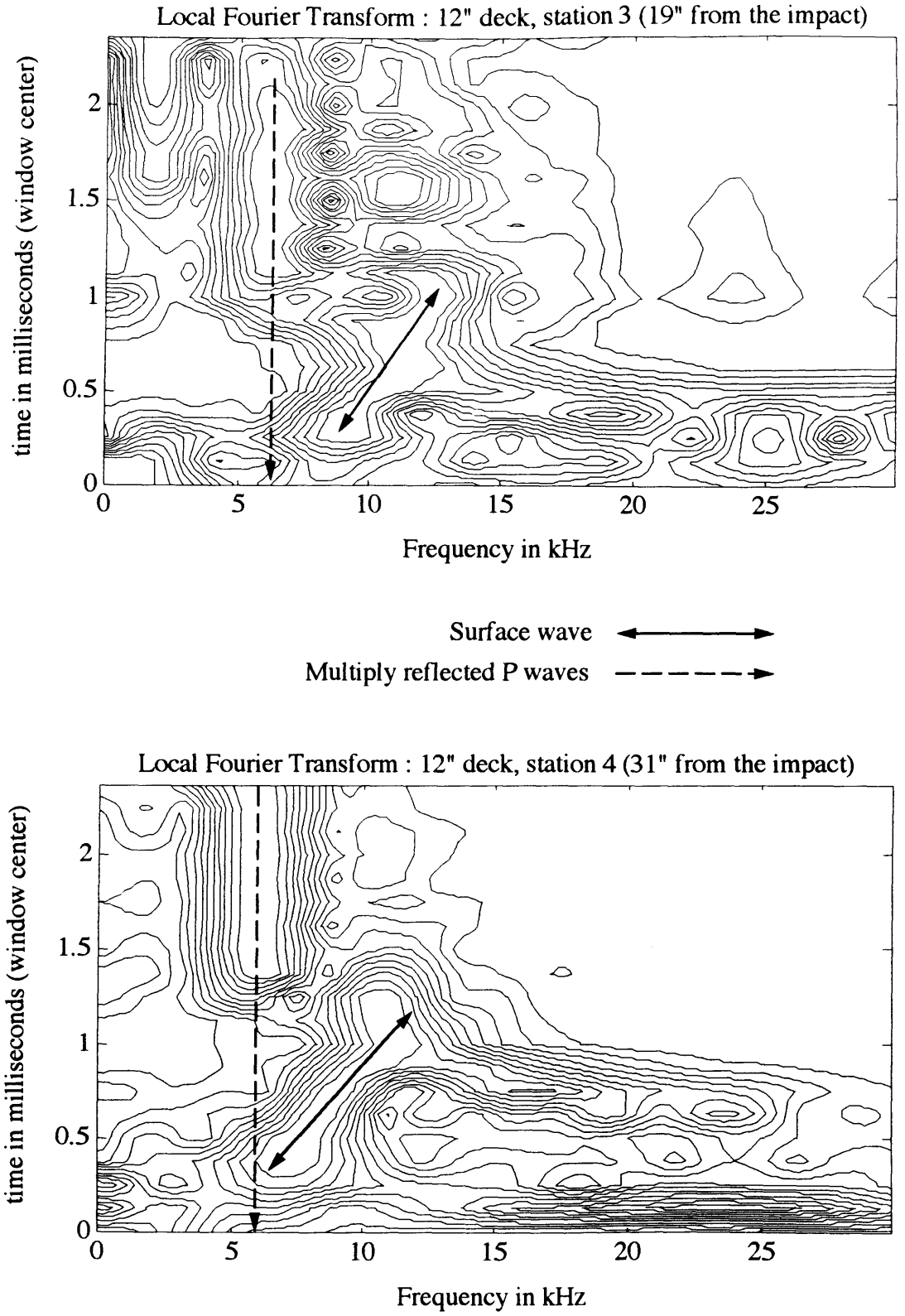

Figure 3.12: Windowed Fourier Transform at station 3 & 4
case 1: 10" concrete deck, 2" asphalt cover

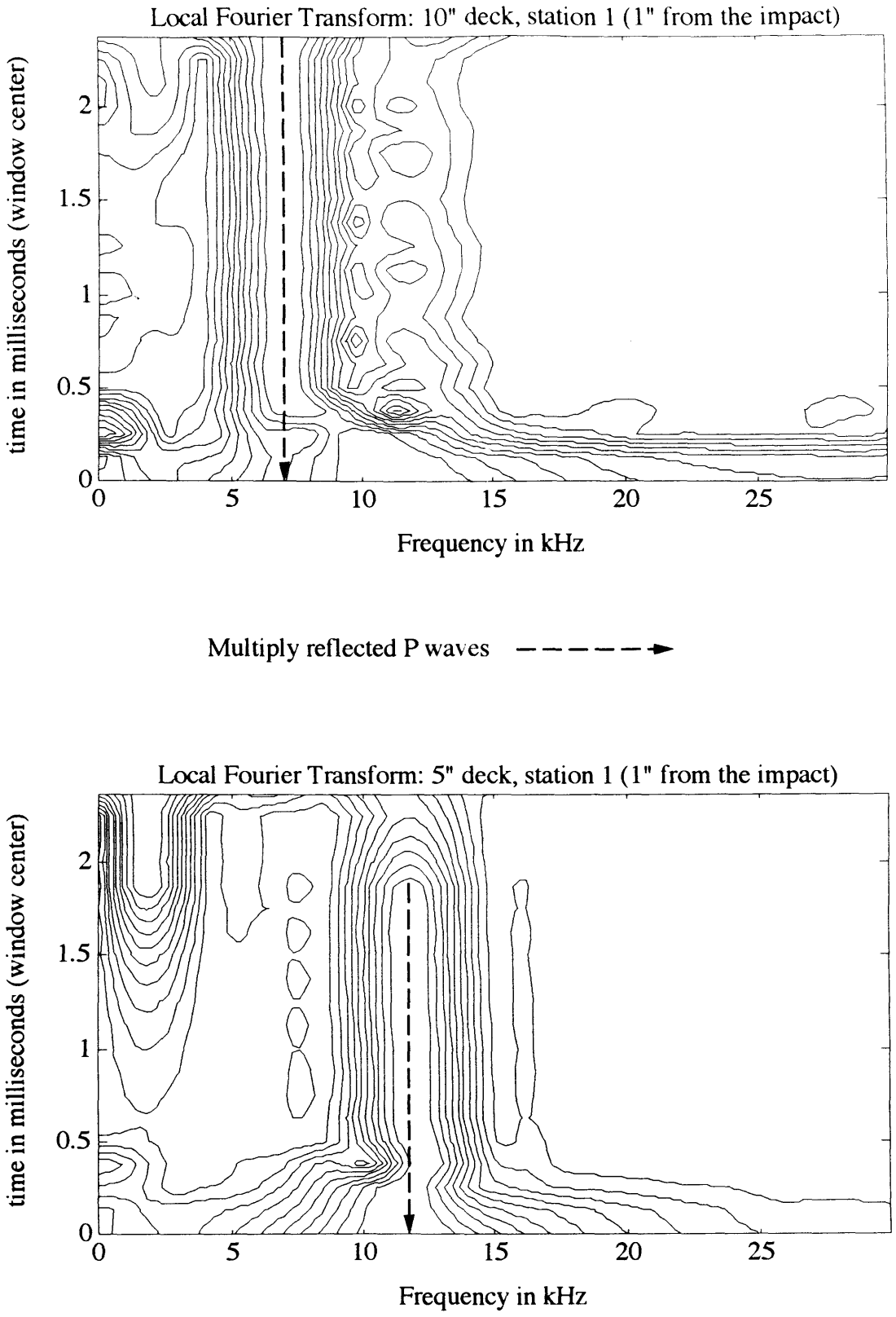

Figure 3.13: Windowed Fourier Transform at station 1
case 2 (8" concrete deck, 2" asphalt cover)
& case 3 (3" concrete deck, 2" asphalt cover)

CHAPTER IV: IMPACT ECHO METHOD

Outline

I- Principles of the Impact-Echo Method

II- Strategy for field data analysis

- II-1) Algorithm
- II-2) Result for simulated data
- II-3) Results for real data at a receiver close to the impact point, station 1

III- Corrections for farther receivers

- III-1) Corrections for skewed rays
- III-2) Validity. Mode conversion problem.
- III-3) Results for station 2

IV- Stiffness Matrix Approach for the Impact-Echo Method

- IV-1) Exact solution for a model with two layers
- IV-2) Resonant frequencies
- IV-3) Heuristic inverse problem
- IV-4) Results for simulations

I- PRINCIPLES OF THE IMPACT-ECHO METHOD

Among other non destructive testing techniques for the evaluation of structures, the Impact-Echo Method based on stress wave propagation has gained interest in recent years. If it gives appealing results for homogeneous materials, metallic for example, development for concrete structures has been relatively slow, in particular because this heterogeneous medium wipes out high frequencies and contains many more failure modes than many mechanical problems. Truly, concrete can suffer from delaminations, weaknesses, flaws, cracks, micro-cracks and so on and so forth. All these defects generally have a complex influence on wave propagation. Besides, reinforcement bars present in most concrete structures again modify the way stress waves propagate through the structure.

In principle, the Impact-Echo Method consists in introducing a stress pulse by means of a mechanical impact at the surface of the structure to be tested, which can be a concrete deck, a road pavement, or a tunnel wall for instance. The waves thus generated are monitored on the same surface at short distances from the impact point. In between, not only do they bounce back and forth between the free or fixed boundaries of the structure but they also interact with the defects of the material. To name only a few effects of structure failures, we note that waves will be reflected by cracks, scattered by the sharp edges of voids and slowed down by a field of micro-cracks.

To locate and identify defects in the structure we must have a good understanding of how transient waves propagate through the structure and we must also be able to point out a few characteristics typical of the alterations that the defects will generate. In [17], M.Sansalone, N.J.Carino, N.N. Hsu focus on wave propagation in a concrete slab very similar to ours, 0.25m thick, with a modulus of elasticity of 33100 MPa, a Poisson's ratio of 0.2 and a density of 2300 kg/m^3. Hence the resulting P, S and R wave velocities are 4000 m/s, 2440 m/s and 2240 m/s respectively which are very close to the values that we used, namely 3919 m/s, 2400 m/s and 2200 m/s. M.Sansalone, N.J.Carino and N.N. Hsu carried their analysis both with Green's functions for an analytical solution and with a finite element solution. Both solutions matched pretty well.

The results for station 2 of the simulation carried out with the code referred to in chapter III, are reproduced in Figure 4.1. They are very similar to those M. Sansalone and N.J. Carino obtained. We note in this graph, that after the passage of the Rayleigh wave, the surface returns to its original position until the arrival of the reflected P waves (that is always a tension wave), when it is drawn below its original position. After the passage of the Rayleigh wave, the upper surface never goes higher than its original position. In fact,

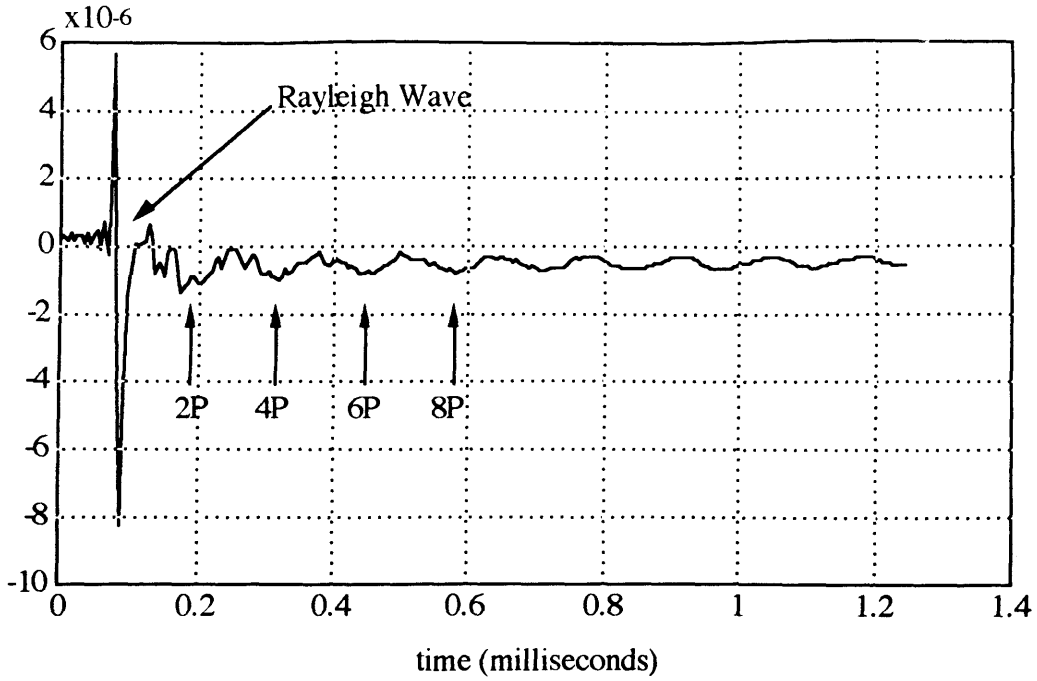

Figure 4.1: Displacements at station 2 (7" from the impact point) for a 16 μs impact on a 10" thick infinite concrete plate

because the amplitude of a stress wave changes sign each time it reflects at a free boundary, it follows that downward waves are always compressive, while upward waves are tensile.

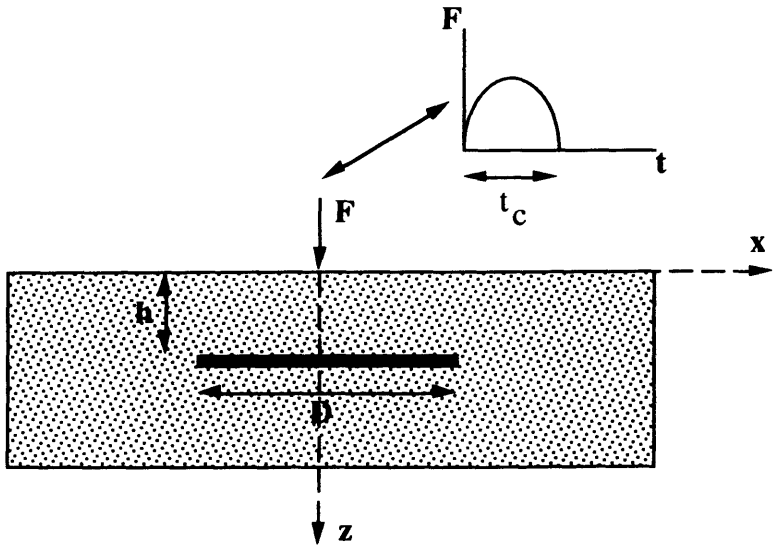

Figure 4.2: Concrete Plate with a Planar Disk-Shaped Void

Confident in their finite element analysis, M.Sansalone, N.J.Carino and N.N. Hsu perform in their later work ([18] - [23]) analyses of several plates with defects, typically horizontal disk shaped voids of various dimensions, as shown on Figure 4.2. In [18], the authors showed noticeable changes in the trace due to waves diffracted on the sharp edge of the flaw, in particular large upward surface displacement caused by the arrivals of the P_dS and S_dP waves (namely P waves diffracted into S waves, and S waves diffracted into P waves). Recalling that in an ideally infinite plate, a point on the surface never moves above its original position after the passage of the Rayleigh wave, these uprising could be used as an indicator of waves diffracted by a sharp edge of a crack.

In [19], a study is presented for a point impact on a finite unsupported circular plate, with a particular focus on the frequency response of a point on the surface, close to the impact location. In the frequency spectrum of the displacement at that point, the authors identify several modes of vibrations: specular reflection modes (i.e. generated by compression waves multiply reflected at the upper and lower free boundaries) and bending modes of the plate. They find that near the impact point, P wave reflections back and forth across the thickness of the plate are predominant over S wave reflections, as expected, since shear wave displacements are relatively weak just below the impact point. Furthermore, they find major reflections coming from the bottom and top corner edges of the circular plate (diameter modes), as well as the first three flexural modes of the finite plate and a rod mode.

If H is the thickness of the plate, L its diameter, C_p the P-wave velocity, then the compression wave thickness mode has a frequency of

$$f_p = \frac{C_p}{2H} \tag{4.1}$$

and the diameter modes have the following frequencies

$$f_p = \frac{C_p}{\left\{L^2 + (nH)^2\right\}^{1/2}} \tag{4.2}$$

where n=0,1,2,3...

For a 25 cm thick plate, 1.6m in diameter, with the material characteristic mentioned earlier, the frequencies of the modes are the following:

1st flexural mode	3.5 kHz
2nd flexural mode	12 kHz
3rd flexural mode	20 kHz
Rod mode	10 kHz
P thickness mode	8 kHz
S thickness mode	4.9 kHz
P diameter mode	2.1 kHz
S diameter mode	0.65 kHz

Table 4.1: Frequencies of the different modes in a finite circular plate

It is worth noting that for our engineering problem we are more interested in the direct reflections from the bottom of the plate than in the side reflections, since one of our objectives is to measure the thickness, of the plate. One way to avoid side reflections that might come from lateral support of the deck, is to cut the recordings sufficiently early so that echoes do not have time to reach the sensor. It is also interesting to note, as mentioned in chapter III, that as the distance along the surface from the impact point increases, displacements due to shear waves grow larger. Moreover, the time lag between the thickness reflections and the side reflections diminishes as the distance between the sensor and the impact location increases, which makes the analysis more difficult in the time domain and might prevent us from cutting the recordings in time to end up only with the thickness modes.

In [20] M. Sansalone and N.J. Carino extend the analysis to a circular plate with a horizontal flaw centered on the plate axis. They compare the frequency spectrum of the displacements of a surface point close to the impact location for a damage-free plate and for a plate with a flaw. In the latter they find two dominant frequencies: the original compression thickness mode frequency of the complete plate and a higher frequency due to multiple P wave reflections on the flaw surface:

$$f=\frac{C_P}{2h} \qquad (4.3)$$

where h is the flaw depth (see Figure 4.2). The full depth thickness mode can still be observed because of P waves diffracted at the edge of the flaw and reflected at the bottom free surface of the plate.

The authors try several sizes of flaws in their numerical analysis, and demonstrate that it is important for the impact time t_c to be short enough in order to generate high frequencies waves (most of the energy being in the frequency range 0 to $1/t_c$), having short wavelengths $\lambda=c_p.t_c$ that are smaller than the diameter of the flaw. To detect a 0.20m diameter void, a contact time shorter than 50 μs is needed. However, we must keep in mind that the interfaces between aggregates and the binder must be transparent to the waves and therefore the wavelength must be larger than the maximum typical size of the aggregate, i.e. 2.5 cm. Hence, t_c should be greater than 0.025(m)/4000(m/s)=6.25 μs.

Again as the flaw is centered about the axis of the circular plate, the best results are obtained when the receiver recording the displacements is placed near the impact location, and as it is dragged away, the frequency peak corresponding to the reflections on the flaw decreases and almost vanishes as the receiver moves outside of the area immediately above the flaw.

We mentioned earlier that in order to avoid interferences with waves reflected on the side edge of the circular plate, recordings must be terminated soon enough. In such a case the spectrum does not contain modes generated by side reflections, but on the other hand, it is computed on a smaller number of points and therefore shows less accuracy. This can be annoying if we are to find precisely the depth of the flaw ($h=C_p/2f$). Hence there is an engineering trade-off between the precision with which the flaw depth can be measured and the amount of spurious information coming from the side boundaries of the inspected structure.

Now, in practical situations, we very seldom face a homogeneous concrete plate. Most of the time, the concrete decks we are interested in, are covered with an asphalt layer, underlain by a layer of steel reinforcing bars or beams, or are lying on an acoustically softer subgrade if we are dealing with road pavements or airport runways. In all those cases, the heterogeneous medium in which waves propagate can be modeled as a layered plate. The difficulty arises in the multiple reflections at interfaces between layers that make the recordings more complicated to interpret. In [21] M.Sansalone and N.J. Carino analyzed several two-layer plates with varying acoustic impedance differences and pointed out how, and to what extent, flaws at the interface or in the lower layer can be detected and located. In the impact echo method, we place the receiver at the surface, very close to the impact point. Hence, since the layers are assumed to be horizontal, we are mainly concerned with reflections of normally incident P waves. Thus the amplitude

of a P wave reflected at an interface between two layers 1 and 2, is proportional to the amplitude of the incident P wave with a factor of

$$A=\frac{Z_2-Z_1}{Z_2+Z_1} \tag{4.4}$$

where Z_1 and Z_2 are the acoustic impedances, i.e. density multiplied by the compression wave velocity, of the first layer (in which the incident P wave propagates initially) and of the second layer respectively. It is of particular interest to note that if the second layer has a lower impedance than the first layer, then the amplitude of the stress wave changes sign as it bounces back on the interface and keeps the same sign otherwise. Hence, as shown on Figure 4.3 taken from [21] the surface displacements are very different in the two cases. In this figure and the following, T and P respectively indicate tension and compression waves.

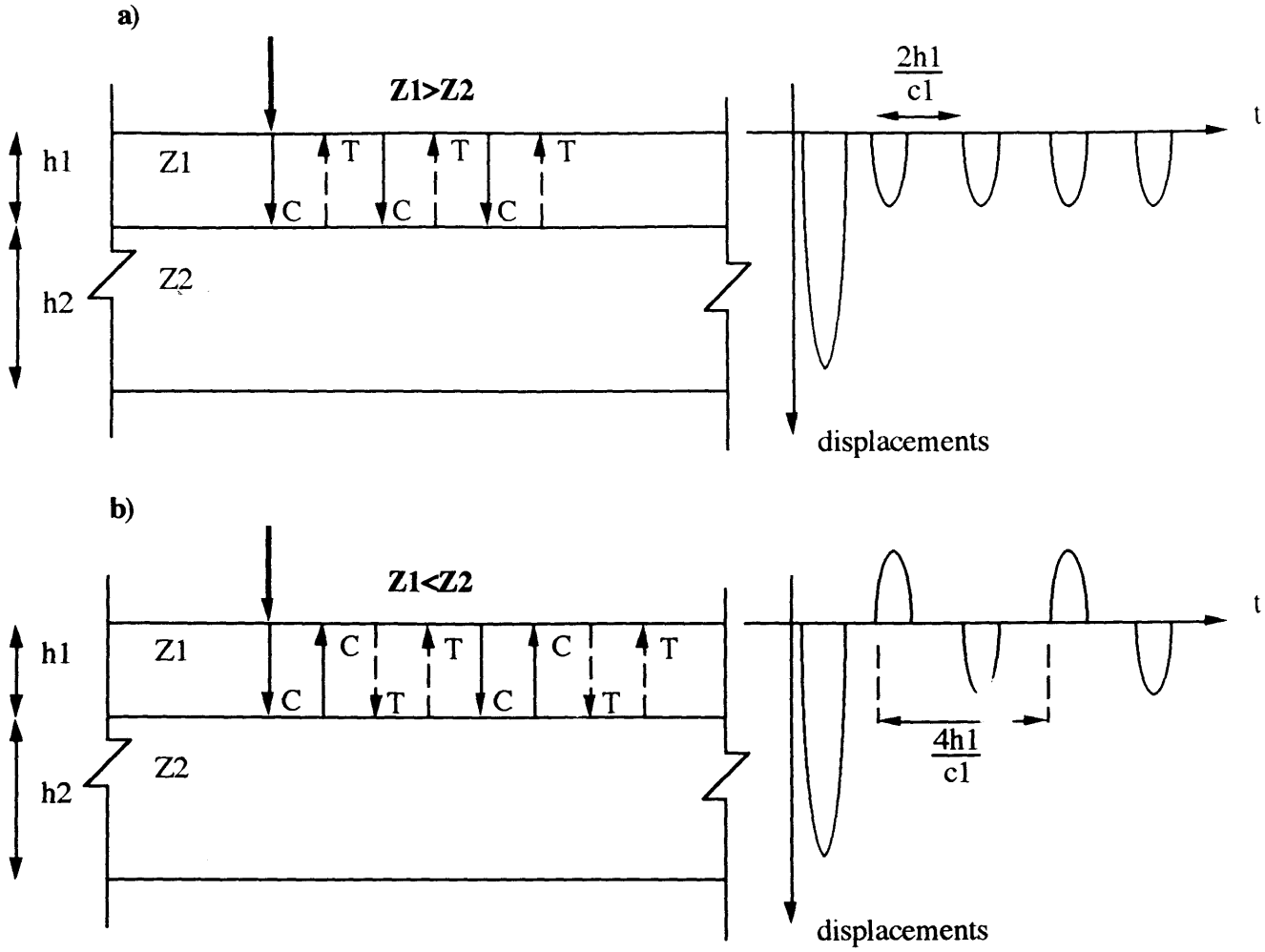

Figure 4.3: Impact response of the top layer
a) harder top layer
b) softer top layer

After the passage of the Rayleigh wave the dominant frequency due to reflections on the interface (hence the subscript i) are:

$$f_i = c_1 / (2h_1) \qquad \text{if } Z_1 > Z_2$$
$$f_i = c_1 / (4h_1) \qquad \text{if } Z_1 < Z_2 \tag{4.5}$$

where h_1 is the thickness of the first layer and c_1 the P wave velocity in this layer. However since the amplitude of the stress wave refracted by the second layer never changes sign, the frequency of the composite plate is (see Figure 4.4)

$$f=\frac{1}{\frac{2h_1}{c_1}+\frac{2h_2}{c_2}} \qquad (4.6)$$

h_2 and c_2 being the thickness and the compression wave velocity of the bottom layer.

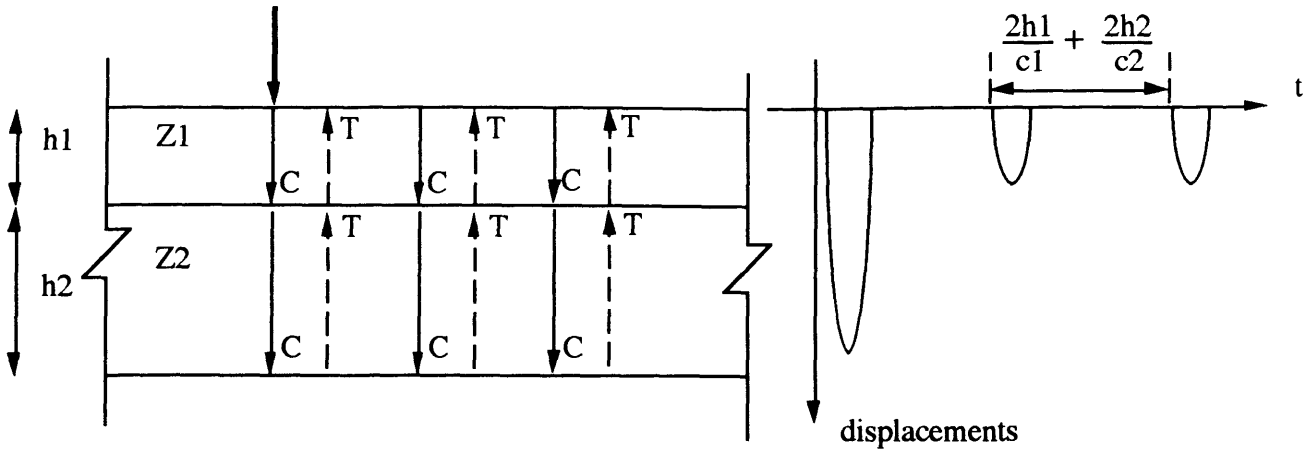

Figure 4.4: Reflections of the complete deck

Eventually the waves trapped in the bottom layer give rise, by refraction in the top layer (see Figure 4.5 taken from [21]), to surface displacements that, according to the relative importance of Z_1 and Z_2 have a fundamental frequency of

$$f_b = c_2 / (4h_2) \qquad \text{if } Z_1>Z_2$$

$$f_b = c_2 / (2h_2) \qquad \text{if } Z_1>Z_2 \qquad (4.7)$$

Of course, in [21] M.Sansalone and N.J. Carino, overlook many other modes and ray paths, but these three modes and their frequencies appear clearly in the numerical simulation the authors carry out and are therefore validated as indicators of the integrity and characteristics of the layered plate.

In a second stage, finite element solutions are used in [21] to study the effect of horizontal voids and flaws on frequency spectra of surface displacements. In the case we are particularly interested in, namely a concrete deck with an asphalt cover, flaws are placed in the mesh of the concrete layer as shown in Figure 4.2 and a simulation is run with a contact time of 15 μs. The frequency spectrum of a surface point in the vicinity of the impact (4 cm away) shows two major peaks, one corresponding to the composite plate frequency (4.6) with a reduced thickness of the concrete layer and the other, a low

frequency, corresponding to the first flexural mode of the delaminated section. It is important to note that with equation (4.6) and the frequency of the specular mode, we can have an estimation of the depth of the flaw. Moreover the pitch of the flexural mode gives an idea of the extent of the delamination: the larger the void is, the lower the frequency of the flexural mode is. M.Sansalone and N.J. Carino show that for small flaws, the specular mode turns out to be unobservable among all the other plate modes, but the flexural mode of the delaminated portion remains observable (with a higher pitch) and becomes the only clear indication of the plate failure.

This observation is also applicable to the case of a concrete pavement on a soft subgrade. Indeed, the low impedance of the soft subgrade layer does not allow dramatic changes in the frequency response for specular waves whenever a zero impedance partial delamination is present at the interface. However a flexural mode appears in the delaminated portion and this is observable.

The situation is very different and easier to deal with, when the impedance order is reversed. For instance we may have an upper layer of asphalt with a relatively low acoustic impedance and a bottom layer of concrete with a high impedance level. With this setting, a very common degradation consists in a debonding of the asphalt cover. If this happens, the impedance difference at the interface is not only altered in amplitude, but its sign also changes. Hence the fundamental frequency of the top layer given by (4.5) doubles from $c_1/(4h_1)$ to $c_1/(2h_1)$ and this shift in the spectrum can be very easy to point out.

The beginning of the trace, consisting mainly of the Rayleigh wave, contains information primarily on the impact, and almost nothing on the structure geometry. Indeed, information that travels at the speed of compression waves, arrives later on. In chapter III, we also mentioned that resonant frequencies are actually well established in the late part of the signal. Hence as mentioned in [22], if we remove the early part of the signal we are left with multiple reflections of body waves only (P waves mainly, if the signal is recorded near the impact) and we thus obtain clearer information about the structure geometry. In addition, since the Rayleigh wave has a very large amplitude compared to the remaining part of the signal, it may be desirable to increase the gain of the sensor so as to clip this portion and have a better resolution on the part of the trace that contains specular reflections.

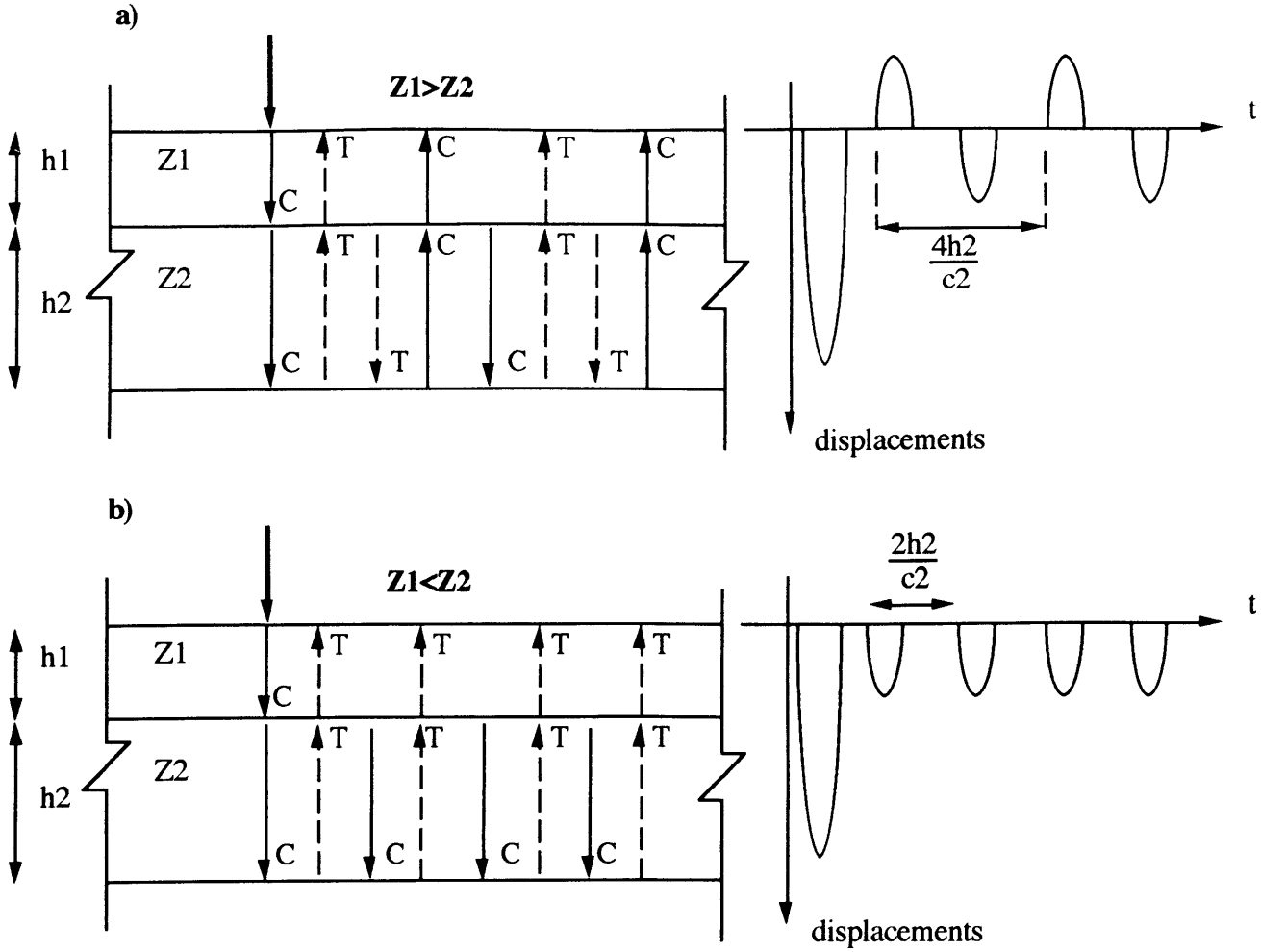

Figure 4.5: Reflection within the bottom layer
a) harder top layer
b) softer top layer

Thus, the main resonance frequencies of the concrete deck generated by multiply reflected P waves, can be used, via equation (4.6), to scan the material in depth. In [23] M.Sansalone and N.J. Carino step towards a solution for an inverse problem in the simple case of a one layer concrete slab containing partial delaminations. They rely on equation (4.1), which is a one layer version of equation (4.6). Along a line at the surface of a concrete plate, they perform a set of seismic measurements, using an impact source, and recording surface displacements next to the impact point. For each seismic trace they compute the Fast Fourier Transform, locate the peaks corresponding to in-depth reflection resonance modes, compute the related depth according to (4.1) and eventually plot those depths versus the horizontal distance on the scan line to obtain a profile of the plate.

In [23] they carry several laboratory tests and obtain good results for simple slabs with voids and delaminations. The authors are for instance able to locate and give the

extent of delaminations, knowing only their existence and nature (horizontal delaminations).

II- STRATEGY FOR FIELD DATA ANALYSIS

II-1) Algorithm

We assume, in the following, that the major frequencies in the late part of the signal, that contains primarily specular reflections, are essentially:

- The frequency related to compression waves bouncing back and forth on the free boundary of the deck:

$$f=\frac{1}{\frac{2h_1}{C_1}+\frac{2h_2}{C_2}} \tag{4.8}$$

- The frequency associated with P waves reflected both at the upper free boundary of the deck and at the interface between the concrete and the asphalt layers:

$$f_i=\frac{C_1}{4h_1} \tag{4.9}$$

The notations were explained earlier and are summarized in Figure 4.7, below.

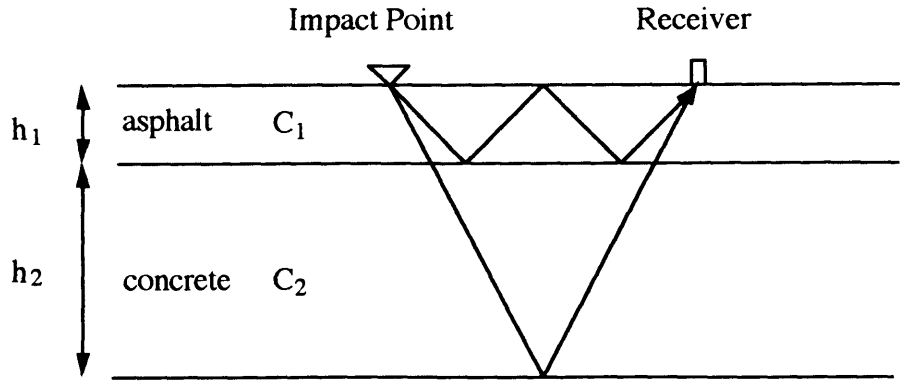

Figure 4.7: Schematic description of the complete deck

We consider of course, the case in which distance between the impact source and the receiver is small in comparison to the deck height h_1+h_2. With typical compression

wave velocities, C_1=2400 m/s, C_2=3920 m/s and thicknesses h_1=2"=5cm, h_2=8"=20cm, the frequency f_i given by (4.9), associated with reflections within the asphalt layer, is much higher than the complete plate frequency f given by (4.8). With the values above, f=5.9kHz and f_i=12kHz. These are, of course, fundamental frequencies and we also expect to detect the presence of overtones.

Hence, our first step is to remove all frequencies that we assume to be associated with the asphalt layer, i.e. frequencies f such that

$$f \geq 0.9 \frac{C_1}{4h_1} \tag{4.10}$$

Then in the remaining low frequency range, we detect major peaks in the spectrum using an appropriate algorithm. Having those major frequencies f, we are able to compute the thickness h_2 of the lower concrete layer as

$$h_2 = \frac{C_2}{2f} - \frac{C_2}{C_1} h_1 \tag{4.11}$$

and the complete thickness of the deck h:

$$h = h1 + h2 = \frac{C_2}{2f} + \left(1 - \frac{C_2}{C_1}\right).h1 \tag{4.12}$$

The MATLAB programs corresponding to that algorithm are reproduced in appendix C.

II-2) Results for simulated data

Our first step, before we apply this technique to field data, is to check its validity on simulated data. For this purpose, we simulate the propagation of waves in three different decks (see table 3.5 in chapter III) with the same material properties, among which we need only mention the P wave velocities in the asphalt layer C_1=2400 m/s and in the concrete layer C_2=3920 m/s. In all simulations the asphalt layer is 5 cm (2") thick. The difference between the three cases is the concrete layer thickness, which is successively taken to be 25.4 cm (10"), 20.3 cm (8"), and 7.62 cm (3") (which represents an 'infinite delamination'). To be consistent with the previous analysis, only

displacements at the first station are considered here, that is 1" away from the impact point.

We choose the time window on which we carry out the analysis, in such a way that we avoid the presence of surface waves and include a sufficient number of reflections. Thus it is possible to perform a Fourier analysis on a clean signal with a time window starting at 0.2 millisecond and 1 millisecond long. The signals are shown in the three cases in Figure 4.8, 4.9, 4.10 along with their discrete Fourier Transforms. Before actually taking the Fourier transforms, we modify the original signal, removing the linear component (free body motion) that takes place in infinite plates, by subtracting the best fit line to the windowed signal. Doing so, frequencies close to zero that do not have any structural significance are removed. Having the frequency amplitude spectrum, we are able to locate the main peak and using equation (4.12) we obtain estimations of the complete deck height, that are particularly close to the real thickness as Table 4.2 shows:

Real deck height	Computed deck height
30.40 cm	29.50 cm
25.30 cm	24.83 cm
12.62 cm	13.03 cm

Table 4.2: Real and computed deck height

This simple method yields particularly accurate results with simulated data, which, as we mentioned earlier, have the enormous advantage to be extendible in time, as accurate as we wish, and noise free.

a)

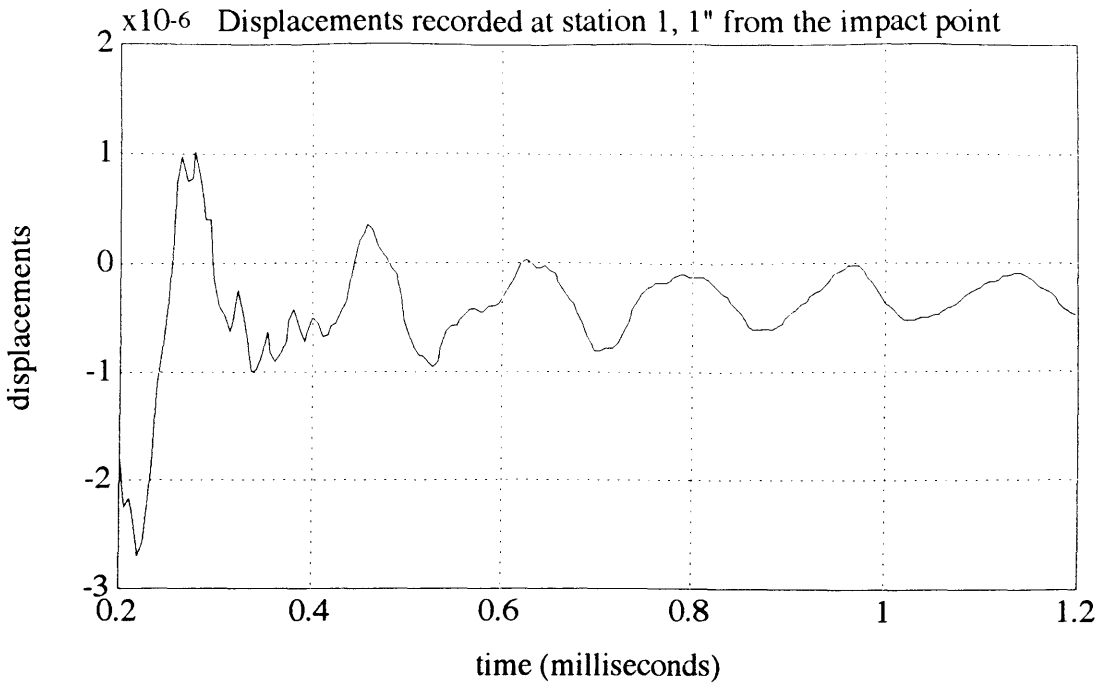

b)

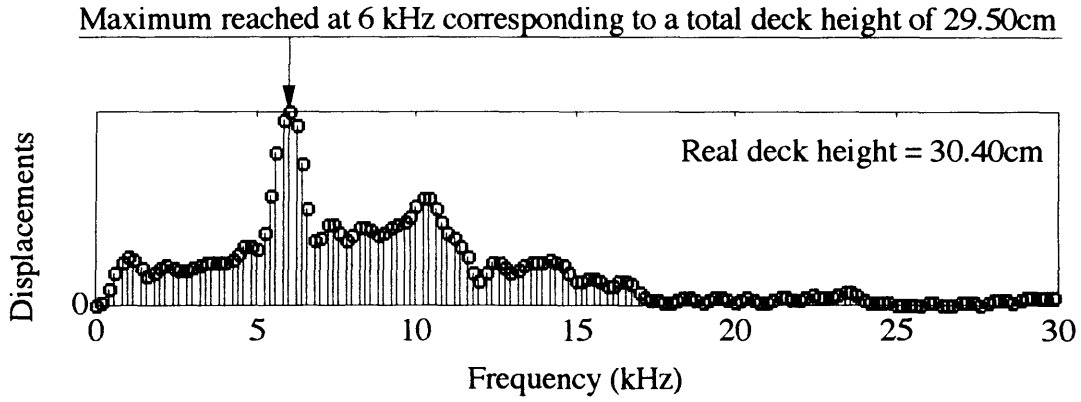

Figure 4.8: Simulated displacements at station 1 (1" from the impact location) for a 30.4 cm thick deck
a) time domain
b) frequency domain (amplitude)

a)

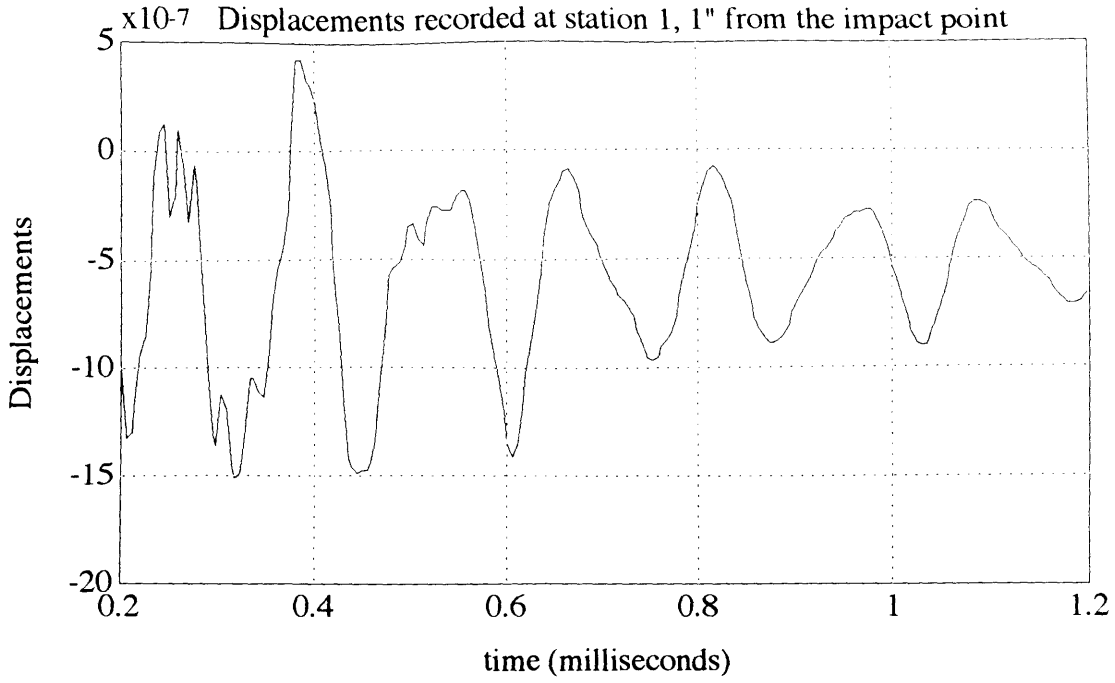

b)

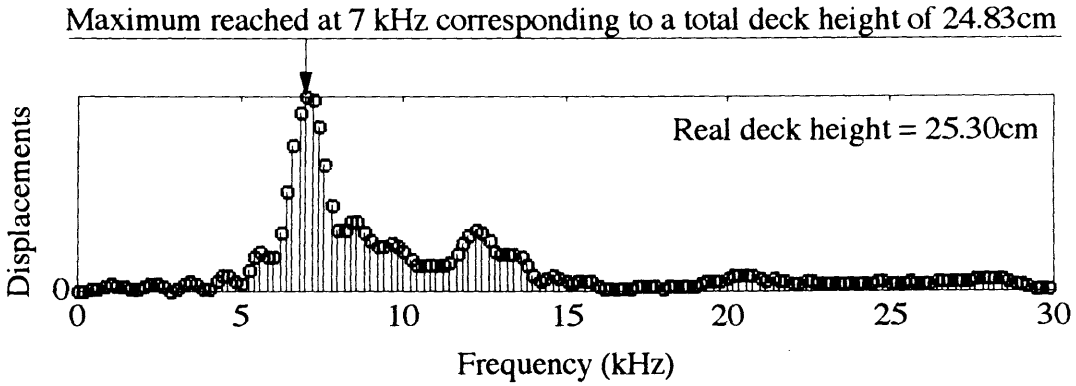

Figure 4.9: Simulated displacements at station 1 (1" from the impact location) for a 25.30 cm thick deck
a) time domain
b) frequency domain (amplitude)

a)

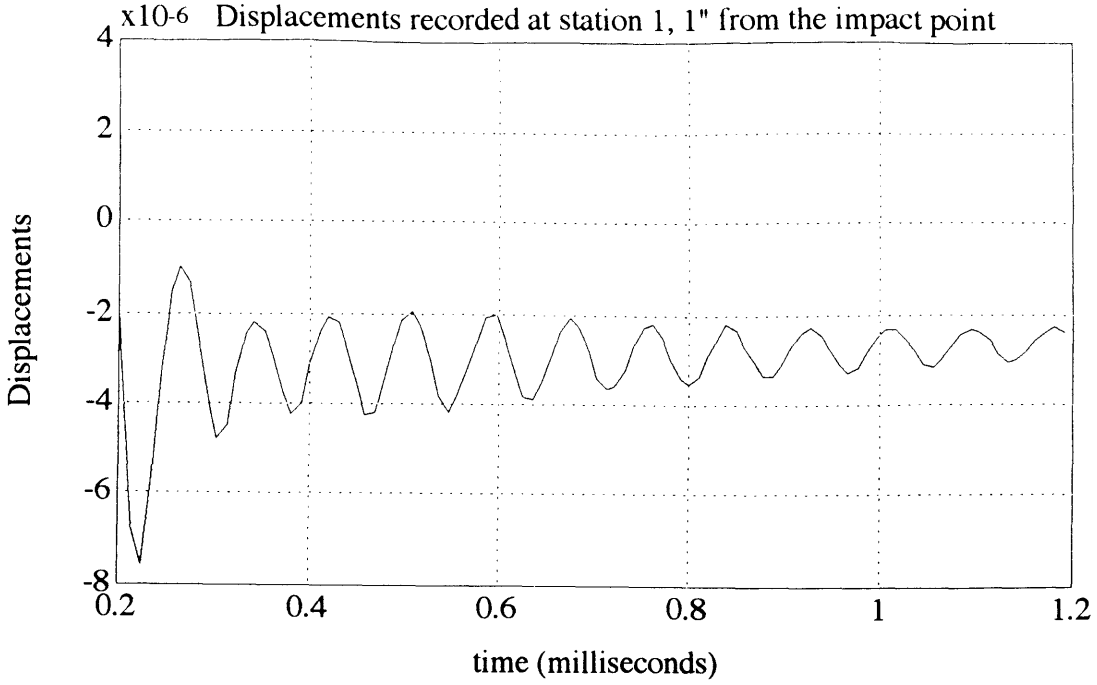

b)

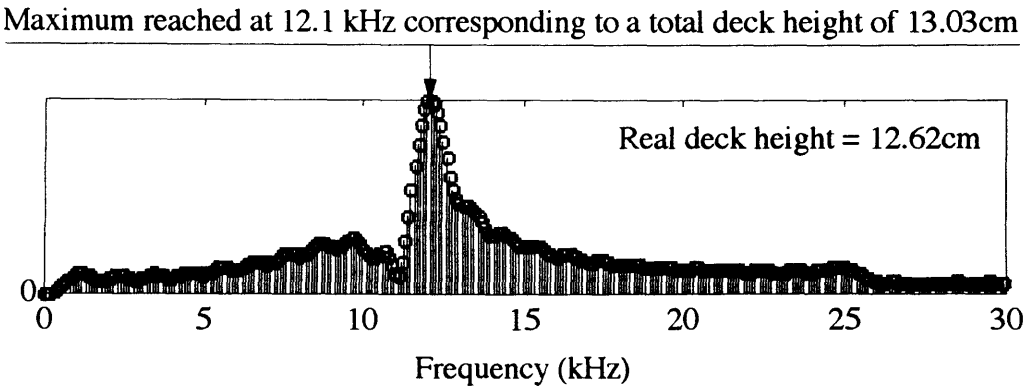

Figure 4.10: Simulated displacements at station 1 (1" from the impact location) for a 12.62 cm thick deck
a) time domain
b) frequency domain (amplitude)

II-3) Results for field data at station 1

We tried the algorithm on field data collected by Weston NDT, but unfortunately the recorded traces for station 1 to 3 were only 0.5 millisecond long. Taking the Rayleigh wave away (say the first 0.125 milliseconds at the first station) we end up with a 0.375 millisecond trace. The bridge deck on which the measurements are performed has a main concrete layer, 8" (20.3 cm) thick, covered with approximately 1.5" (3.8 cm) of asphalt. According to (4.6) the travel time back and forth in the thickness direction of the deck of a compression wave is more or less 0.133 milliseconds. This means that only two reflections arriving at the top surface are within this window, which is very little.

However, the results presented in Figures 4.11 to 4.13 show interesting structural features. All the way through, we assumed a compression wave velocity of 4000 m/s in the concrete and 2400 m/s in the asphalt. In Figure 4.11, we present results for a portion of a bridge deck that was scanned twice: the first time with bare concrete and the second time with an asphalt layer. We compute the depth of the echoes in accordance with the procedure described in section II-1) and we plot them versus the horizontal distance in feet along the bridge deck. Different types of echoes are represented in Figure 4.11. Strong echoes, corresponding to frequency peaks whose amplitudes are at least 50% of the amplitude of the major frequency peak of the same trace, are marked with black filled circles. The weak echoes, corresponding to all the other peaks are identified by hollow circles. We also mention, when relevant, the theoretical location of the asphalt-concrete interface. The complete deck has a maximum thickness of 10" (25.4 cm) but we represent the echoes up to depth of one meter, in order to show that multiply reflected compression waves are not the only one detected.

In Figure 4.11.a we can easily see a concentration of echoes around the assumed deck thickness of 8" (20.3 cm) which is even more visible and sharp when the asphalt is present. The asphalt layer echoes are also noticeable in Figure 4.11 b) and are quite well distributed about the theoretical line.

Let us mention that the strong echo around 0.7 m is only a numerical artifact. Namely, in order to remove the surface wave, we deal only with the last 0.375 milliseconds of the original trace; therefore, the Fourier transform exhibits a fundamental frequency of 1/0.375e-03=2666 Hz, which, when plugged into equation (4.12), and assuming C_1=2400 m/s, C_2=4000 m/s, yields a spurious thickness of 0.72m.

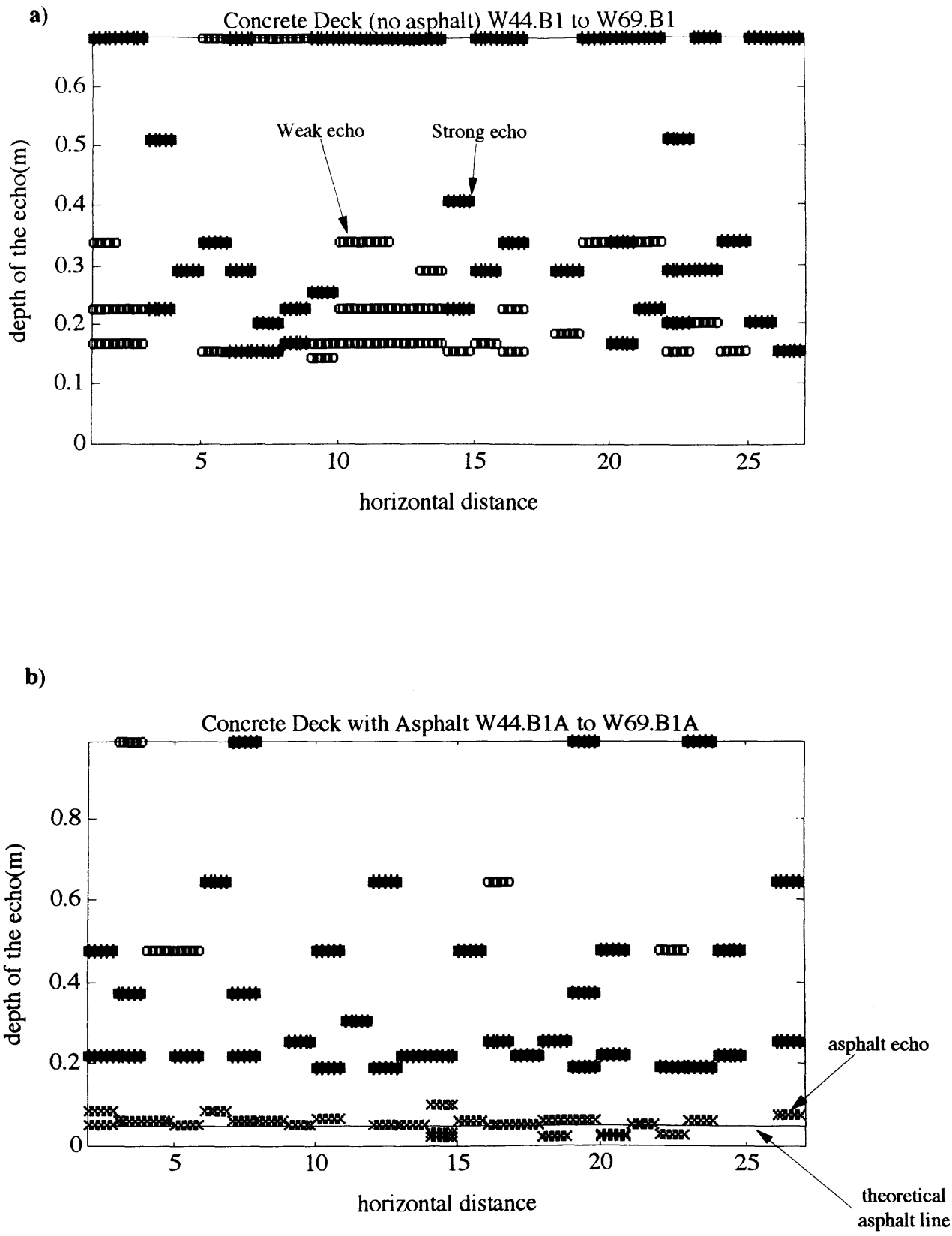

Figure 4.11: Impact Echo method performed on a same concrete deck
a) without the asphalt cover (8"=20.3cm thick concrete deck)
b) with the asphalt cover (1.5"=3.8cm thick)

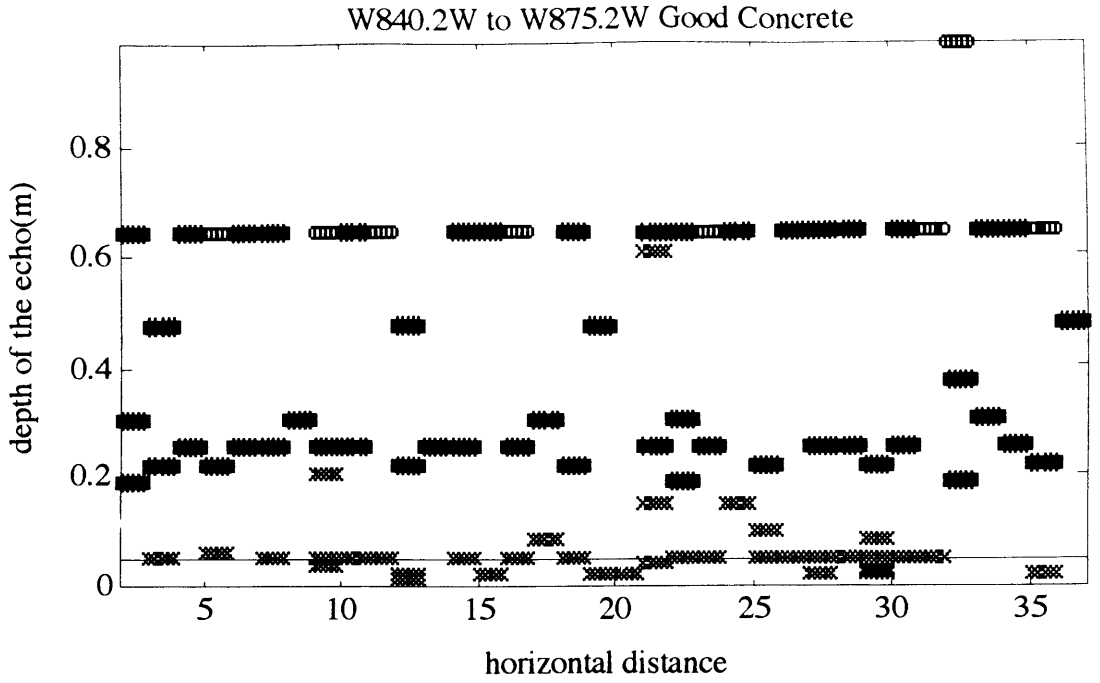

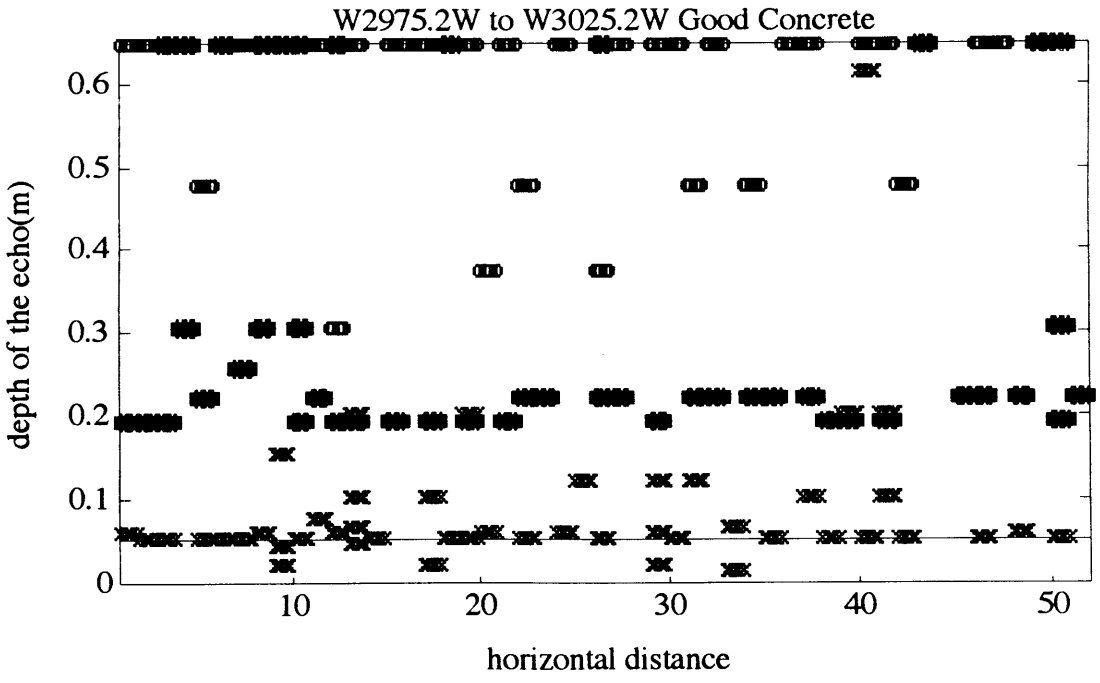

Figure 4.12: Impact Echo Method performed on two portions of the same deck that revealed to contain only sound concrete

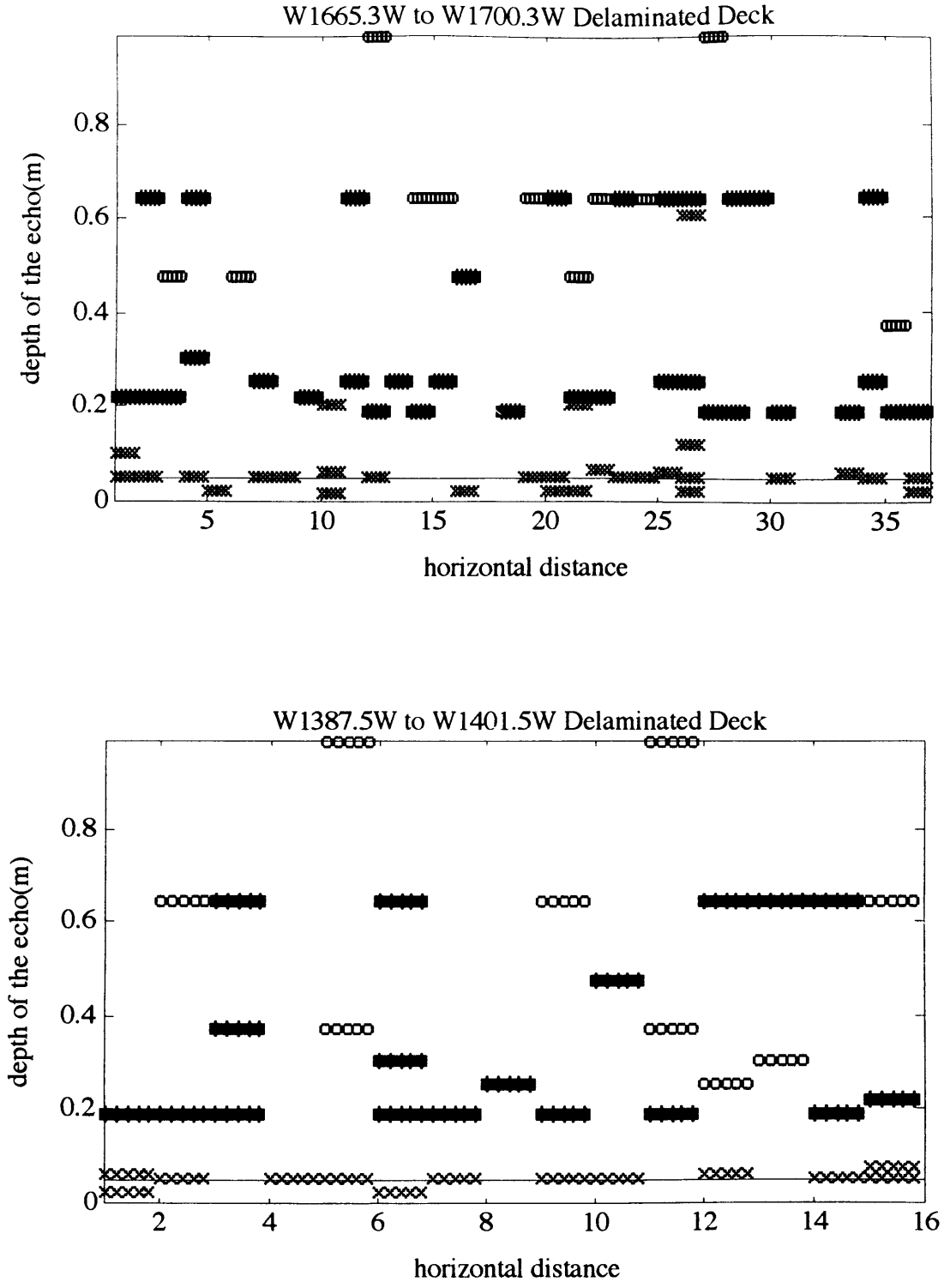

Figure 4.13: Impact Echo Method performed on two portions of the same deck that revealed to contain delaminated portions

Figure 4.12 shows the outcome of the procedure for two portions of the same 8" deck, covered with 1.5" of asphalt, where ulterior coring tests have shown that the concrete was in fairly good condition. And indeed, the main echo corresponding to the complete plate mode shows some regularity. By comparison, Figure 4.13 illustrates that for portions containing delaminations, as demonstrated by destructive tests, that regularity is disrupted. However, even if we are able to point out degradation, the picture is not clear enough to give further precision, such as the location or the extent of the degradation. For that, we would definitely need longer traces so as to collect more information.

III- CORRECTIONS FOR FARTHER RECEIVERS

III-1) Corrections for skewed rays

The preceding ray approach can be extended to slightly farther receivers if we account for the increase in travel path. However, compression waves received by remote surface sensors reflect back and forth at the top and bottom free boundaries with an oblique incidence with respect to the normal of the surface, thus producing mode conversion as will be discussed in the next paragraph. Let us first examine the necessary correction to the computations.

Assume that we have a homogeneous plate, on the surface of which an impact source and a receiver stand at a distance D from each other. The plate thickness is noted H, as shown in Figure 4.11. The rays are numbered r_0, r_2, r_4,... The index accounts for the number of reflections on free surfaces.

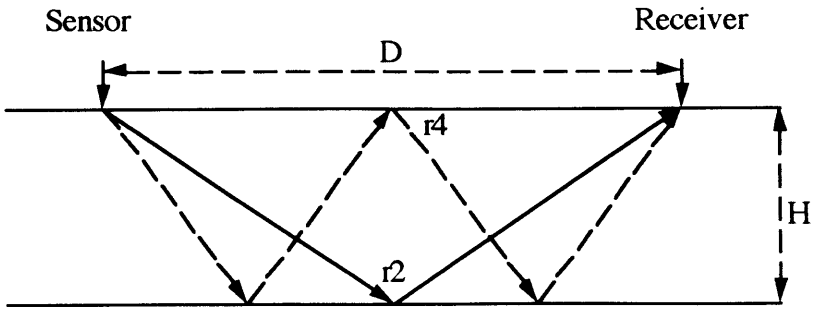

Figure 4.11: Multiply reflected waves at remote stations

The path distance for ray r_{2n} is

$$d_{2n} = \sqrt{D^2 + 4n^2H^2} \tag{4.13}$$

and the corresponding travel time is given by

$$t_{2n} = \frac{2nH}{C_p}\sqrt{1+\left(\frac{D}{2nH}\right)^2} \tag{4.14}$$

Now, if we expand (4.14) for n large we obtain

$$t_{2n} = \frac{2nH}{C_p}\left\{1+\frac{1}{2}\left(\frac{D}{2nH}\right)^2 - \frac{1}{8}\left(\frac{D}{2nH}\right)^4 + O\left(\frac{1}{n^6}\right)\right\} \tag{4.15}$$

from which we can compute an expansion for the time interval between two successive compression wave arrivals

$$\Delta t_n = t_{2(n+1)} - t_{2n} = \frac{2H}{C_p} - \frac{D^2}{4C_pH}\frac{1}{n^2} + O\left(\frac{1}{n^3}\right) \tag{4.16}$$

Now, from (4.14), we infer that

$$\frac{1}{n^2} = \frac{4H^2}{C_p^2t^2 - D^2} \tag{4.17}$$

that enables us to express the time interval between two P wave arrivals as a function of time:

$$\Delta t = \frac{2H}{C_p}\left\{1 - \frac{D^2}{2\left(C_p^2t^2 - D^2\right)} + O\left(\frac{1}{t^3}\right)\right\} \tag{4.18}$$

We then understand that the mode frequency of multiply reflected P waves is also a function of time for remote sensors. This frequency is given by

$$f = \frac{1}{\Delta t} = \frac{C_p}{2H}\left\{1 + \frac{1}{2\left(\left(\frac{C_pt}{D}\right)^2 - 1\right)} + O\left(\frac{1}{t^3}\right)\right\} \tag{4.19}$$

Of course, this formula only makes sense for $t>D/C_p$, that is after the passage of the first P wave that travels directly below the upper surface and which is not reflected by the lower free surface. Therefore $C_p/2H$ is only a lower limit to the resonant frequency. Even though such limit is reached quickly since the convergence is in $1/t^2$, it is worth evaluating the correction factor

$$r = \frac{1}{2\left(\left(\frac{C_p t}{D}\right)^2 - 1\right)} \tag{4.20}$$

For example, if we wish that r remains below 5% then we must also have $t>3.31D/C_p$, that is $t>0.15$ms for the second station.

The correction term depends on time and therefore it is difficult to perform an exact rectification. Instead an average correction term based on boundary values of the time window was introduced in the analysis program given in appendix C. Results are presented in paragraph III-3.

III-2) Validity. Mode conversion problem.

The derivation depends on the dominance P waves among all multiply reflecting waves. Therefore, its validity usage depends on the wave composition after impact, as discussed in chapter III, and on the absence of mode conversions into SV waves as the P waves are reflected at the free surfaces. As shown in [1] and in Figure 4.12, an oblique compression wave having an incident angle θ_0 with the surface normal is reflected into a P wave with the same angle $\theta_1=\theta_0$ and an SV waves having an angle θ_2 given by

$$\sin(\theta_2) = \kappa^{-1}\sin(\theta_0) \tag{4.21}$$

where

$$\kappa = \left\{\frac{2(1-\nu)}{1-2\nu}\right\}^{\frac{1}{2}} \tag{4.22}$$

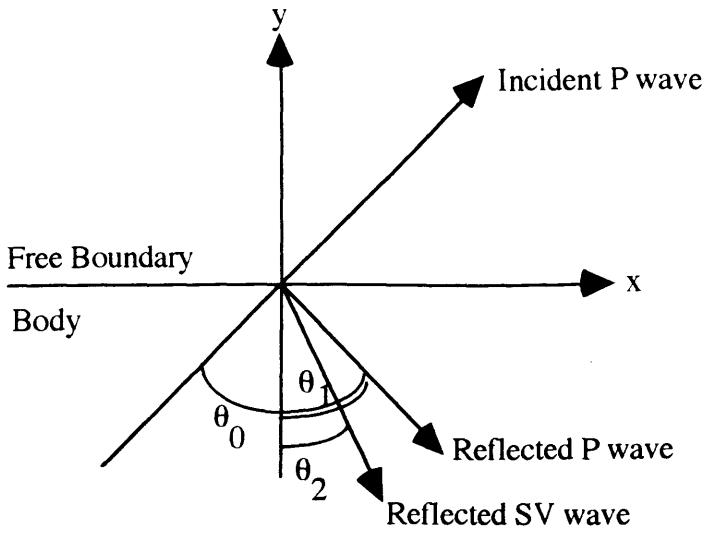

Figure 4.12: Mode conversion

The fraction of energy reflected as compression wave, equals the square of the ratio of displacement amplitudes expressed in (4.21). This fraction depends only on Poisson's ratio and the incident angle. Figure 4.13 shows the energy ratio as a function of incidence angle, for a Poisson's ratio of 0.20, which is typical of concrete. We can see in this figure that reflected P waves decay rapidly as θ_0 increases and disappear completely for an incident angle of 50°. The P wave is then totally converted into a SV wave.

$$\frac{A_1}{A_0} = \frac{\sin(2\theta_0)\sin(2\theta_2) - \kappa^2\cos^2(2\theta_2)}{\sin(2\theta_0)\sin(2\theta_2) + \kappa^2\cos^2(2\theta_2)} \tag{4.23}$$

All of this shows that it is very unreasonable to consider models in which P waves radiate from the impact point and strike the first free surface at an incidence angle greater than 20°. With that particular angle, a P wave ray is first reflected at the lower free surface and then reaches the upper surface at a distance 0.73H of the impact location. For a 10" thick plate this distance is 7.3", which is more or less where the second receiver is positioned. Therefore it really only makes sense to apply the impact echo method to receivers 1 and 2. Beyond, most of the body waves are be a mixture of compression and shear waves that do not travel at the same speed which makes the procedure unworkable.

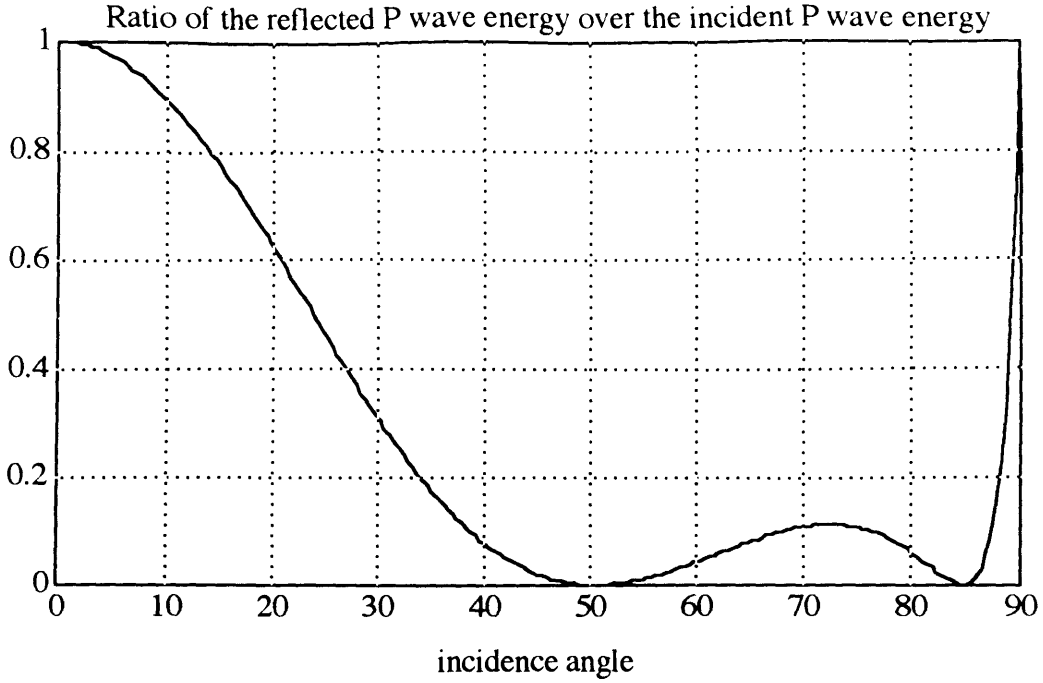

Figure 4.13: Energy Ratio (Reflected P wave / Incident P wave)

III-3) Results for station 2

We tried the impact echo method with recordings at station 2, 7" (17.8 cm) from the impact location and we went through the same procedure. Starting with the simulated data, as shown on Figure 4.15, we find a resonant frequency at 6.2 kHz, which is slightly above the 6 kHz peak detected at station 1 (see Figure 4.8). The corrective term r, for the time window selected (0.35 to 1.35 milliseconds) varies from 0.8% to 0.05% and is, therefore, negligible. Using equation (4.12) we find a total deck height of 28.5 cm which is still very close to the true thickness of 30.4 cm.

We processed the field data in a similar way. However, since the time window for these data is much closer to the time origin, as it does not extend beyond 0.5 millisecond, the corrective term r of equation (4.20) is this time close to 1% for the concrete layer and 5% for the asphalt layer. The results reproduced in Figure 4.15, already show less accuracy than those obtained for the first station. A main deck thickness is still visible but the echoes have a strong tendency to be mixed up. Again longer traces would be necessary to secure a better resolution.

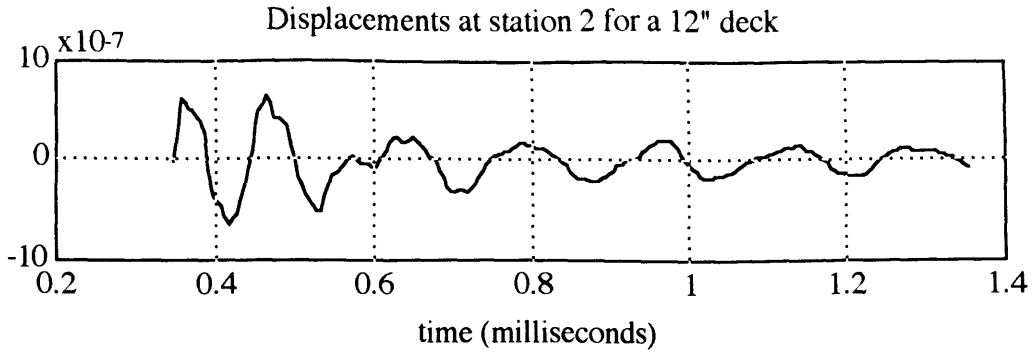

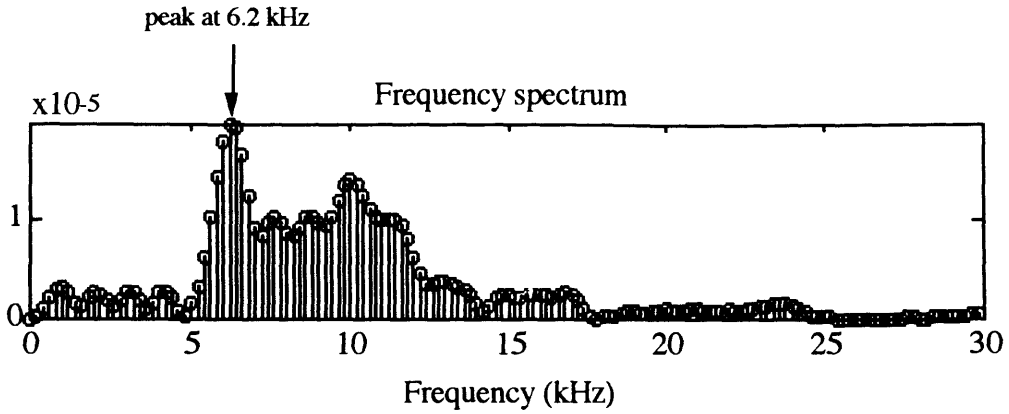

Figure 4.14: Impact Echo Method at station 2 for a simulated 12" deck

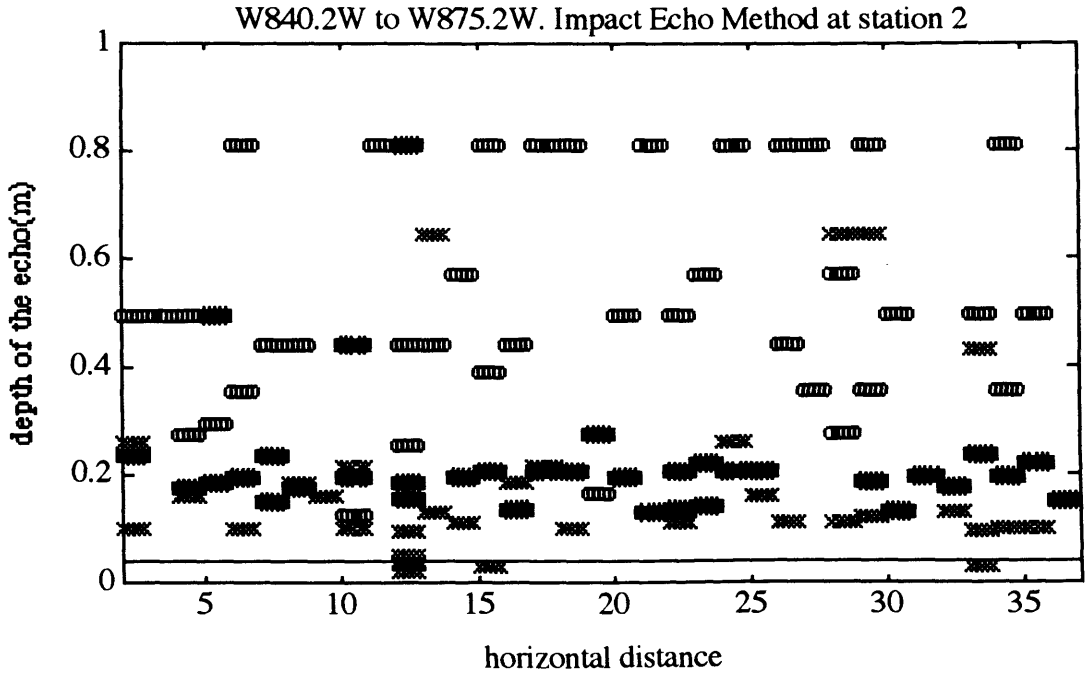

Figure 4.15: Impact Echo Method for field data at station 2

IV- STIFFNESS MATRIX APPROACH FOR THE IMPACT-ECHO METHOD.

The impact-echo method used in the previous section is tied to the assumption that only certain ray paths are of significant importance, namely reflections within the top asphalt layer and within the complete deck. This assumption may have some credit during the primary phase of wave propagation in the plate but is not valid after oscillation modes are well established in the plate. In such case we must trade our ray path approach with a modal analysis which accounts for coupling effects between the two oscillating layers.

IV-1) Exact solution for a model with two layers

To derive the exact solution for our model consisting of two layers, we use the Haskell-Thompson transfer matrix method, originally developed by Haskell [5] and enhanced by E. Kausel and J.M. Roësset in [7]. The layered system that we have in mind is represented in Figure 4.16 and is composed of an upper asphalt layer and a lower concrete layer. It is, of course, an axially symmetric problem in the conditions of impact that we are facing.

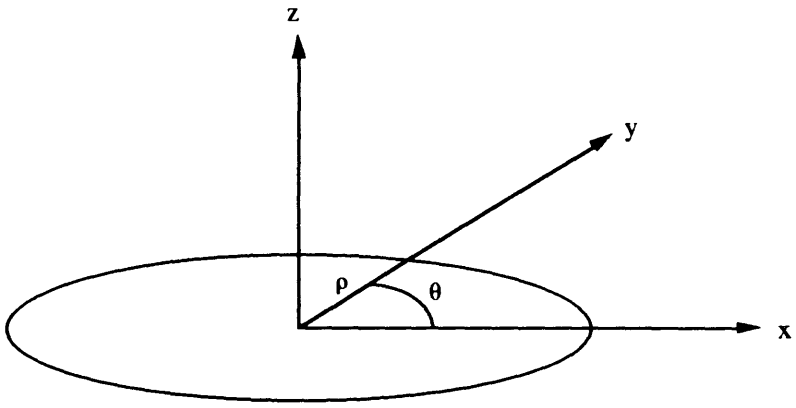

Figure 4.16a: Cylindrical Coordinates

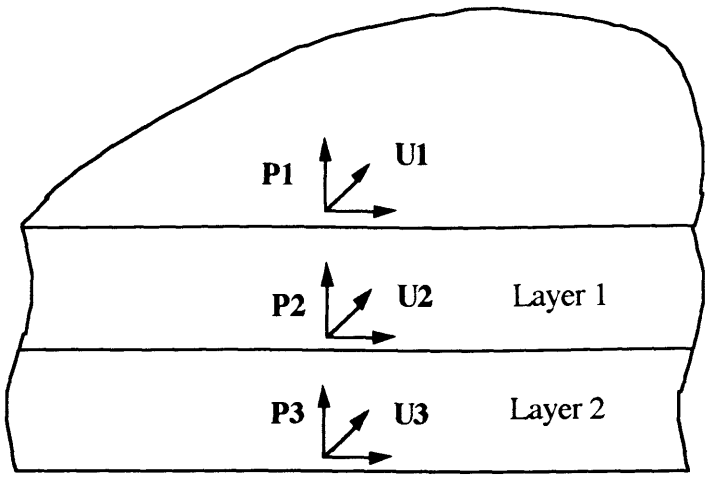

Figure 4.16b: Layered Plate

For a particular frequency ω and a wave number k in the axial direction, we define the state vector in the cylindrical coordinates as

$$\mathbf{Z} = \{\bar{u}_\rho, \bar{u}_z, \bar{\tau}_{\rho z}, \bar{\sigma}_z\}^T = \begin{Bmatrix} \bar{\mathbf{U}} \\ \bar{\mathbf{S}} \end{Bmatrix} \tag{4.24}$$

where the superscript bar indicates that the coordinates are functions of z only. We derive the total displacement and stress field as follow:

$$\begin{Bmatrix} \mathbf{U} \\ \mathbf{S} \end{Bmatrix} = \begin{bmatrix} \mathbf{C} & 0 \\ 0 & \mathbf{C} \end{bmatrix} \begin{Bmatrix} \bar{\mathbf{U}} \\ \bar{\mathbf{S}} \end{Bmatrix} \tag{4.25}$$

$$\mathbf{C} = \begin{bmatrix} \frac{d}{d(k\rho)}C_0 & & \\ & \frac{d}{d(k\rho)}C_0 & \\ & & -C_0 \end{bmatrix} \tag{4.26}$$

C_0 being a Bessel, Neumann or Hankel function of order zero. More precisely the transformation into the wave number domain and back into the spatial domain is given by

$$\bar{\mathbf{U}} = \frac{1}{2\pi}\int_0^\infty \rho \mathbf{C}\mathbf{U}\, d\rho \tag{4.27}$$

$$\mathbf{U} = \int_0^\infty k\mathbf{C}\overline{\mathbf{U}}\, dk \tag{4.28}$$

For each layer we define the external load vectors $\overline{\mathbf{P}}_1 = \overline{\mathbf{S}}_1$ at the upper interface and $\overline{\mathbf{P}}_2 = -\overline{\mathbf{S}}_2$ at the lower interface. Expressing the generalized loads in terms of generalized displacements, we obtain

$$\overline{\mathbf{P}} = \mathbf{K}\ \overline{\mathbf{U}} \tag{4.29}$$

in which we understand **K** to be stiffness matrix of a particular layer. It usually has a complicated form. However, focusing on the recordings at station 1, we are primarily interested in waves that do not propagate in the radial direction, namely waves that have a null wave number k. The expression of **K** is then much simpler and was derived exactly by E. Kausel and J.M. Roësset in [7]. In the particular case of an axisymmetric problem, with non zero frequency ω and zero wave number k, it reduces to

$$\mathbf{K} = \rho C_s \omega \begin{Bmatrix} \cot an\ \eta & & -\frac{1}{\sin \eta} & \\ & \frac{1}{\alpha}\cot an\ \alpha\eta & & -\frac{1}{\alpha}\frac{1}{\sin \alpha\eta} \\ -\frac{1}{\sin \eta} & & \cot an\ \eta & \\ & -\frac{1}{\alpha}\frac{1}{\sin \alpha\eta} & & \frac{1}{\alpha}\cot an\ \alpha\eta \end{Bmatrix} \tag{4.30}$$

where $\eta = \omega\eta / C_S$ is a normalized frequency and $\alpha = C_S / C_P$ is the ratio of the shear wave velocity to the compression wave velocity. Blanks represents zeros. We note that this stiffness matrix covers only the propagation of SV-P waves, SH waves being irrelevant with our particular conditions of loading (vertical point load).

As in a finite element procedure we assemble the total stiffness matrix for the complete plate by overlapping the contribution of the layer matrices at each interface. We thus obtain a 6x6 matrix (for the 3 interfaces). At this stage, it is interesting to notice that S and P waves uncouple and therefore it is advisable to rearrange the order of the coordinates as:

$$\bar{\mathbf{P}} = \left\{ P_{\rho z}^1 \quad P_{\rho z}^2 \quad P_{\rho z}^3 \quad P_z^1 \quad P_z^2 \quad P_z^3 \right\}^T \tag{4.31}$$
$$\bar{\mathbf{U}} = \left\{ U_\rho^1 \quad U_\rho^2 \quad U_\rho^3 \quad U_z^1 \quad U_z^2 \quad U_z^3 \right\}^T$$

Hence the total stiffness matrix is of the form

$$\mathbf{K} = \omega \begin{Bmatrix} \mathbf{A} & \\ & \mathbf{B} \end{Bmatrix} \tag{4.32}$$

where the matrices **A** and **B** are defined below:

$$\mathbf{A} = \rho_1 C_{s_1} \begin{bmatrix} \cot \eta_1 & -\dfrac{1}{\sin \eta_1} & \\ -\dfrac{1}{\sin \eta_1} & \cot \eta_1 + r_s \cdot \cot \eta_2 & -\dfrac{r_s}{\sin \eta_2} \\ & -\dfrac{r_s}{\sin \eta_2} & r_s \cdot \cot \eta_2 \end{bmatrix} \tag{4.33}$$

$$\mathbf{B} = \rho_1 C_{p_1} \begin{bmatrix} \cot \bar{\eta}_1 & -\dfrac{1}{\sin \bar{\eta}_1} & \\ -\dfrac{1}{\sin \bar{\eta}_1} & \cot \bar{\eta}_1 + r_s \cdot \cot \bar{\eta}_2 & -\dfrac{r_p}{\sin \bar{\eta}_2} \\ & -\dfrac{r_p}{\sin \bar{\eta}_2} & r_p \cdot \cot \bar{\eta}_2 \end{bmatrix} \tag{4.34}$$

in which

$$\bar{\eta}_m = \frac{\omega h_m}{C_p}$$

is the frequency normalized by the compression wave velocity and the thickness of the layer, and

$$r_s = \frac{\rho_2 C_{s_2}}{\rho_1 C_{s_1}}, \; r_p = \frac{\rho_2 C_{p_2}}{\rho_1 C_{p_1}}$$

are the impedance contrasts for S and P waves, respectively.

The derivation of the resonant frequencies is then straightforward. Under free vibration conditions, $\bar{\mathbf{P}} = \mathbf{0}$, there can be a solution if and only if the determinant of **K**, det(**K**) is zero, which in turn, is equivalent to the nullity of either det(**A**)=0 or det(**B**)=0. It

is also clear that det(**A**)=0 will yield resonant frequencies of shear modes and det(**B**)=0 addresses compression modes. As mentioned in chapter III, shear waves carry very little energy just below the impact point, in comparison to compression waves. Therefore, although shear modes exists, they will not be taken into account in the following.

Hence the exact characteristic equation for compression modes in our model with two layers is det(**B**)=0 or,

$$r_p \cdot \operatorname{cotan}(h_1 \cdot \overline{\eta_1}) + \operatorname{cotan}(h_2 \cdot \overline{\eta_2}) = 0 \tag{4.35}$$

and if we define the fundamental resonant frequency of each layer being fixed at the interface, f_1 and f_2 respectively as

$$f_1 = \frac{C_{p_1}}{4 \cdot h_1} \quad \text{and} \quad f_2 = \frac{C_{p_2}}{4 \cdot h_2} \tag{4.36}$$

then the characteristic equation can be rewritten as

$$r_p \cdot \operatorname{cotan}(\frac{\pi}{2} \cdot \frac{f}{f_1}) + \operatorname{cotan}(\frac{\pi}{2} \cdot \frac{f}{f_2}) = 0 \tag{4.37}$$

IV-2) Resonant frequencies

The solution to the characteristic equation (4.37) can be found numerically within a range of acceptable frequencies. Typically we are interested in a band of frequencies between 0 and 40 kHz since most of the energy of the impact is located in this region. For each possible combination of compression wave velocities in both the asphalt and the concrete layer and thicknesses h_1 and h_2, we obtain a different characteristic equation and, of course, different frequencies. In the following, we assume three of those parameters, namely C_{p_1}, C_{p_2}, h_1 and vary the depth h_2 of the concrete layer so as to obtain from (4.37), curves for resonant frequencies versus unknown deck height.

In the simulations, we use the following values: h_1=0.05m, C_{p_1}=2400m/s, ρ_1=2100 kg/m^3, ρ_2=2200 kg/m^3, C_{p_2}=3920m/s, the subscript 1 referring to the asphalt layer and the subscript 2 referring to the concrete layer. The MATLAB program given in appendix D solves (4.37) for a given range of deck thickness and plots the first three (or more) resonant frequencies versus the deck height (see Figure 4.17).

It is clear that we can choose to represent any arbitrary number of resonant frequencies for each deck height and that we can focus on any range of frequencies. This allows us to produce a flexible scheme for an inverse problem.

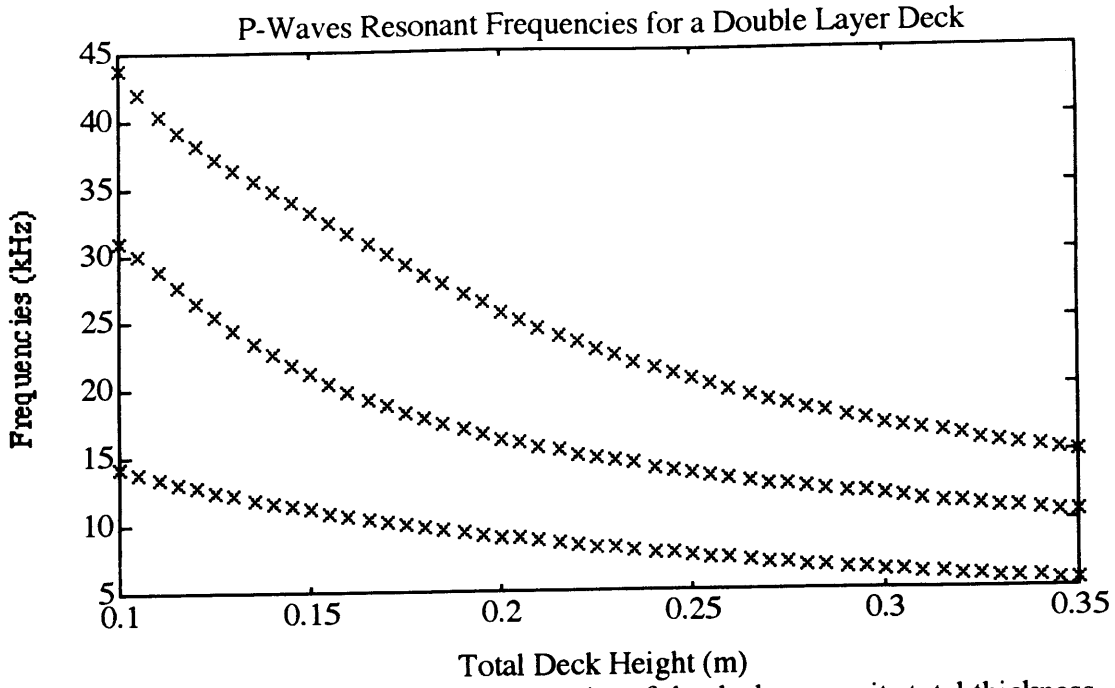

Figure 4.17: First three resonant frequencies of the deck versus its total thickness

IV-3) Heuristic inverse problem

The methodology for conducting an inverse problem, that is solving for the total deck thickness (our principal unknown), follows naturally from our preceding study. First we pick up major peaks in the frequency content of the recorded signal. Again, we confine ourselves in the time domain to that portion where specular reflections are dominant. Then, we try to match, as close as possible, the experimental values of the resonant frequencies with those of the theoretical model above. If a delamination is present, the shift towards high frequencies should be detected and translated into a decrease in the total thickness. Of course, we do not expect the field information to match exactly the previous model for several reasons. First, the values of P waves velocities in the model may not match exactly the values in the field; and second, depending on experimental conditions, not all the modes might be excited. Therefore, we need to find a norm that will enable us to find the most probable height and evaluate the error.

For that purpose, the MATLAB program reproduced in appendix D is organized in the following way:

step 1: specify a time window for the signal corresponding to specular reflections, (that selection is left to the user)

step2: compute a Fast Fourier Transform of the chosen part, locate the peaks of magnitude in the Fourier spectrum and sort them with respect to their importance.

step3: select the n largest peaks (n being up to the user) and their relative amplitude (weight): (f_j, W_j) j=1..n

step 4: for each possible concrete layer thickness (h_i), and within the assumed range, compute the distance e_i of the n largest peaks of the experimental signal to the resonant frequencies of the theoretical model corresponding a concrete layer thickness h_i:

$$e_i = \sum_{j=1}^{n} W_j . dist[f_j, f(h_j)] \qquad (4.38)$$

where

$$dist[f_j, f(h_j)] = min|f_j - f(h_i)| \qquad (4.39)$$

in which $f(h_i)$ describes all theoretical resonant peaks corresponding to h_i.

step5: Find the h_{io} that minimizes e_i: $e_{io}=min\{e_i\}$. h_{io} is the estimated thickness, $h=h1+h_{io}$ becomes the estimated total deck height, and e_{io} is the value of error function.

IV-4) Results for simulations

In order to check the validity of the procedure described above, we apply it to several simulated traces corresponding to different deck heights (see Table 3.5 in chapter III). In all cases, the asphalt layer is 5 cm (2") thick and the concrete layer is taken to be successively 25.4 cm (10"), 20.3 cm (8") and 7.6 cm (3"). The total deck heights are therefore 0.304 m, 0.253 m, and 0.126 m. The Fourier analysis is carried out on the first station output. The best results are obtained for a time window ranging from t=0.2ms to 1.2ms, that is after the passage of the direct surface waves and before the multiply

reflected waves in the asphalt have completely died out. Hence, in that time window we should only get specular reflection modes with a strong coupling between the two layers. Later on, it is likely that the damping in the asphalt will wipe out the contribution of the top layer, so that the concrete layer will be the only oscillator. In fact, when we tried to take a Fourier transform for later time windows (e.g. 0.5ms<t<1.5ms) the second peak visible in Figures 4.8 and 4.9 disappeared.

The retained frequencies ranged from 2kHz to 25 kHz and only two peaks (n=2) were used to match the simulation results with the exact model solutions. The clear shift in frequency seen in Figures 4.8 to 4.10 as the thickness of the deck decreases, is perfectly detected by the automatic procedure described earlier, which gives the results listed in Table 4.3.

Real deck thickness	Estimated thickness
0.304m	0.320m
0.253m	0.270m
0.126m	0.130m

Table 4.3: Estimation of deck thicknesses with the stiffness matrix approach

This approach, more rigorous than the impact echo method since it accounts for all coupling effects and does not emphasize any of the ray paths shown in Figure 4.3, 4.4 or 4.5, yields estimated thicknesses that are slightly overestimated and that are not significantly more accurate.

However, this procedure points out a few possible pitfalls in the interpretation of the data, whatever method we choose. In particular, Figure (4.17) shows that the first resonant mode has approximately the same frequency for a 0.1m deck than the second mode for a 0.35m deck. Therefore a small error in the location of a frequency peak, or biased elastic properties, could easily lead the algorithm to jump from one branch of Figure (4.17) to another, and thus, the estimation of the bridge deck height could be false.

This is precisely what happened, when we tried to apply this method to field data. The algorithm turned out to be quite unstable and we could actually see jumps from one branch to the other. Of course, as we mentioned before, the field traces are very short.

The problem should improve with longer traces, which could probably help in defining more precisely the location of frequency peaks, thus ensuring a more accurate procedure.

CHAPTER V : SURFACE WAVE METHOD

Outline

I- Theory and validity domain of the Surface Wave Method

- I-1) Introduction - Motivations
- I-2) Principle
- I-3) Exact solution for an infinite two layer plate

II- Numerical Results

- II-1) Numerical results on simulations
- II-2) Stability and limitations

III- Comparison with the local spectral analysis

- III-1) Location in time of frequency peaks
- III-2) Numerical results

I- THEORY AND VALIDITY DOMAIN OF THE SURFACE WAVE METHOD

I-1) Introduction - Motivations

As we mentioned in chapter III, body waves attenuate for geometrical reasons much faster than surface waves. Namely, as body waves expand, their amplitude follow a decaying law in proportion to r^{-1} along their spherical front whereas surface waves decrease only in proportion to $r^{-0.5}$. The direct body waves decline even faster just below the free surface (see Table 3.3 in chapter III). Hence, at station 3 and 4, Rayleigh waves are indeed predominant. In this chapter, we focus on their study, starting from a technique that has been developed for layered half spaces. In particular, surface waves have been used extensively to measure shear wave velocities of horizontally layered soil. We apply a similar technique in our case, essentially to find out the shear wave velocities of the two materials we are dealing with, concrete and asphalt.

I-2) Principle

For a complete description of the theory, we refer to S.N. Nazarian and K.H. Stokoe II in [9]. We only present here a summary. Assume that sufficiently far away from the impact location, only surface waves propagate in the plate and they do so, along an almost plane front. Also, assume that only one mode of surface wave dominates, i.e. for each frequency ω, there is only one surface wave propagating at that frequency, and the displacements that wave generates at the upper free surface depends only on the horizontal distance x and the time t as:

$$u = A(\omega)\cdot e^{-i(k(\omega)x-\omega t)} \tag{5.1}$$

where $A(\omega)$ is the amplitude (that can be complex), $k(\omega)$ is the wave number in the x direction (supposing that the plane surface wave propagates in that direction). Hence, the complete surface displacement at time t, and abscise x is given by:

$$u(x,t) = \frac{1}{2\pi}\int_{-\infty}^{+\infty} A(\omega)\cdot e^{-i(k(\omega)x-\omega t)}\cdot d\omega \tag{5.2}$$

With these basic assumptions, if we fix the abscissa x and take the Fourier transform in time of (5.2), we obtain for a given x:

$$u(x,\omega) = A(\omega)\cdot e^{-ik(\omega)x} \tag{5.3}$$

The phase difference between station 3 and station 4 is thus expressed by

$$\phi_3-\phi_4=k(\omega)\Delta x \tag{5.4}$$

where $\Delta x=x_4-x_3$ is the horizontal distance between the two receivers. From (5.4) we can extract $k(\omega)$ and the associated wavelength:

$$\lambda(\omega) = \frac{1}{2\pi\cdot k(\omega)} = \frac{\Delta x}{2\pi\cdot(\phi_3-\phi_4)} \tag{5.5}$$

The Rayleigh wave velocity follows immediately:

$$C_R(f) = f\cdot\lambda(f) \tag{5.6}$$

where $f=2\pi\omega$ is the frequency in Hertz. From (5.6), we can draw an experimental dispersion curve: surface wave velocity versus frequency or versus wavelength.

Let us note here, that in some cases, it is advantageous to introduce the Cross Power Spectrum: for two temporal series X and Y, of the same length, whose Fourier transforms are respectively $S_X(f)$ and $S_Y(f)$, the cross power spectrum as defined by S. Nazarian and K. H. Stokoe II in [9], is

$$G_{YX}(f) = S_Y(f)\cdot S_X^*(f) \tag{5.7}$$

It is clear that the phase difference (5.4) is simply the cross power spectrum phase with a minus sign. In its form (5.7), the cross power spectrum offers the advantage of being independent of the time origin. Hence, to attenuate the effect of noise, it is possible to average the cross power spectra of several recordings at the same location. An indicator to assess the quality of the observed signal is the coherence function, which is the ratio of the output power caused by the measured input to the total measured output. Its expression isgiven by (5.8).

$$\gamma^2(f) = \frac{G_{YX}(f)\cdot G_{YX}^*(f)}{G_{XX}(f)\cdot G_{YY}(f)} \tag{5.8}$$

where the auto power spectra G_{XX} and G_{YY} are defined as

$$G_{XX}(f) = S_X(f) \cdot S_X^*(f) \quad \& \quad G_{YY}(f) = S_Y(f) \cdot S_Y^*(f) \tag{5.9}$$

The coherence function is a real number in the range of 0 to 1, close to 1 when the transfer of information between stations 3 and 4 is free of noise. The signal to noise ratio (S/N) is related to the coherence function via

$$S/N = \gamma^2(f) / \left[1 - \gamma^2(f)\right] \tag{5.10}$$

In case the experiment is not to be repeated, there is only one trace X and one trace Y. The cross power spectrum can still be used if the traces are long enough: they must then be divided in overlapping segments, windowed accordingly, and several cross power spectra must be computed on corresponding windows in X and Y. The spectra can then be averaged as if they had been produced by several experiments.

We note, that for stationary vibrations, as opposed to short transient signals that we are dealing with, it is necessary to replace the original quantities X and Y by their auto-correlation and cross correlation functions (see [11]).

However, the necessity to have an operational system, in particular the necessity to scan a huge area in little time, prevents us from repeating the measurement several times at the same location. Therefore, we have to cope with a single trace, that in addition, is too short to be efficiently treated with a cross power spectrum algorithm. We actually obtain better results, if we directly take the Fourier transforms of the signals at stations 3 and 4 and compute the dispersion curve according to equations (5.4) to (5.6).

Thus, starting from the simulation 'case 1' defined in chapter III (see Table 3.5), we select the first 1.2 milliseconds of the traces at station 3 and station 4 (Figure 5.1), compute the phase lag versus frequency and unwrap it as shown on Figure 5.2. Experience has shown, that only frequencies up to 30 or 40 kHz were of real importance. We then calculate the dispersion curve with equations (5.4) to (5.6), and represent first the wave velocity versus frequency in Figure 5.3. Up to 6 kHz, i.e. the frequency of the plate thickness mode, the curve is rather irregular, but it becomes smooth for higher frequencies.

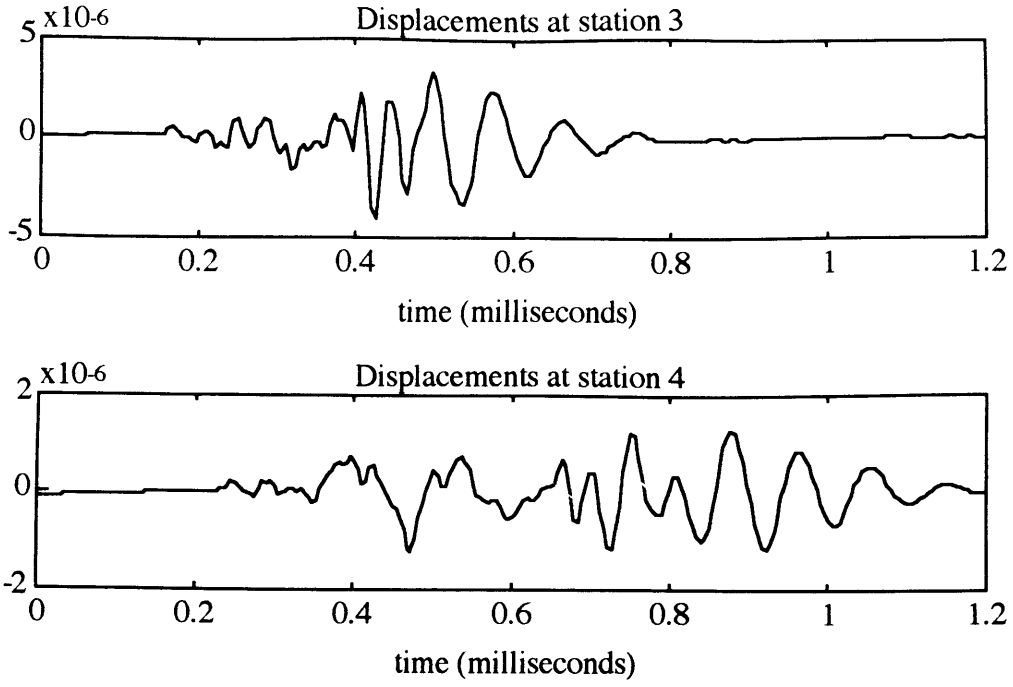

Figure 5.1: Simulated displacements at station3 and station 4

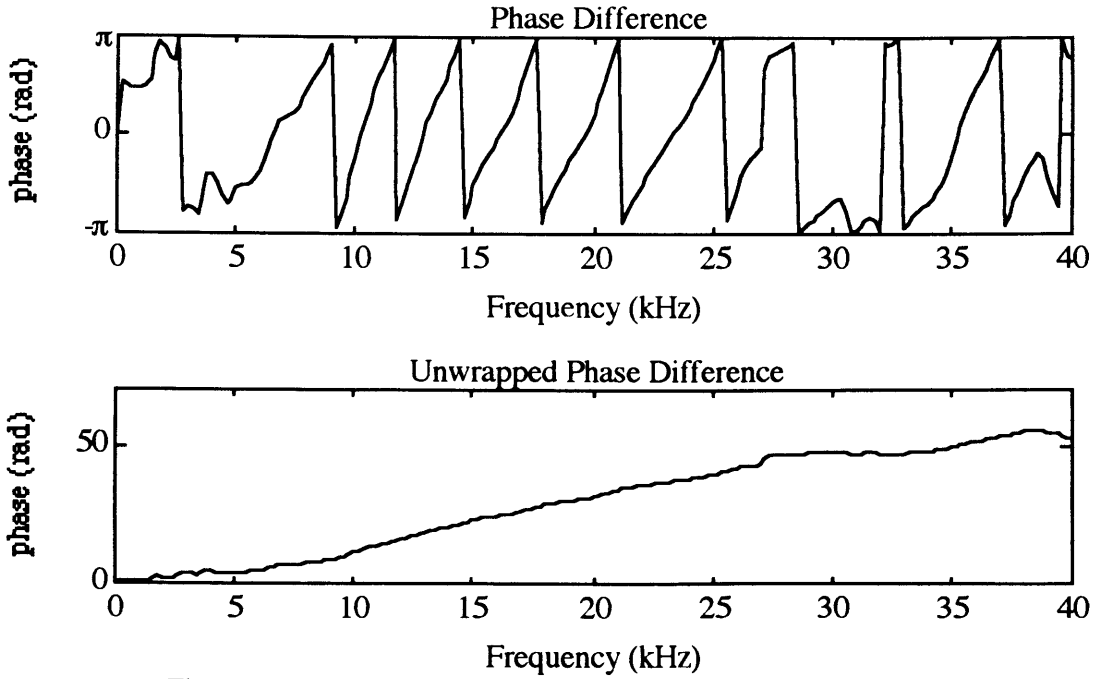

Figure 5.2: Phase difference between station 3 and station 4

Another interesting point of view is presented on Figure 5.4, where we show wave velocities versus wavelengths. The latter on the horizontal axis, are restricted to the range 0 to 0.30 m, that is within the dimension of the plate thickness. We, indeed, expect to see for short wavelengths, the occurrence of surface waves. In effect, as the wavelength

approaches the thickness of the asphalt layer, the experimental wave velocity gets closer to the Raylaigh wave velocity in the asphalt, yet without reaching it. Even though its wavelength is small, the surface wave extends in the concrete layer and, therefore, the total wave is faster than if it were entirely in the asphalt. Similarly, as the wavelength extends towards the thickness of the plate, the wave velocity increases but remains below the Rayleigh wave velocity in the concrete: the asphalt slows down the surface waves that are mainly in the concrete layer.

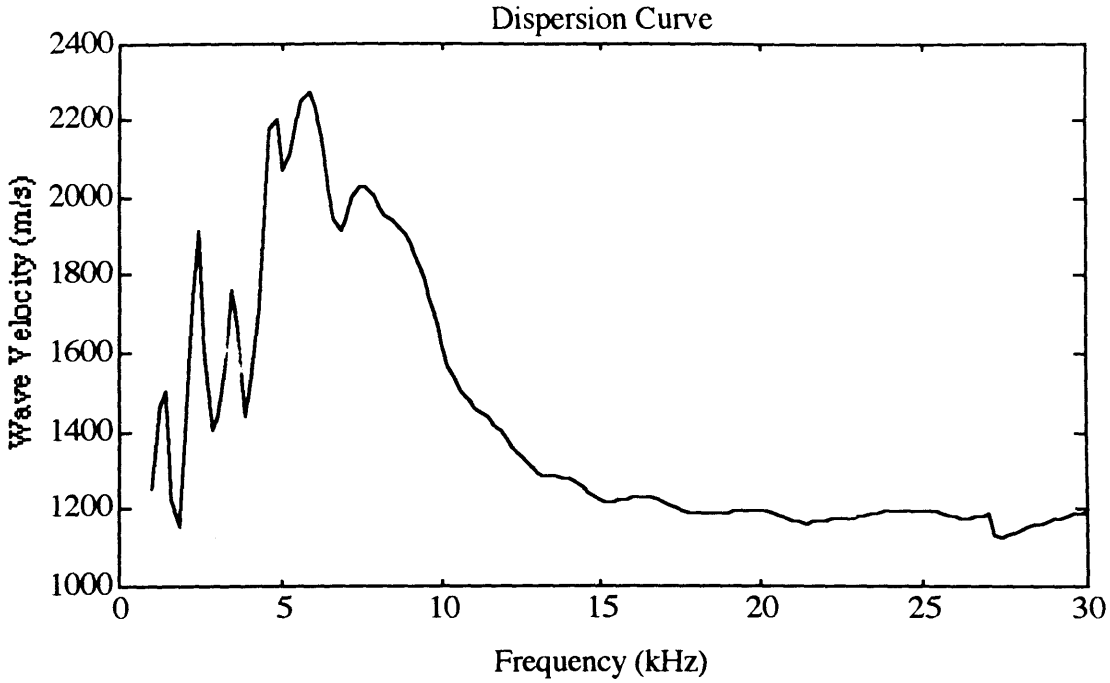

Figure 5.3: Experimental dispersion curve, wave velocity versus frequency

We now wish to extract from this dispersion curve, some information about the structure. We proceed as we did in chapter IV, by adjusting some parameters of a theoretical model to match the experimental results. In [9] and [10], S.N. Nazarian and K.H. Stokoe II use a theoretical model for a half space or an infinite layered plate, based on a Haskell-Thomson approach. In brief, it involves dividing the half space or the plate in a finite number of elastic sublayers whose elastic properties, namely shear wave velocities, Poisson's ratios and mass densities, are adjusted gradually until the theoretical dipersive curve actually matches the experimental one. The authors thus obtain a profile of soils with respect to their elastic properties. S.N. Nazarian and K.H. Stokoe II demonstrate in [9], that the influence of the variation of Poisson's ratio and the mass density can neglected. Hence, in our procedure, we fix once and for all those parameters and we adjust only the shear wave velocities.

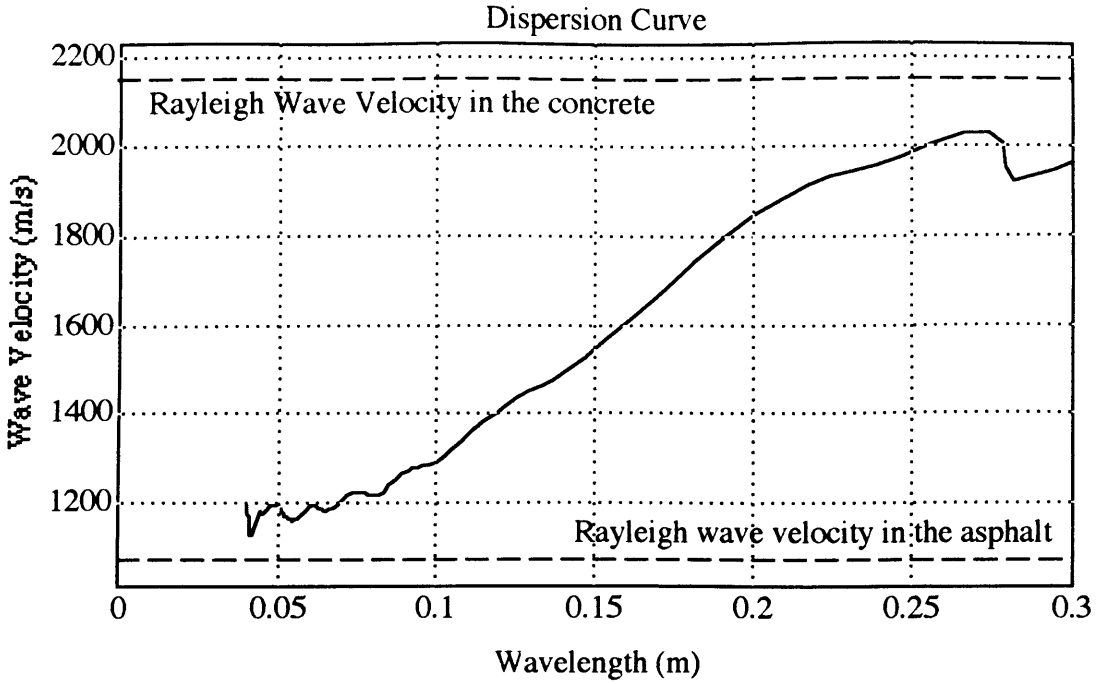

Figure 5.4: Experimental dispersion curve, wave velocity versus wavelength

I-3) Theory for an infinite two layer plate

In order to represent the variation of soil elastic properties with depth, S.N. Nazarian and K.H. Stokoe II use a model that contains many layers resting on an infinite half space. The situation with a bridge deck is, of course, very different. We assume the asphalt and the concrete layers to be homogeneous and therefore, we need only represent two layers. Furthermore, both the upper and lower surfaces are free. The characteristic equation that yields the propagation modes and the dispersion curve is thus quite different.

For the determination of the exact solution of the two-layer plate, we refer to E. Kausel and J.M. Roësset [7] as in chapter IV, but this time we introduce strictly positive wavenumbers k, to represent propagating surface waves. The model is again a two-layer infinite plate, shown on Figure 4.16. Equations (4.24) to (4.29) remain valid, but the stiffness matrix must be changed so as to account for non zero wave numbers and non zero frequencies.

Thus, for each layer, we define the dynamic stiffness matrix **K**, as follow:

$$\mathbf{K} = 2kG\begin{Bmatrix} \mathbf{K}_{11} & \mathbf{K}_{12} \\ \mathbf{K}_{21} & \mathbf{K}_{22} \end{Bmatrix} \tag{5.10}$$

where

$$\mathbf{K}_{11} = \frac{1-s^2}{2D}\begin{Bmatrix} \frac{1}{s}\left(C^rC^s - rsC^sS^r\right) & -\left(1-C^rC^s+S^sS^s\right) \\ -\left(1-C^rC^s+S^sS^s\right) & \frac{1}{r}\left(C^sS^r - rsC^rS^s\right) \end{Bmatrix} - \frac{1+s^2}{2}\begin{Bmatrix} 0 & 1 \\ 1 & 0 \end{Bmatrix} \qquad (5.11.a)$$

$$\mathbf{K}_{22} = \frac{1-s^2}{2D}\begin{Bmatrix} \frac{1}{s}\left(C^rC^s - rsC^sS^r\right) & \left(1-C^rC^s+S^sS^s\right) \\ \left(1-C^rC^s+S^sS^s\right) & \frac{1}{r}\left(C^sS^r - rsC^rS^s\right) \end{Bmatrix} - \frac{1+s^2}{2}\begin{Bmatrix} 0 & -1 \\ -1 & 0 \end{Bmatrix} \qquad (5.11.b)$$

$$\mathbf{K}_{12} = \frac{1-s^2}{2D}\begin{Bmatrix} \frac{1}{s}\left(rsS^r - S^s\right) & -\left(C^r - C^s\right) \\ C^r - C^s & \frac{1}{r}\left(rsS^s - S^r\right) \end{Bmatrix} = \mathbf{K}_{21}^T \qquad (5.11.c)$$

$$\begin{array}{ll} \omega>0 & k>0 \\ C^r = \cosh(krh) & S^r = \sinh(krh) \\ C^s = \cosh(ksh) & S^s = \sinh(ksh) \end{array}$$

$$D = 2(1 - C^rC^s) + \left(\frac{1}{rs} + rs\right)S^rS^s$$

with the notation

ω = frequency of excitation

k = wavenumber

h = layer thickness

G = shear modulus

$\alpha = C_S / C_P$ = shear wave velocity / compression wave velocity

$r = \sqrt{1-\left(\omega/kC_p\right)^2}$

$s = \sqrt{1-\left(\omega/kC_s\right)^2}$

We then assemble the layer matrices in the total stiffness matrix of the plate. For each wavenumber, or wavelength, we can find the frequencies of the propagating modes as the roots of the characteristic equation (5.12):

$$\det(\mathbf{K}) = 0 \tag{5.12}$$

We solve this equation numerically, with the MATLAB program reproduced in appendix E. The results are shown on Figure 5.5, for the same range of wavelengths that we used in the analysis of the simulated signal, i.e. 0 to 0.30 meter. The studied plate is again that of 'case 1' of chapter III: 10" (25.4 cm) of concrete, covered with 2" (5 cm) of asphalt. The material properties are mentioned on the graph. We note that several modes exist for each wavelength, but we do not know their relative importance. K.F. Graff has shown in [4], that the slowest of the surface waves in a infinite plate, propagates with the velocity of the Rayleigh wave, as soon as the wavelength is smaller than the thickness of the plate. Therefore, we concentrate on the slowest mode, that we name Rayleigh wave, and assume that it is the mode that actually predominates in between station 3 and station 4. In order to verify this, we confront in the next paragraph the theoretical model and the simulations.

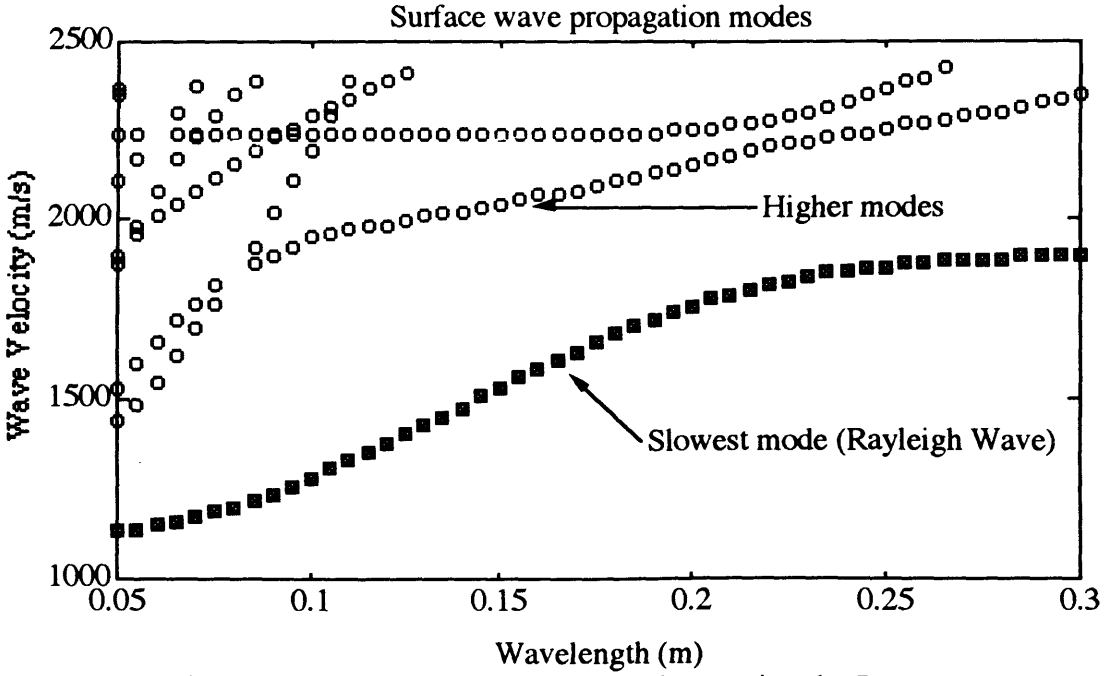

Figure 5.5: Solution of the characteristic equation det(**K**)=0

II- NUMERICAL RESULTS

II-1) Numerical results on simulations

To lay the ground for an inverse process, we now bring together the dispersion curves resulting from the simulations and those predicted by the exact two-layer model. In the exact model, we compute the Rayleigh wave dispersion curves, for different concrete conditions. Namely, the MATLAB program 'sweep' reproduced in appendix E, computes the dispersion curves for a set of plates with concrete layers that have a constant Poisson's ratio ν=0.2 and a compression wave velocity C_{p2} that ranges from 2000 m/s to 5000 m/s at 250 m/s intervals. The shear wave velocity C_{s2} is of course proportional to the compression wave velocity C_{p2}, in the ratio given by equation (3.1). The asphalt characteristics are the same for all plates: the compression wave velocity C_{p1} the shear wave velocity C_{s1} are taken to be 2400 m/s and 1200 m/s respectively. In Figures 5.6 and 5.7, the dispersion curves of the exact two-layer problem are indicated by little dots, whereas the dispersion curve resulting from the simulation is a full line curve. The parameters for the simulation are different in both figures. In Figure 5.6, the simulated plate correspond to 'case 1' of chapter III and has a concrete layer in good condition with a P wave velocity of 3920 m/s and a S wave velocity of 2400 m/s. In Figure 5.7, the simulated plate has a weak concrete layer, whose compression wave and shear wave velocities are 2940 m/s and 1800 m/s respectively. We first note that the surface wave velocity, in the exact model, tends to the Rayleigh wave velocity in the asphalt, as the wavelength approaches the thickness of the asphalt layer. This is true, whatever the compression and shear wave velocities might be in the concrete layer (as long as it is larger than the shear wave velocity in the asphalt). Comparing Figure 5.6 and Figure 5.7, we also note that the dispersion curve of the simulated plate drops dramatically when the concrete is weak. Moreover, in both figures, the simulated dispersion curve follows quite well the curve of the exact model that has the same characteristics, as far as the wavelength remains smaller than 0.20 m (i.e. 2/3 of the plate thickness).

Thus, by comparing the dispersion curve of the simulated plate with those of two-layer exact models, we can have a good idea of the condition of the underlying concrete. Of course, to start this comparison, we need the value of the compression and shear wave velocity in the asphalt layer. To obtain those value, we can look at the small wavelengths

in the experimental dispersion curve and say that the wave velocities converge to the Rayleigh wave velocity in the asphalt as the wavelength tends to the thickness of the asphalt layer. Now, assuming a reasonable Poisson's ratio of 1/3, we can easily infer the P and S wave velocity. With those values, we can build theoretical two-layer models for different characteristics of the concrete layer. The comparison between the experimental (simulated) curve and the theoretical ones, allows us to estimate the wave velocities in the concrete layer and hence, the concrete condition.

The procedure also applies to field data. Unfortunately, at this time, the field recordings are too short to conduct such an analysis. We indeed need traces of at least 1.2 to 1.5 milliseconds. Presently, the signals available are only 0.5 and 0.75 milliseconds long for station 3 and station 4 respectively.

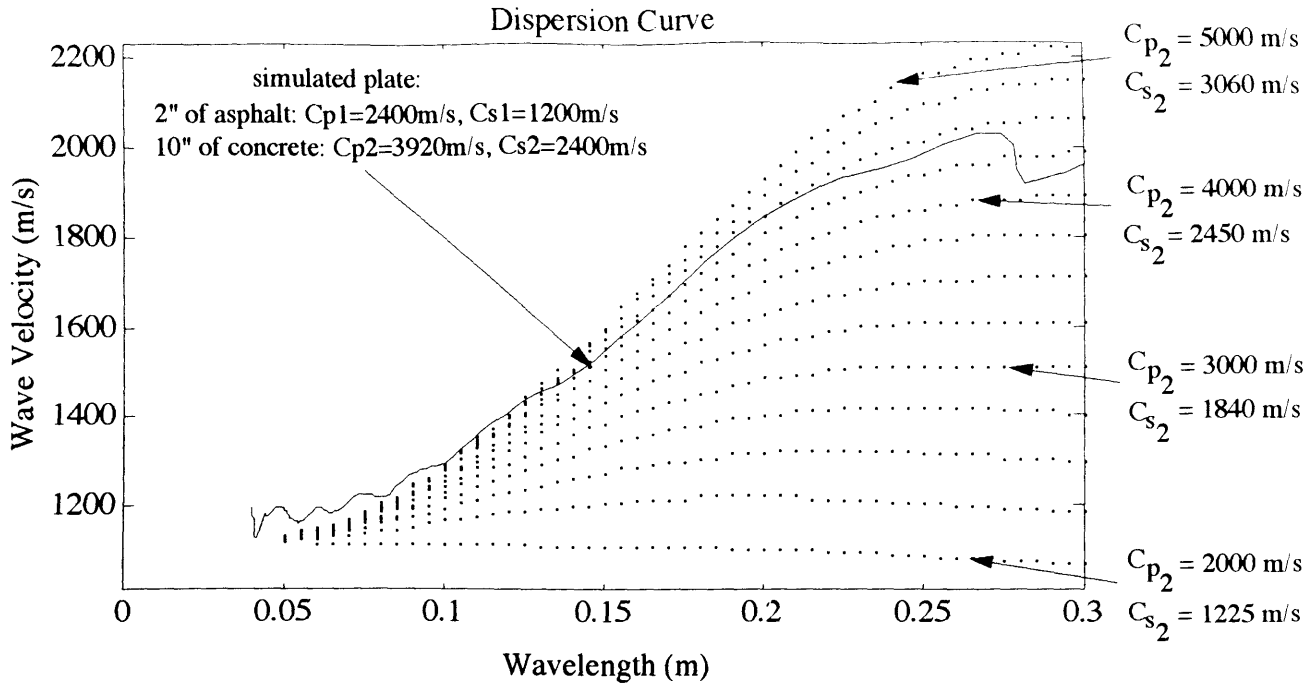

Figure 5.6: Dispersion curve for a simulated plate with a concrete layer in good condition

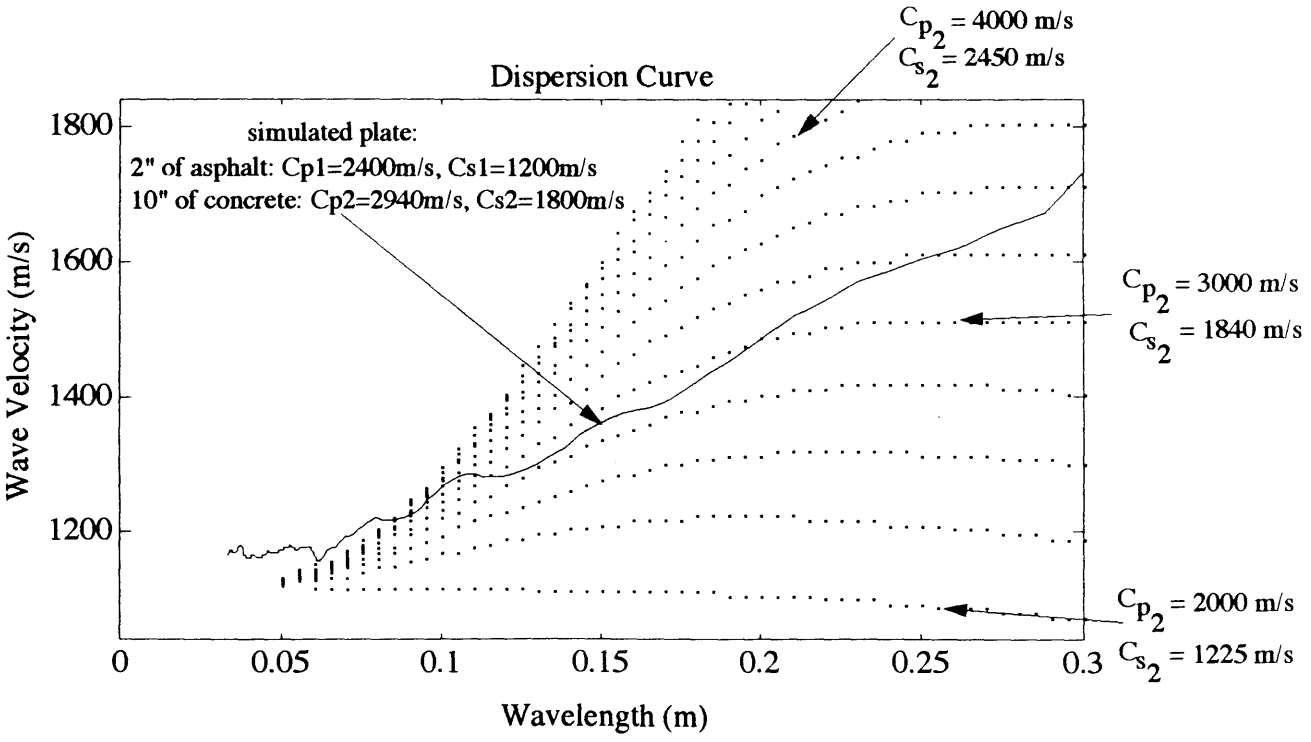

Figure 5.7: Dispersion curve for a simulated plate with a concrete layer in poor condition

II-2) Stability and limitations

Conducting the preceding analysis, we sometimes face stability problems due to the unwrapping of the phase. This operation consists in making the phase continuous by adding or subtracting 2π to the phase function whenever it shows a step of approximately 2π. Unfortunately, this operation is sometimes delicate to carry out automatically, in particular because the definition of 'an approximately 2π step' is ambiguous. Yet, an error of 2π in the phase, in particular in the low frequencies, can bring dramatic changes to the dispersion curve. Most of the unwrapping errors are located around 6 kHz, i.e. around the frequency of the thickness mode. In this area, the phase changes much more rapidly than in other areas of the frequency range, which makes the unwrapping difficult.

Other limitations to this surface wave analysis come from the definition of our model. In the first place, we assume that at each frequency, there exists only one propagating mode, and therefore one wavenumber. We saw, that this is only an approximation that relies on another assumption, that only the first surface wave mode is observable. The unwrapping difficulties that we face around the frequency of the thickness mode, show that this is not entirely the case. Other modes, although small in amplitude, bring some instability to the automatic data processing described above.

A second major assumption in our model, is that surface waves propagate along a plane front. It indeed enables us to define a wavenumber k in the direction of propagation. It is obviously not exactly the case, since the problem is axially symmetric about the vertical line of the impact. To be consistent with that symmetry, we should adopt the transformations defined by equations (4.27) and (4.28), that lead to the characteristic equation that we actually use. The difference in the procedure would be in the definition of the phase. We would indeed have to use Hankel functions to describe waves, instead of complex exponentials as in equation (5.1). However, in the range of wavelengths and distances to the impact point, that we are interested in, this additional complication does not bring a much better precision, mainly because, in that range, the phase of the Hankel functions behave very much like that of complex exponentials.

III) COMPARISON WITH THE LOCAL SPECTRAL ANALYSIS

III-1) Location in time of frequency peaks

In the preceding analysis, we assumed that between station 3 and station 4, there existed only one type of propagating wave, namely the Rayleigh wave. However, we mentioned that equation (5.12) had many other solutions, although, at that time, we could not tell which were indeed observable. In this section, we propose to use a local spectral analysis, a little more refined than that of chapter III, in order to estimate the relative importance of the different propagating modes.

In chapter III, we performed a local Fourier analysis using a fixed window, defined in equations (3.5) and (3.6). Although, this method enabled us to point out several types of waves, its resolution, in particular in the high frequencies, was not sufficient to reveal more than one mode. This problem arises with a single window, that must be able to detect low frequencies as well as high frequencies. Indeed, the width of the window is dictated by the smallest frequency $f_{minimum}$ that we want to include in the analysis. A good rule of thumb to select the parameters ω_0 and t_0 of the window is to chose

$$f_0 = \frac{\omega_0}{2\pi} = \frac{1}{3} f_{minimum} \tag{5.13}$$

and

$$f_0 t_0 = \frac{1}{2} \tag{5.14}$$

With that choice of the parameters ω_0 and t_0, the window has a compact support $[-t_0 ; t_0]$, or, which is equivalent, is zero outside this interval. The Fourier analysis conducted afterward, represents fairly well frequencies above $f_{minimum}$. This remark induces us to adapt the width of the window to the frequencies we wish to locate. Indeed, a wide window, suitable to detect low frequencies, loses accuracy when it comes to locate high frequencies in the time domain.

The MATLAB program 'wavelet' reproduced in appendix F, uses this idea to carry out an detailed local frequency analysis. In this program, we first choose a set of frequencies, typically 1,000 Hz to 25,000 HZ at 500 Hz intervals. For each frequency f of that set, we define an new window, whose parameters ω_0 and t_0 are given by equations

(5.13) and (5.14), where we replace $f_{minimum}$ by f. We then slide this window along the time axis, i.e. shift it by regular amounts Δt (typically 10 μs). Hence, for each frequency f in our given set and for each time step r Δt , where r is an integer, we compute

$$X(f, r\,\Delta t) = \sum_{n=0}^{N-1} e^{-i2\pi f n\,dt} x(n\,dt)\, W_f(n\,dt - r\,\Delta t) \qquad (5.15)$$

where x is the sampled surface displacement (at station 3 or 4), dt the sampling period, N the number of samples in the displacement trace, and W_f the window adapted to frequency f. In equation (5.15), we note that the window W_f, originally centered about the time origin, is shifted by an amount of r Δt. The amplitude of X(f, r dt) is indeed representative of the importance of frequency f in the vicinity of r dt in the time domain.

With this local spectral analysis, in comparison to the one developed in chapter III, we improve the resolution in time, of high frequencies. In particular, as we show in the next paragraph, we are able to differentiate several propagating modes. Also, in the following results, the local spectra are not normalized in any way, so that the coming graphs truly represent the amplitude X given by equation (5.15).

III-2) Numerical results

With the technique described above, we analyze here the simulated displacements at station 3 and station 4 of the typical deck 'case 1' described in Table 3.5 of chapter III. The amplitude of the local Fourier transform, as expressed in equation (5.15) is defined on a discrete time-frequency grid. Figure 5.8 represents a three dimensional view of that amplitude, for displacements at both station 3 and station 4. We note that the top graph, depicting the local Fourier spectrum of displacements at station 3, shows smooth variations, whereas the bottom graph corresponding to station 4, exhibits several peaks and more irregularities. In addition, the local spectrum of station 4 reveals large amplitudes for zero frequency that are produced by the free body motion of the plate.

Figure 5.9, displays the same information as Figure 5.8, but this time, on a contour plot. We can see that waves that have frequencies of 10 kHz and higher, are dominant at station 3 around 0.5 millisecond and propagate towards station 4 where they arrive later on, around 0.9 milliseconds. We assume that these propagating modes are the surface waves. Other modes with frequencies around 7 kHz, are hardly observable at station 3, but appear clearly at station 4. They obviously travel faster than the surface waves and are not at all negligible as Figure 4.8 clearly shows.

In Figure 5.10, we gather the information of both stations, to produce dispersive curves. On the top graph of Figure 5.10, we represent the arrival time of the amplitude maxima of the local Fourier transforms at station 3 (marked with 'x') and at station 4 (marked with 'o') versus frequency. Namely, for each frequency, we pick up the time when the maximum amplitude occurs for each station. As expected, the arrival times at station 3 of the maximum peaks form a smooth curve, but it is not the case at station 4.

To compute the surface wave velocity, we divide, for each frequency, the distance between stations 3 and 4 (i.e. 12"=0.305m) by the time lag between the arrival of peak at the two stations. Namely, if $t_3(f)$ and $t_4(f)$ are the arrival times of the maximum amplitude of frequency f, and d_{34} is the distance between stations 3 and 4, the computed Rayleigh wave velocity is

$$C_R = \frac{d_{34}}{t_4(f) - t_3(f)} \tag{5.16}$$

The middle graph of Figure 5.10 shows the surface wave velocity versus frequency. Between 8 and 16 kHz, the curve is very regular but it shows a step at 16 kHz, due to the discontinuity of the station 4 curve on the top graph. Below 8 kHz, the top graph shows peaks that arrive at station 4, before they appear at station 3, which proves that cannot come from the same propagating mode. The dispersion curve is therefore erratic below 8 kHz.

The bottom graph also represents the dispersion curve, but this time the wave velocity is represented as a function of the wavelength. For short wavelength, there seem to be two observable modes: the first one has a wave velocity close to the Rayleigh wave velocity in the asphalt (1080 m/s); the other one has a lower wave velocity.

The discontinuities in the dispersion curve induce us not only to take into consideration the major amplitude peak for each frequency, but also the second peak. We display the result in Figure 5.11. The top graph shows in particular, that the discontinuity in the station 4 arrival times curve in the top graph of Figure 5.10, is nothing more than a jump from one propagating mode to the other. Indeed, both modes exist, but one dominates the other below 16 kHz, and the other dominates above 16 kHz. A sophisticated algorithm would be needed to form the arrival times curves of the different modes and then to draw the corresponding dispersion curves. This goes beyond the scope of the qualitative analysis that we are carrying out in this paragraph.

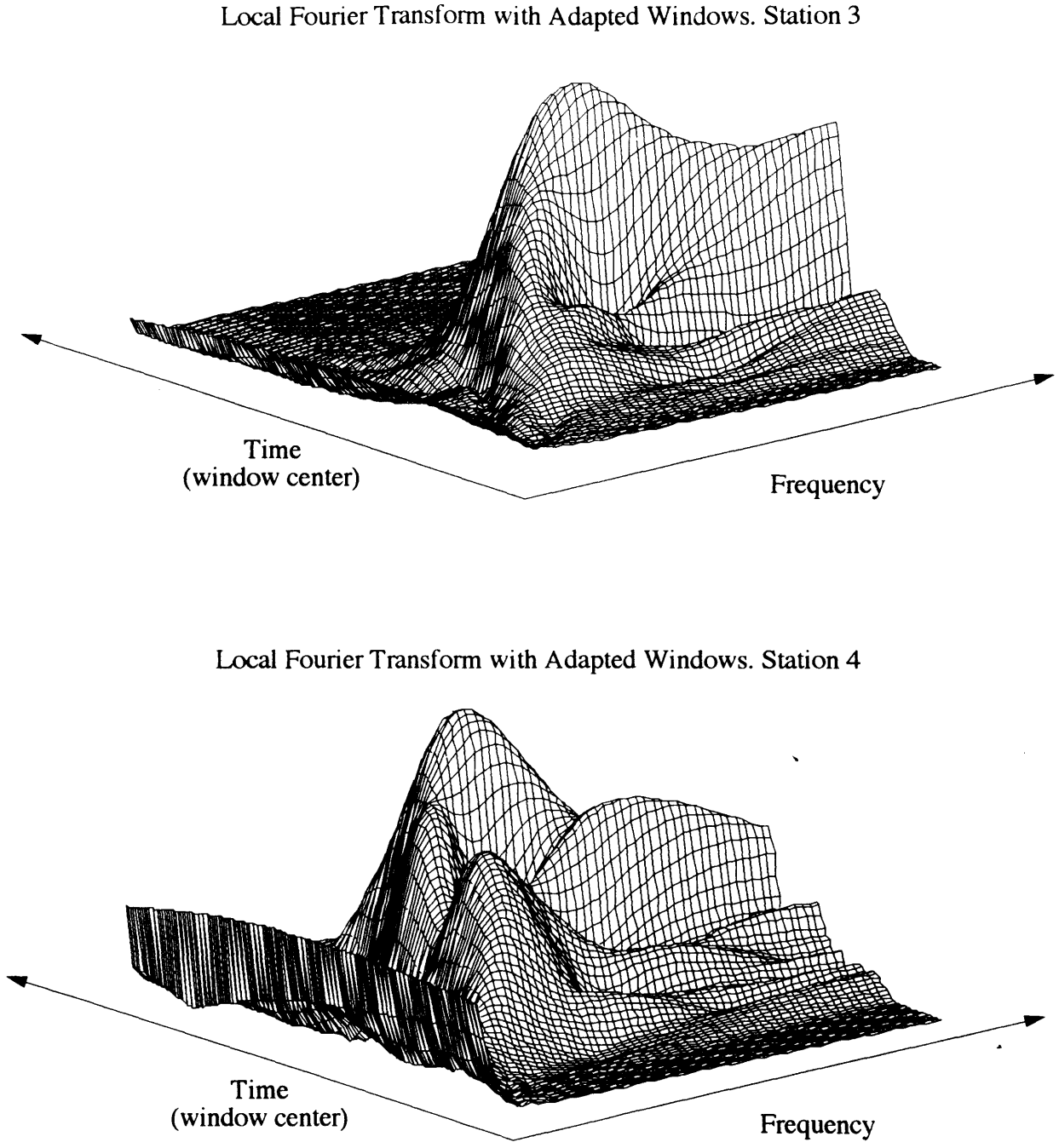

Figure 5.8: 3-D mesh of the local Fourier transform with adapted windows at station 3 and station 4 for the 'case 1' deck

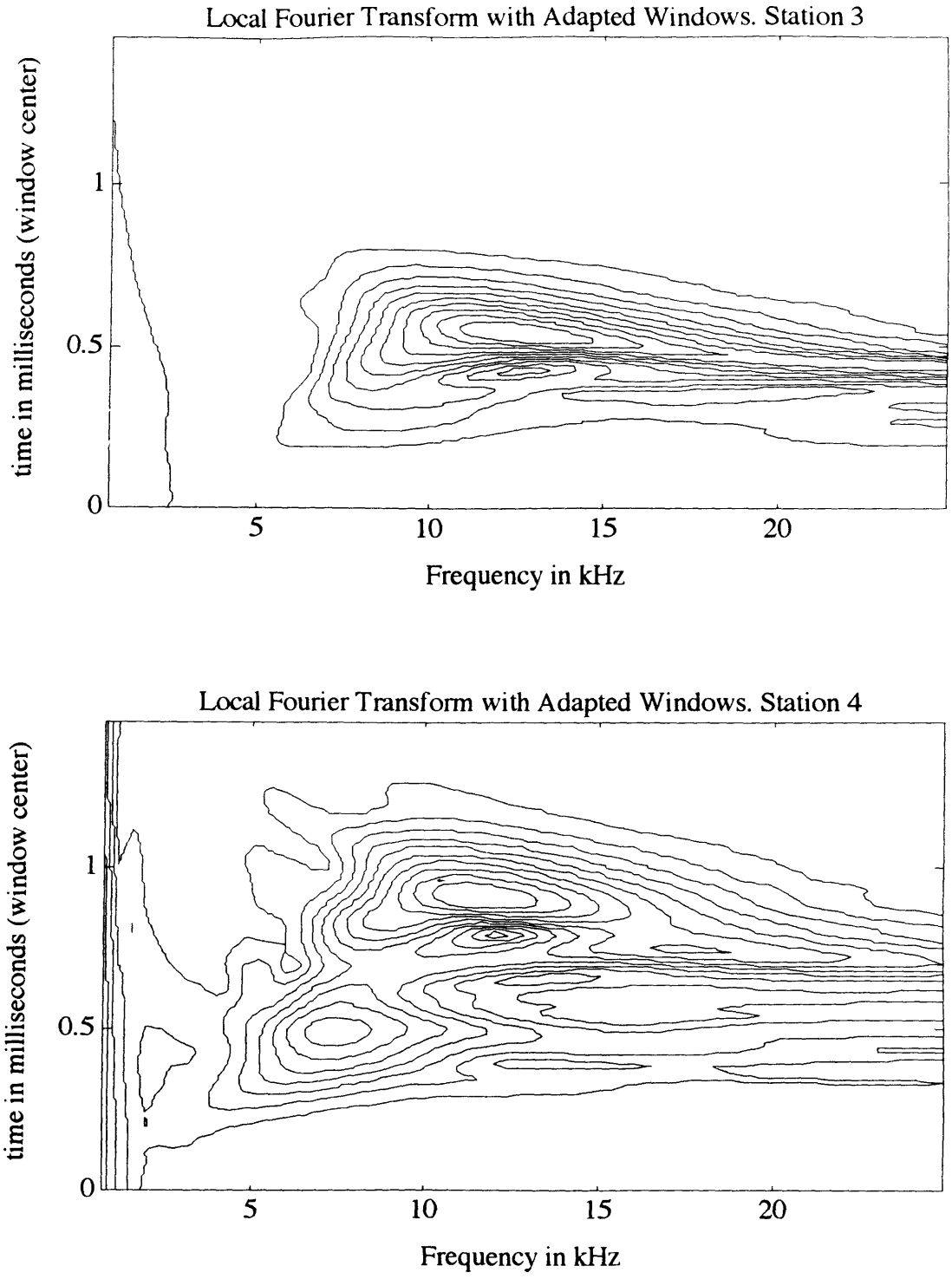

Figure 5.9: Contour plot of the local Fourier transform with adapted windows at station 3 and station 4 for the 'case 1' deck

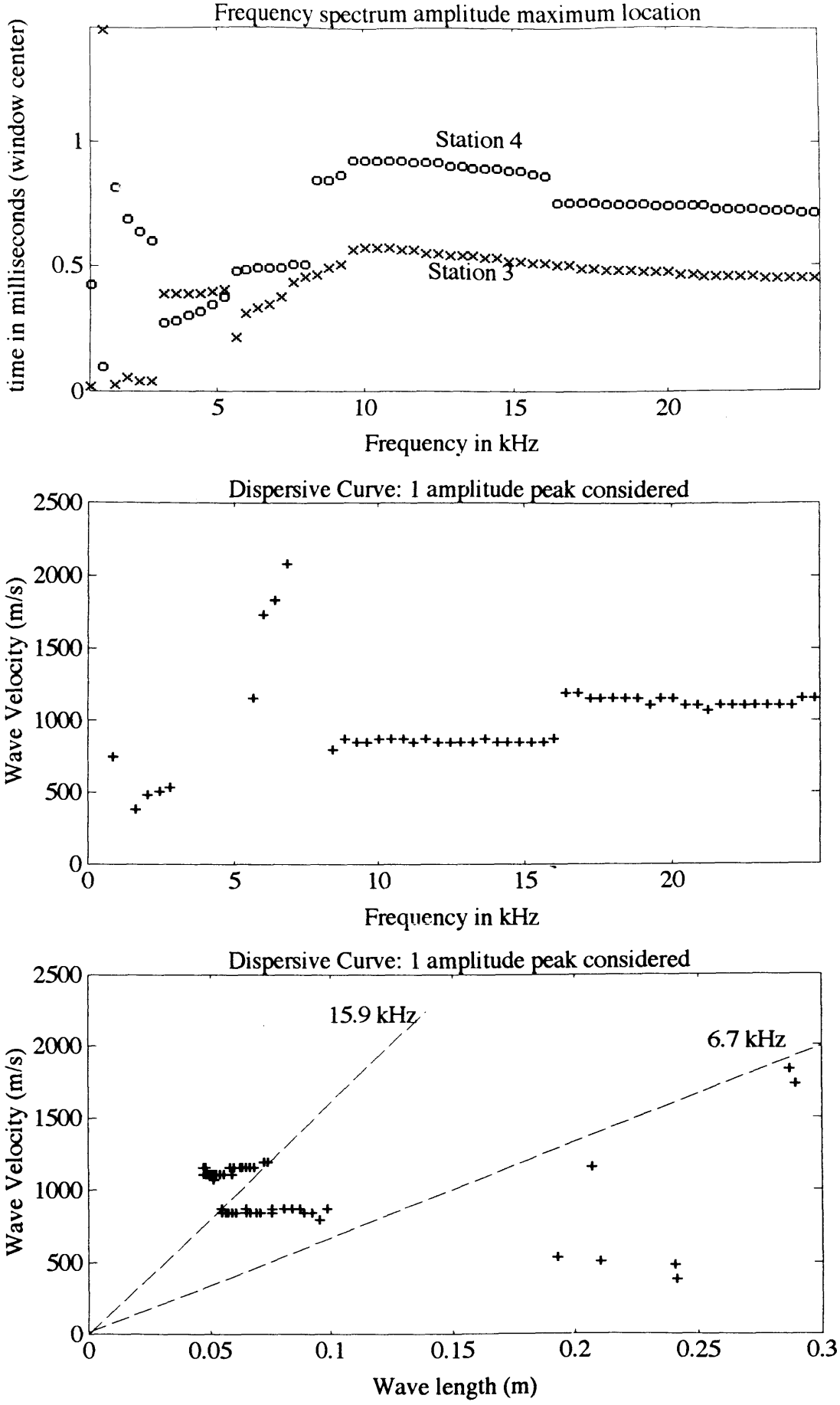

Figure 5.10: Dispersive curves of surface waves when only one peak per frequency is selected in the local Fourier transform

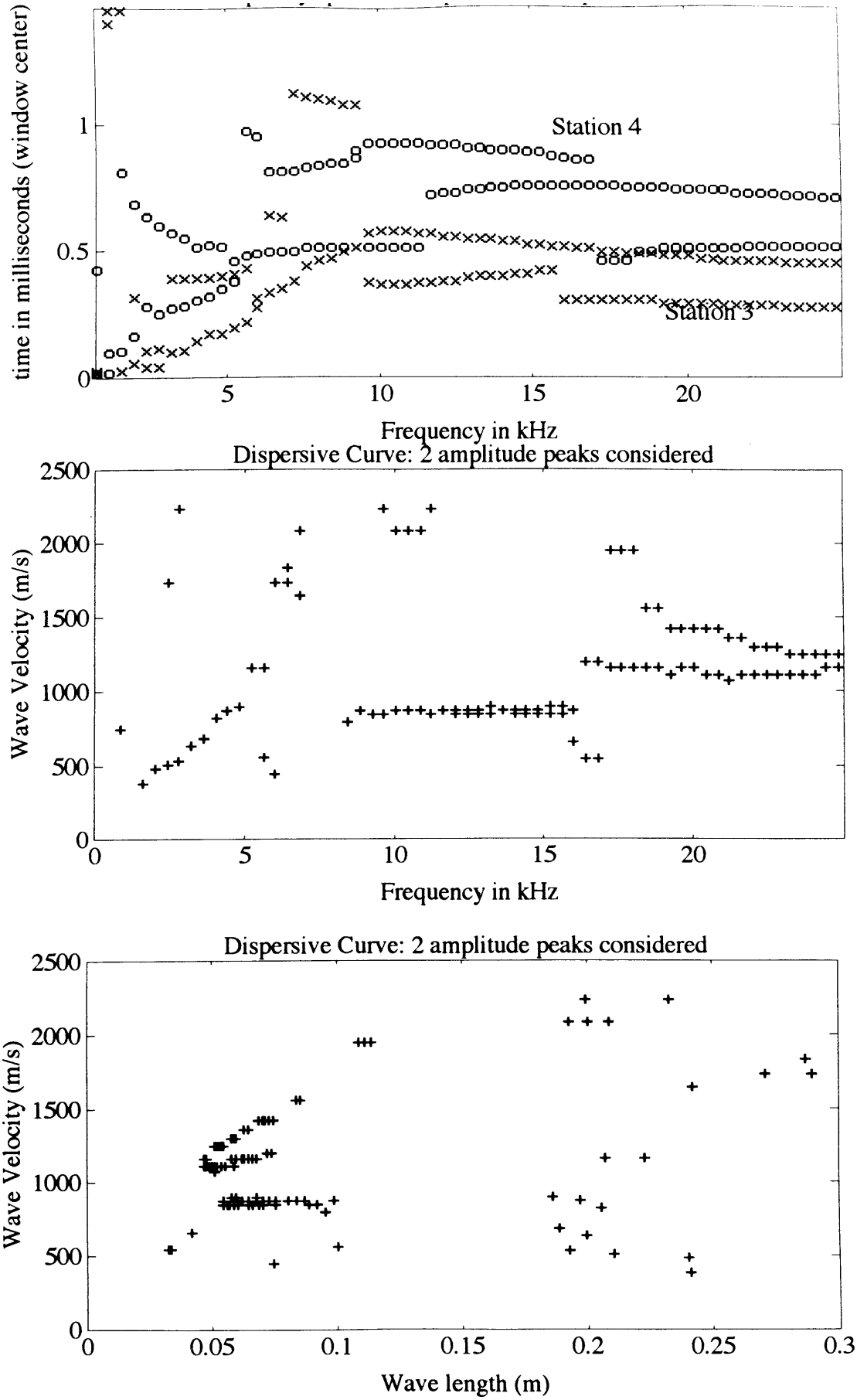

Figure 5.11: Dispersive curves of surface waves when two peaks per frequency are selected in the local Fourier transform

The dispersion curves of the middle and bottom graphs of Figure 5.11 were simply computed as in equation (5.16), with the exception that $t_3(f)$ and $t_4(f)$ are successively the arrival times of the major peaks of frequency f and the arrival times of the second major peak of frequency f. We can indeed see that several modes appear.

In Figure 5.12, we compute the surface wave velocity in a slightly different way: for each station (3 and 4), we divide the distance from the impact point to the station by the arrival times of the peak at the station. This way, we obtain a dispersion curve at each station. Again, the curve at station 3 is very smooth (above 7 kHz), whereas the curve at station 4 exhibits quite a few discontinuities. Both curves match pretty well above 8 kHz, which basically means that a same propagating mode reaches station 3 and station 4 and that its velocity does not change in between. Below 8 kHz, we can hardly speak of such a mode, since the dispersion curves at station 3 and 4 do not match at all.

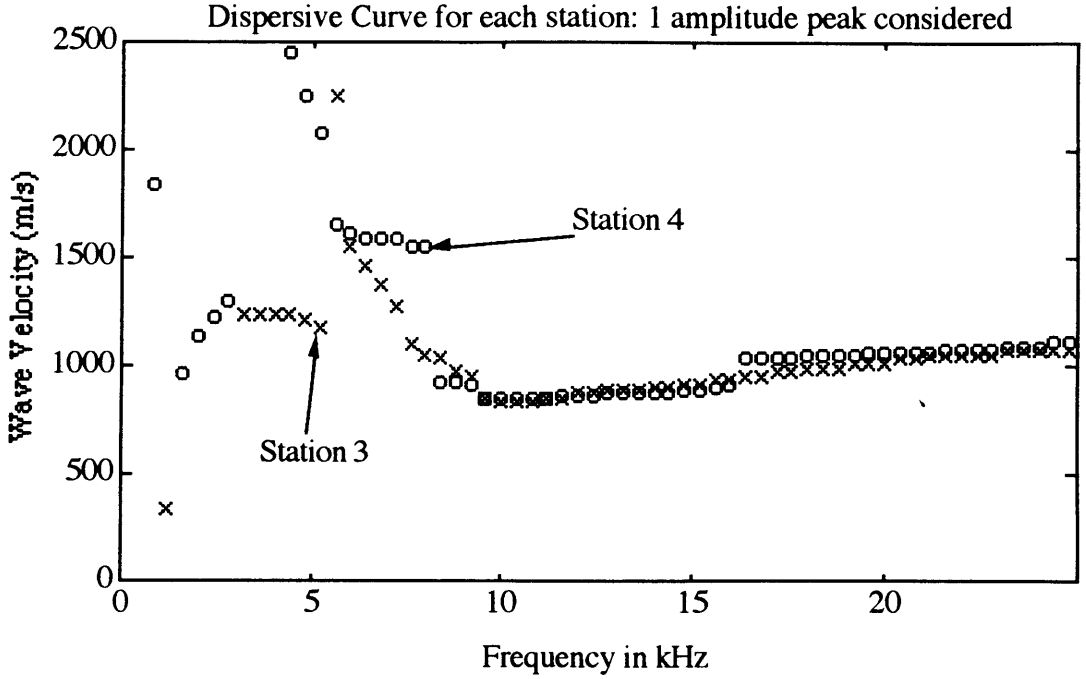

Figure 5.12: Dispersion curves at each station (3 & 4)

We have shown here, on simulated displacements, that the basic assumption of the surface wave method, namely that only one mode of propagating waves is actually observable, is not quite satisfied below 8 kHz, in the case of a concrete deck with an asphalt cover. This explains in part, the instability in the unwrapping of the phase that we mentioned in paragraph II-2.

At this stage, the available field data traces are too short to allow us to carry a local Fourier transform analysis on them . This could definitely be the object of further works.

CHAPTER VI: CONCLUSION

Outline

I- Summary
II- Implications
III- Further Works

I- SUMMARY

In order to extract structural information from seismic traces generated by an impact and recorded at the surface of a bridge deck by four sensors, we examined two numerical analysis techniques, namely the impact-echo method and the surface wave method. These analyses were performed on data recorded on the field and on numerical simulations. We demonstrated that the two techniques were not to be applied to the same recordings.

The impact-echo method, that deals with the traces recorded by the first two sensors, close to the impact point, locates, in the frequency domain, major peaks corresponding to multiply reflected compression waves. It enables us to measure with a good precision the thickness of the concrete deck. It is particularly effective with the simulated data.

The surface wave method addresses recordings by sensors that are far enough from the impact location. At such a distance, it is assumed that only Rayleigh waves are observable. The method consists in computing an experimental dispersion curve from the field or simulated data, and in comparing it to theoretical dispersion curves. It is meant to determinate elastic properties, essentially the shear wave velocities, of the deck materials (concrete and asphalt). Applied to numerical simulations, this technique enables us to point out weak portions of concrete. However, it turns out that this method suffers from numerical instability due to the fact that more than one propagating mode actually exist and that the extra modes are not negligible.

Unfortunately, the field data that are available to us for the time being, are much too short to process properly any of those techniques.

II- FURTHER WORKS

In the first place, the two procedures must be tested on longer field data, in order to corroborate the results found with numerical simulations. With the help of the two techniques, we can sketch a procedure for an analysis of a bridge deck. The surface wave method could in the first place, determine the wave velocities in the asphalt and in the concrete layers. Those velocities could then be used in the impact-echo method to measure the deck thickness and to locate possible delaminations.

Several methods in acoustics make use of arrays of sensors (many more than four) to obtain a good resolution in the measurements of wavenumbers or wave velocities. The

modal-slowness analysis is one of those methods. It might be interesting to increase the number of sensors to obtain a better accuracy in the surface wave method.

III-IMPLICATIONS

An automatic process able to determine, in the field, the condition of a concrete structure would be extremely useful for the maintenance engineer. However, the seismic techniques that we have been dealing with, must be used in combination with other non destructive techniques. Indeed, radar scanning reveals defects that are not always detected by acoustic measurements, such as the presence of moisture, or problems with the reinforcing bars.

It is of particular interest to know what quantity the acquisition system is actually recording, in particular if we are to compare field information with numerical simulations. Of course, such a quantity depends very much on how the recording device is mounted. Therefore we examine two possible mounting of the sensor, that give two different recorded quantities.

I- SENSOR FIXED TO THE WHEEL

In the first place, we model the piezo as a spring fixed at one end on the wheel and in permanent contact with the asphalt on the other end. We assume that the piezo behaves quasi-statically, that is well below its first resonant frequency. Thus, this elastic cylindrical rod reacts as a massless spring. For reasons of simplicity, we model the asphalt layer as an infinite half space, which already gives us a good idea of the plate-sensor interaction.

As A. Pais and E. Kausel stated in [13], that an approximate formula for the vertical dynamic stiffness of a cylinder of radius R in contact with an elastic infinite half space is given by

$$K_v^D = K_v^S(1 + ia_0 c)$$

where

$$K_v^S = \frac{4GR}{i - \nu}$$

is the static stiffness. G is the asphalt shear modulus, ν its Poisson's ratio; a_0 is the normalized frequency

$$a_0 = \frac{\omega R}{C_s}$$

and c is a dimensionless factor given by

$$c = \frac{\pi C_p / C_s}{K_v^S / GR}$$

With the typical values for the asphalt:

C_p= 2400 m/s

C_s= 1200 m/s

ρ= 2100 kg/m^3

ν= 0.33

and a radius of the sensor R=8mm, we obtain

$$K_v^s = 144.4 \times 10^6 \text{ N/m}$$

$$c = 1.052$$

Hence,

$$K_v^D \approx K_v^s\left(1 + i\omega \cdot 7 \cdot 10^{-6}\right)$$

which shows that for reasonable values of the frequency $f = 2\pi\omega \leq 20$ kHz, the imaginary term, dependent on ω, remains negligible. The half space responds quasi-statically.

Our model is now very simple: it consists of two springs in series as shown on Figure A-1

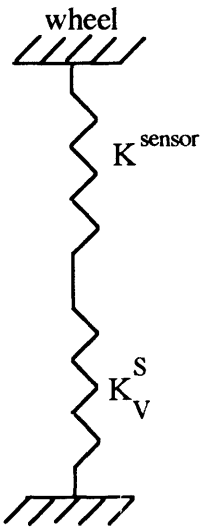

Figure A-1

As for a comparison, we note that the equivalent spring constant of the sensor is

$$K^{sensor} = \frac{EA}{L} = \frac{E\pi R^2}{L} = 31.6 \times 10^9 \text{ N/m}$$

Hence, the sensor spring is 219 times stiffer than the equivalent spring of the half space. The asphalt layer sees the sensor as a rigid rod that applies a force, proportional to the depth d it has penetrated in the layer as shown in Figure A-2. The recorded value, that is the electric voltage generated by the piezo, is proportional to the constant stress in the sensor rod, hence to the contact force and eventually to the surface displacement at the location of the sensor.

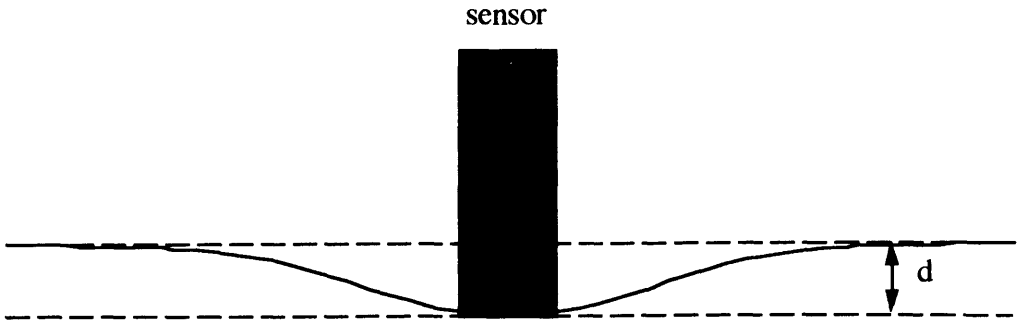

Figure A-2: Sensor aphalt contact

II- SENSOR CONNECTED TO THE WHEEL VIA A SOFT SPRING

In this case, the sensor behaves approximately as a mass held by a soft spring at one end and excited by a vertical ground motion at the other end. The contact force between the sensor and the asphalt is then essentially the inertia force of the sensor $m\omega^2X(\omega)$, where m is the mass of the sensor, ω the frequency of the excitation, and $X(\omega)$ the amplitude of the ground displacements at frequency ω. Hence, the force and the recorded voltage is proportional to $\omega^2X(\omega)$, that is proportional to the vertical surface acceleration of the ground.

We see here, that with a slight change in the experimental setting, we can select the recorded quantity to be either displacement or acceleration. So far, the sensors are mounted on soft springs and therefore record accelerations.

APPENDIX B: MATLAB PROGRAMS FOR LOCAL FOURIER ANALYSIS

In this appendix are listed the MATLAB Program we used for the local spectral analysis. The only necessary input data are the vector X of successive displacements at a particular station and dt, the time interval between two successive samples. Once those variables are defined or loaded, the whole process can be launched by typing *local_analysis.*

LOCAL_ANALYSYS.M

```
% LOCAL_ANALYSIS
% main program for a windowed Fourier analysis
% X is the main variable
% dt is the sample time interval
[m,n]=size(X);
if (n==1)
  X=X';
end
N=length(X);  %is the total number of samples = length(X)
t=[0:N-1]*dt;

% CONSTRUCTION OF THE BASIC WINDOW


f0=2000; % (Hz) as defined in chapter III
t0=0.25e-03; % (seconds)
Low0=floor(-1/2/f0/dt);
High0=ceil(1/2/f0/dt);
Interval0=[Low0*dt:dt:High0*dt];
g0=my_window(t0,f0,Interval0);
plot(Interval0*1e3,g0);title('Fundamental Window');
xlabel('Time (milliseconds)');
pause;

main_loop;
```

MAIN_LOOP.M

```
% MAIN LOOP
% sweep the time domain at 'step' intervals
% to obtain a grid of spectral amplitude stored in GFW

GFW=[];
step=0.5*t0;
for K_shift=0:floor((N-1)*dt/step)  % beginning of the main loop

 % CONSTRUTION OF THE SHIFTED WINDOW

 t_shift=K_shift*step;
```

```
 n_shift=floor(t_shift/dt)+1;
 g=zeros(t);
 for k=1:N
  if ((Low0+n_shift<=k) & (k<=n_shift+High0) )
   g(k)=g0(k-n_shift-Low0+1);
  end
 end
 %plot(t*1e03,g);

 % MULTIPLICATION AND FOURIER TRANSFORM
 Max_Freq=30000;
 Min_Freq=0;
 % range of represented frequencies;

 % computation of the average value of X on the support of g
 max_g=max(g);
 one_g=g ./ (g+max_g/10000);
 % approximately 1 for non zero values of g, zero elsewhere
 mean_X=sum(X .* one_g)/sum(one_g);
 WX=(X-mean_X) .* g;
 plot(t*1e03,WX);title('Windowed Trace');

 fft_length=2^(ceil(log(length(WX))/log(2))+1);
 f=[0:fft_length/2-1]/fft_length/dt;
 fmin=floor(Min_Freq*fft_length*dt)+1;
 fmax=floor(Max_Freq*fft_length*dt)+1;
 FWX=fft(WX,fft_length);
 FWX=abs(FWX(1:fft_length/2));
 Max_FWX=max(FWX);
 GFW=[(FWX(fmin:fmax))/Max_FWX  ; GFW ];
 plot(f/1000,FWX);

end  % OF MAIN LOOP
mesh(GFW);pause;
contour(GFW,10,[(fmin-1):(fmax-1)]/fft_length/dt/1000,[0:floor((N-
1)*dt/step)]*step*1000);
xlabel('Frequency in kHz');
ylabel('time in milliseconds (window center)');
```

MY_WINDOW.M

```
function g=my_window(t0,f0,x);

w0=2*pi*f0;
% t0*w0>=pi and t0*w0<=2*pi
[m,n]=size(x);
if (m==1)
  x=x';
end;
[m,n]=size(x);
% x is now a column vector of size m
```

```
if (t0*w0<pi)
  disp('Warning t0*f0 must be larger than 1/2');
elseif (t0*w0>2*pi)
  disp('Warning t0*f0 must be smaller than 1');
elseif ( (t0*w0>=pi) & (t0*w0<=2*pi))
  g=zeros(x);
  for k=1:m
    if ( (-pi/w0<=x(k)) & (x(k)<=pi/w0-t0) )
       g(k)=sin(pi/2*nu((pi+w0*x(k))/(2*pi-w0*t0)));
    elseif ( (pi/w0-t0<=x(k)) & (x(k)<=-pi/w0+t0))
       g(k)=1;
    elseif ( (-pi/w0+t0<=x(k)) & (x(k)<=pi/w0) )
       g(k)=sin( pi/2*nu( (pi-w0*x(k)) / (2*pi-w0*t0) ) );
    elseif (x(k)<-pi/w0)
       g(k)=0;
    elseif (pi/w0<x(k))
       g(k)=0;
    end
  end
  g=t0^(-0.5) * g;
end
```

NU.M

```
function n=nu(x);

if (x<=0)
  n=0;
elseif ((x>0) & (x<1))
  n=sin(pi/2*x)^2;
elseif (x>=1)
  n=1;
end
```

In this appendix are listed the MATLAB Program we used for the impact echo method. The analysis is launched under MATLAB by typing *SPP*

SPP.M

```
% Spectral Peak Plotting

clear;
SPPload;
SPPgraph;
SPP2layers;
```

SPPload.M

```
% Spectral Peak Plotting

% File Loading
n1=input('First row to be tested: ');
n2=input('Last  row to be tested: ');
extension=input('Extension: ','s');
safe=input('Name of the save file: ','s');
titre=input('title for the graphs: ','s');
station=input('station [ :');
if (station==1)
  mmm='(1:125)" ];';
elseif (station==2)
  mmm='(126:250)" ];';
elseif (station==3)
  mmm='(251:375)" ];';
elseif (station==4)
  mmm='(376:563)" ];';
end

v=[];
for n=n1:n2
  name=['W' int2str(n) '.' extension];
  action=['load ' name ];
  eval(action);
  name=['W' int2str(n)];
  action=['v=[v; ' name mmm]
  eval(action);
  action=['clear ' name];
  eval(action);
  disp([name ' loaded']);
end

N=n2-n1+1;
if (station<4)
   t=[0:124]*4e-06*1000; % time in milliseconds
   axis([0,0.5,-2,N+1])
```

```
else t=[0:187]*4e-06*1000; % time in milliseconds
  axis([0,0.752,-2,N+1])
end
for n=1:N
 v_actif=v(n,:);
 v_max=max(abs(v_actif));
 v_actif=v_actif/v_max;
 plot(t,v_actif*2+n-1);
 if (n==1)
   hold on;
 end
end
axis
hold off;

action=['save ' safe]
eval(action);
```

SPPgraph.M

```
% Spectral Peak Plotting

% velocity graph

d=[];
axis([0,0.5,-2,N+1])
for n=1:N
 v_actif=v(n,:);
 v_actif=v_actif-mean(v_actif(1:8));
 d_actif=integral(v_actif,4e-06,0);
 d=[d; d_actif];
 v_max=max(abs(v_actif));
 v_actif=v_actif/v_max;
 plot(t,v_actif*2+n-1);
 if (n==1)
   hold on;
 end
end
axis;
xlabel('Time (milliseconds)');
ylabel('velocities');
title(titre);
hold off;
pause;
clg;

% Displacement Graph

axis([0,0.5,-2,N+1])
for n=1:N
 d_actif=d(n,:);
 d_max=max(abs(d_actif));
 d_actif=d_actif/d_max;
 plot(t,d_actif*2+n-1);
 if (n==1)
```

```
    hold on;
  end
end
axis;
xlabel('Time (milliseconds)');
ylabel('displacements');
title(titre);
hold off;
pause;

% Fourier Spectrum
fft_length=512;
v_or_d=input('Fourier Transform on displacements (d) or velocities (v): ','s');
tmin=input('Start Fourier Transform at time: ');
tmax=input('Stop  Fourier Transform at time: ');
if (v_or_d=='d')
  FP=[];
  for n=1:N
    d_actif=d(n,:);
    FP_actif=fit_spectrum(d_actif,4e-06,tmin,tmax,fft_length,'c',' ',' ');
    FP=[FP; FP_actif];
  end
else
  FP=[];
  for n=1:N
    v_actif=v(n,:);
    FP_actif=fit_spectrum(v_actif,4e-06,tmin,tmax,fft_length,'c',' ',' ');
    FP=[FP; FP_actif];
  end
end

axis([0,40,-1,N+3])
k=[0:fft_length/2-1]/fft_length/4e-06/1000; % frequency in kHz
for n=1:N
  FP_actif=FP(n,:);
  FP_max=max(abs(FP_actif));
  FP_actif=FP_actif/FP_max;
  plot(k,abs(FP_actif)*4+n-1);
  if (n==1)
    hold on;
  end
end
axis;
hold off;
xlabel('Frequency in kHz');
if (v_or_d=='d')
   ylabel('displacements');
else
   ylabel('velocities');
end
title(titre);
pause;

action=['save ' safe]
```

```
eval(action);
```

SPP2layers.M

```
% SPP2layers
% draws an estimated cross section along the scan

ca=2400; % P wave velocity in asphalt (m/s)
cp=4000; % P wave velocity in concrete (m/s)
Ta=2*0.0254; % estimated depth of the asphalt layer
Ta=input('estimated depth of the asphalt layer(m): ');
threshold=0.99;
if (Ta==0)
  cut_off=15000;
else
  cut_off=0.9*ca/(4*Ta);
end
% frequency above which nothing is considered

depth_max=input('assumed maximum depth(m): ');
dt=4e-06;
offset=Ta*(1-cp/ca);

% correction for skewed rays
taverage=(tmin+tmax)/2;
if (station==1)    H=1*0.0254;
elseif (station==2) H=7*0.0254;
elseif (station==3) H=19*0.0254;
elseif (station==4) H=31*0.0254;
end
rp=0.5*1/((cp*taverage/H)^2-1);
disp(['rp= ' num2str(rp)]);
ra=0.5*1/((ca*taverage/H)^2-1);
disp(['ra= ' num2str(ra)]);

% all local maxima
m_cut_off=floor(cut_off*fft_length*4e-06)+1;
impact_echo=[];
for n=1:N
 FP_actif=FP(n,1:m_cut_off);
 FP_max=max(abs(FP_actif));
 FP_actif=abs(FP_actif)/FP_max;
 impact_echo=[impact_echo; maximum_detection(n,FP_actif(1:m_cut_off),4e-
06,fft_length,cp,threshold,0)];
end
x=impact_echo(:,1);
depth=(impact_echo(:,2)+offset)*(1+rp);
axis([min(x),max(x)+1,0,min(max(depth),depth_max)]);

for m=0:0.2:0.8
  plot(x+m,depth,'o');
  if (m==0) hold on;
  end
end
```

```
%major echos peak>0.5
impact_echo=[];
for n=1:N
  FP_actif=FP(n,1:m_cut_off);
  FP_max=max(abs(FP_actif));
  FP_actif=abs(FP_actif)/FP_max;
  impact_echo=[impact_echo; maximum_detection(n,FP_actif(1:m_cut_off),4e-
06,fft_length,cp,threshold,0.5)];
end
x=impact_echo(:,1);
depth=(impact_echo(:,2)+offset)*(1+rp);

for m=0:0.2:0.8;
  plot(x+m,depth,'*');
end


% echos in the asphalt layer
if (Ta==0)
  disp('Fini');
else
impact_echo=[];
clear FP_actif;
for n=1:N;
  FP_actif=FP(n,m_cut_off:fft_length/2);
  FP_max=max(abs(FP_actif));
  FP_actif=abs(FP_actif)/FP_max;
  impact_echo=[impact_echo; max_detect_asp(n,FP_actif,dt,fft_length,ca,threshold,0.5)];
end
x=impact_echo(:,1);
depth=impact_echo(:,2)*(1+ra);

for m=0:0.2:0.8;
  plot(x+m,depth,'x');
end
end

% assumed asphalt line;
n=0:N+1;
interface=ones(n)*Ta;
plot(n,interface);

xlabel('horizontal distance');
ylabel('depth of the echo(m)');
title(titre);
axis;
hold off;
```

APPENDIX D: MATLAB PROGRAMS FOR THE EXACT TWO LAYER MODEL IN THE IMPACT-ECHO METHOD

In this appendix we reproduce the MATLAB programs for the exact two layer model in the impact-echo method. The program Resonant computes the resonant frequencies for a set of deck thickness. The other programs, starting with LOAD_DATA, proceed with the inverse problem

% AAA

```
clear;
Resonant;
clear H0 N NbMaxZeros Nb_zeros alpha f f1 f2 h2 m signe_y; clear theo_peak y yzero z
z0;
clc;
LOAD_DATA;
```

% Resonant;

```
clc;
disp('*****************************************************');
disp('*      Computation of the Resonant Frequencies      *');
disp('*****************************************************');
disp(");
asphalt=input('asphalt layer (y/n) ? ','s');
if (asphalt=='y')
   disp('Assumptions about the asphalt layer');
   disp('***********************************');
   h1=input('Assumed thickness h1 (m) : ');
         cp1=input('P wave velocity cp1 (m/s): ');
   ro1=input('mass density (kg/m3)    : ');
%    nu1=input('Poisson"s ratio         : ');
   disp(");
end
disp('Assumptions about the concrete layer');
disp('***********************************');
h2min=input('Minimum thickness h2min (m) : ');
h2max=input('Maximum thickness h2max (m) : ');
h2step=input('Precision desired h2step(m) : '); cp2=input('P wave
velocity cp2 (m/s): '); ro2=input('mass density (kg/m3)    : ');
%nu2=input('Poisson"s ratio         : '); disp(' ');
NbMaxZeros=input('Maximum Number of Resonances = ');
Frequence_sup=input('Maximum Resonant Frequency (kHz)= ')*1000; if (asphalt=='y')
   r=ro2*cp2/(ro1*cp1);
   one_over_r=1/r;
   f1=cp1/4/h1;
else
   one_over_r=0;
```

```
    h1=0;
    f1=1000;
end

H=[];
U=[];
theo_peak=[];
h=[];
for h2=h2min:h2step:h2max
      disp(['h2 = ' num2str(h2) ' m']);
      f2=cp2/4/h2;
      cherche_zero;
      if (Nb_zeros>0)
                h=[h (h1+h2*ones(1:Nb_zeros))];
                theo_peak=[theo_peak z];
      end
end

axis([1 2 3 4]); axis;
plot(h,theo_peak/1000,'x');
title('P-Waves Resonant Frequencies for a Double Layer Deck');
xlabel('Total Deck Height (m)');
ylabel('Frequencies (kHz)');

H=H';
U=U';
```

% LOAD_DATA

```
clc;
disp('FIELD DATA OR SIMULATION DATA LOADING');
disp('************************************');
TypeData=input('Field data (f) or Simulation (s): ','s');
if (TypeData=='f')
    disp('Go to the subdirectory');
    pause;
%     On a Macintosh, during the pause, the user should go to the
%     directory where the file is located using the menu bar 'LOAD'
%     function; however, no file need be loaded and the user should click
%     the cancel button, once in the proper directory
%     On other machines, this program and the data files sholud be located
%     in the same directory, and the last two lines can be omitted
    row1=input('First row = ');
    row2=input('Last row  = ');
    extension=input('Extension  = ','s');
    station=input('station = ');
    if (station==1)
          mmm='(1:125)" ];';
          Nb_points=125;
    elseif (station==2)
          mmm='(126:250)" ];'; Nb_points=125;
    elseif (station==3)
          mmm='(251:375)" ];'; Nb_points=125;
    elseif (station==4)
```

```
        mmm='(376:563)" ];'; Nb_points=188;
    end
    v=[];
    for row=row1:row2
        name=['W' int2str(row) '.' extension];
        action=['load ' name ]; eval(action);
        name=['W' int2str(row)]; action=['v=[v; '
        name mmm]; eval(action);
        action=['clear ' name]; eval(action);
        disp([name ' loaded']);
    end
    Nb_Traces=row2-row1+1;
    dt=4e-06;
elseif (TypeData=='s')
    disp('Go to the subdirectory');
    pause;
    Nb_points=1024;
    station=input('station = ');
D_or_A=input('displacement (d) or acceleration (a) = ','s');
 if (D_or_A=='d')
        action=['load DPLT' int2str(station) '.ZZ;']; eval(action);
        name=['DPLT' int2str(station)];
        action=['v=' name ';'];
        eval(action);
        action=['clear ' name ';'];
        eval(action);
    elseif (D_or_A=='a')
        action=['load APLT' int2str(station) '.ZZ;'];
        eval(action);
        name=['APLT' int2str(station)];
        action=['v=' name ';'];
        eval(action);
        action=['clear ' name ';'];
        eval(action);
    end
    Nb_Traces=1;
    dt=v(2,1)-v(1,1);
    v=-v(:,2); % notice the - sign
end

v=v';

main;


%    cherche_zero

f=100:100:Frequence_sup;

N=length(f);
y=one_over_r*(tan(pi/2*f/f1))+ (tan(pi/2*f/f2));
yy=(tan(pi/2*f/f1)).^(-1)+one_over_r*((tan(pi/2*f/f2)).^(-1));
%axis([min(f),max(f),-10,10]);plot(f,y);axis;pause;
```

```
signe_y=sign(y);
yzero=1/2*abs(diff(signe_y));

signe_yy=sign(yy);
yyzero=1/2*abs(diff(signe_yy));

%comb(f(1:(N-1)),yzero);

z=[];
for m=1:(N-1)
   if ( (yzero(m)>0) & (y(m+1)>y(m)) ) alpha=y(m)/(y(m)-y(m+1));
        z0=f(m)+alpha*(f(m+1)-f(m));
        z=[z z0];
   elseif ( (yyzero(m)>0) & (yy(m+1)<yy(m)) ) alpha=y(m)/(y(m)-y(m+1));
        z0=f(m)+alpha*(f(m+1)-f(m));
        z=[z z0];
   end
end

if (length(z)>NbMaxZeros)
      z=z(1:NbMaxZeros);
end
Nb_zeros=length(z);
H0=ones(1:NbMaxZeros)*(-1e+05);
H0(1:min(Nb_zeros,NbMaxZeros))=z(1:min(Nb_zeros,NbMaxZeros));
H=[H ; H0];
U=[U ; ones(1:NbMaxZeros)];
```

% main

```
clg;
subplot;
answer='n';
if (TypeData=='f') Nb_points=length(v(:,1));
elseif (TypeData=='s') Nb_points=length(v);
end
while (answer=='n')
    tmin=input('Tmin (ms)= ')*1e-03; tmax=input('Tmax (ms)= ')*1e-03;
    nmin=floor(tmin/dt)+1; nmax=min(ceil(tmax/dt)+1,Nb_points); if (TypeData=='f')
        vactif=v(nmin:nmax,1:Nb_Traces);
    elseif (TypeData=='s') vactif=v(nmin:nmax);
    end
    t=[(nmin-1):(nmax-1)]*dt;
axis([(nmin-1)*dt*1000,(nmax-1)*dt*1000,-1,Nb_Traces]); for n=1:Nb_Traces
    if (TypeData=='f')
        vactifMax=max(abs(vactif(:,n))); plot(t*1e03,vactif(:,n)/vactifMax+n-1);
    elseif (TypeData=='s')
        vactifMax=max(abs(vactif));
        axis([1 2 3 4]);axis; plot(t*1e03,vactif/vactifMax*3+n-1);
    end
        if (n==1)
           hold on;
```

```
            end
        end
        hold off;
        axis;
 answer=input('Do you agree with that time window? (y/n) ','s'); end

 fft_length=input('FFT length = ');
 Nb_points=nmax-nmin+1;
 fft_length=max(fft_length,Nb_points);
 fft_length=2^(ceil(log(fft_length)/log(2)))

 if (TypeData=='f')
      FP=[];
      for n=1:Nb_Traces
          FP0=AAA_spectrum(v(:,n)',dt,nmin,nmax,fft_length,0,'c','AAA','field data ');
          FP=[FP abs(FP0)'];
      end
      FP=FP';
 elseif (TypeData=='s')
      FP=AAA_spectrum(v,dt,nmin,nmax,fft_length,0,'c','AAA',D_or_A);
      FP=abs(FP);
 end

 F_cut_off=input('Cut-off frequency (kHz): ');
 F_cut_off=F_cut_off*1000;
 m_cut_off=min(floor(F_cut_off*dt*fft_length)+1,fft_length/2);
 NbMaxPeaks=input('Maximum number of peaks to consider: ');
 peak_min=input('Minimum Frequency for retained peaks (kHz): ')*1000;
 if (TypeData=='f')
      H_estimate=[];
      for n=1:Nb_Traces
          FP0=FP(n,1:m_cut_off);
          [f_peak,weight,Nb_of_peaks]=locate_peak(FP0,dt,fft_length,NbMaxPeaks,peak_min);
          match_frequency;
          H_estimate=[H_estimate h_guess];
      end
      axis([1 2 3 4]);axis;
      comb(H_estimate);
 elseif (TypeData=='s')
      FP0=FP(1:m_cut_off);
      [f_peak,weight,Nb_of_peaks]=locate_peak(FP0,dt,fft_length,NbMaxPeaks,peak_min);
      match_frequency;
      H_estimate=h_guess
 end


 function FP=AAA_spectrum(x,dt,n1,n2,fft_length,integration,p_or_c,titre,label);


 n=[1:(n2-n1+1)];
 P=x(n1:n2);

 % regress P on a line and remove that linear displacement best_line=polyfit(n,P,1);
 LP=P-polyval(best_line,n);
```

```
% Fourier Transform
FP=fft(LP,fft_length);
FP=FP(1:fft_length/2); f=[0:fft_length/2-1]/fft_length/dt;
factor=i*2*pi*f;
factor=factor .^ (-integration);
FP=FP .* factor;

% graphs
clg;
axis([0,1,0,1]);
axis;
subplot(211);
plot([(n1-1):(n2-1)]*dt*1000,LP);
xlabel('time (milliseconds)');
ylabel(label);
title(titre);
grid;

axis([0,20,0,max(abs(FP))]);% display limited at 20 kHz
subplot(212);
if (p_or_c=='c')
                comb(f/1000,abs(FP));
elseif (p_or_c=='p')
      plot(f/1000,abs(FP));
      grid;
end
xlabel('Frequency (kHz)');
ylabel(label);
title(titre);
subplot;
axis;
```

%match_frequency

```
for mm=1:Nb_of_peaks
   if (mm==1) e=(weight(mm)^2)*min(abs(f_peak(mm)*U-H));
   else e=e+(weight(mm)^2)*min(abs(f_peak(mm)*U-H));
   end
end

[err,i0]=min(e);
h_guess=h1+h2min+(i0-1)*h2step
```

function [F,Intensity,Nb_of_peaks]=**locate_peak**(x,dt,fft_length,NbMaxPeaks,fmin);

```
x=abs(x);
Nx=length(x);
F1=[];
```

```
Intensity1=[];
sup=max(x);

for mm=3:(Nx-2)
if ( (x(mm)>x(mm-1)) & (x(mm)>x(mm+1)) & (x(mm)>x(mm-2)) & (x(mm)>x(mm+2)) )
        f0=(mm-1)/fft_length/dt;
        if (f0>fmin)
            F1=[F1 f0];
            Intensity1=[Intensity1  x(mm)/sup];
        end
   end
end

if (length(F1)<NbMaxPeaks)
     Nb_of_peaks=length(F1);
else
     Nb_of_peaks=NbMaxPeaks;
end

[Intensity,Index]=sort(-Intensity1);
Intensity=-Intensity(1:Nb_of_peaks);
F=zeros(1:Nb_of_peaks);
for mm=1:Nb_of_peaks
   F(mm)=F1(Index(mm));
end
```

APPENDIX E: MATLAB PROGRAMS FOR THE SURFACE WAVE METHOD

The MATLAB program SASW performs the surface wave analysis analysis on simulated data or field data. All the other program address the inverse problem.

```
%       SASW
clear;
hold off;axis([1 2 3 4]);axis;subplot;
clc;
disp('*************************************');
disp('********** SASW ANALYSIS ************');
disp('*************************************');
disp('FIELD DATA OR SIMULATION DATA LOADING');
disp('*************************************');
TypeData=input('Field data (f) or Simulation (s): ','s');
if (TypeData=='f')
   disp('Go to the subdirectory');
   pause;
   row=input('row = ');
   extension=input('Extension  = ','s');
   station1=input('station [1 = ');
   station2=input('station [2 = ');
distance=input('distance between station [1 and [2 = ');

   if (station1==1)
        mmm='(1:125);';
        Nb_points=125;
   elseif (station1==2)
        mmm='(126:250);';
        Nb_points=125;
   elseif (station1==3)
        mmm='(251:375);';
        Nb_points=125;
   elseif (station1==4)
        mmm='(376:563);';
        Nb_points=188;
   end

   name=['W' int2str(row) '.' extension];
   action=['load ' name ];
   eval(action);
   name=['W' int2str(row)];
   action=['v1=' name mmm];
   eval(action);

   if (station2==1)
        mmm='(1:125);';
        Nb_points=125;
   elseif (station2==2)
        mmm='(126:250);';
        Nb_points=125;
   elseif (station2==3)
        mmm='(251:375);';
```

```
        Nb_points=125;
    elseif (station2==4)
        mmm='(376:563);';
        Nb_points=188;
    end

    name=['W' int2str(row)];
    action=['v2=' name mmm];
    eval(action);
    action=['clear ' name];
    eval(action);
    disp([name ' loaded']);

    dt=4e-06;

elseif (TypeData=='s')
    disp('Go to the subdirectory');
    pause;
    Nb_points=1024;
                    D_or_A=input('displacement (d) or acceleration (a) = ','s');
    station1=input('station [1= ');
    station2=input('station [2= ');
     distance=input('distance between station [1 and [2 = ');
     if (D_or_A=='d')
                            action=['load DPLT' int2str(station1) '.ZZ;'];
        eval(action);
        name=['DPLT' int2str(station1)];
        action=['v1=' name ';'];
        eval(action);
        action=['clear ' name ';'];
        eval(action);
        action=['load DPLT' int2str(station2) '.ZZ;']; eval(action);
        name=['DPLT' int2str(station2)]; action=['v2=' name ';'];
        eval(action);
        action=['clear ' name ';'];
        eval(action);
    elseif (D_or_A=='a')
        action=['load APLT' int2str(station1) '.ZZ;']; eval(action);
        name=['APLT' int2str(station1)]; action=['v1=' name ';'];
        eval(action);
        action=['clear ' name ';'];
        eval(action);
        action=['load APLT' int2str(station2) '.ZZ;']; eval(action);
        name=['APLT' int2str(station2)]; action=['v2=' name ';'];
        eval(action);
        action=['clear ' name ';']; eval(action);
    end
    dt=v1(2,1)-v1(1,1);
    v1=-v1(:,2); % notice the - sign v2=-v2(:,2);
end

tmin=input('Tmin (ms)= ')/1000; tmax=input('Tmax (ms)= ')/1000;

n1=1+floor(tmin/dt); n2=1+floor(tmax/dt);
```

```
fft_length=2^ceil(log(n2-n1)/log(2))*4 t=[(n1-1):(n2-1)]*dt;

v1=v1(n1:min(n2,length(v1)))';
v2=v2(n1:min(n2,length(v2)))';
if (n2-n1+1>length(v1))
v1=[v1 zeros((length(v1)+1):(n2-n1+1))];
end
if (n2-n1+1>length(v2))
v2=[v2 zeros((length(v2)+1):(n2-n1+1))];
end

%       regresses v1 and v2 on a line and removes that linear displacement
best_line=polyfit([1:length(v1)],v1,1);

v1=v1-polyval(best_line,[1:length(v1)]);

 best_line=polyfit([1:length(v2)],v2,1);

 v2=v2-polyval(best_line,[1:length(v2)]);

subplot(211);plot(t*1000,v1);
xlabel('time (milliseconds)');
if D_or_A=='d'
titre=['Displacements at station 'int2str(station1)];
else
titre=['Accelerations at station 'int2str(station1)];
end
title(titre);
subplot(212);plot(t*1000,v2);
xlabel('time (milliseconds)');
if D_or_A=='d'
titre=['Displacements at station 'int2str(station2)];
else
titre=['Accelerations at station 'int2str(station2)];
end
title(titre);
pause;

subplot;
f1=fft(v1,fft_length);
f2=fft(v2,fft_length);
f1=f1(1:fft_length/2);
f2=f2(1:fft_length/2);
cp=conj(f1).*f2;
phase=-unwrap(angle(cp)); f=[0:(fft_length/2-1)]/fft_length/dt;
clg;
%axis([1 2 3 4]);axis;
subplot(211);
axis([0 40 -pi pi]);
plot(f/1000,-angle(cp));
xlabel('Frequency (kHz)');ylabel('phase (rad)'); title('Phase Difference');
subplot(212);
%axis([1 2 3 4]);axis;
axis([0 40 min(phase) max(phase)]); plot(f/1000,phase);
```

```
xlabel('Frequency (kHz)');ylabel('phase (rad)'); title('Unwrapped Phase Difference');pause;

axis([1 2 3 4]);axis;
subplot;
Min_Freq=input('Minimum Frequency (kHz) = ')*1000;
N_Min_Freq=ceil(Min_Freq*(fft_length*dt))+1; N_Min_Freq=min(N_Min_Freq,fft_length/2);

Max_Freq=input('Maximum Frequency (kHz) = ')*1000;
N_Max_Freq=ceil(Max_Freq*(fft_length*dt))+1; N_Max_Freq=min(N_Max_Freq,fft_length/2);

fStar=f(max(2,N_Min_Freq):N_Max_Freq);
phaseStar=phase(max(2,N_Min_Freq):N_Max_Freq); plot(fStar/1000,phaseStar);
xlabel('Frequency (kHz)');ylabel('phase (rad)');title('Cross Power Spectrum Phase');pause;

delay=1/(2*pi)*phaseStar./fStar;
Vr=distance*(delay.^(-1));
Lr=Vr./fStar;


plot(fStar/1000,Vr);
xlabel('Frequency (kHz)');ylabel('Wave Velocity (m/s)');title('Dispersion Curve');pause;

Max_WaveLength=input('Maximum Wavelength (m)= ');
sup=0;inf=1e+12;;
for mm=1:length(Vr);
   if ((Vr(mm)>sup) & (Lr(mm)<=Max_WaveLength))
      sup=Vr(mm);
   end
   if ((Vr(mm)<inf) & (Lr(mm)<=Max_WaveLength))
      inf=Vr(mm);
   end
end
axis([0,Max_WaveLength,inf*0.9,sup*1.1]);plot(Lr,Vr);
xlabel('Wavelength (m)');ylabel('Wave Velocity (m/s)');title('Dispersion Curve');

%axis([1 2 3 4]); axis;


%      sweep.m

Vpmin=2000;
Vpmax=5000;
Vpstep=250;
nu=0.2;

lmin=0.05;
lstep=0.005;
lmax=0.30;

Vp1=1200;
Vs1=600;
h1=0.05;
ro1=2100;
```

```
Nb_V=(Vpmax-Vpmin)/Vpstep+1;
Nb_l=(lmax-lmin)/lstep+1;

VRayleigh=zeros(Nb_l,Nb_V);

for N=1:Nb_V
   Vp2=Vpmin+(N-1)*Vpstep; Vs2=Vp2*((1-2*nu)/2/(1-nu))^(1/2);
                        disp(['Vp2=' int2str(Vp2) '   Vs2=' int2str(Vs2)]);
   two_layer;
   VRayleigh(1:Nb_l,N)=Vr;
   name=['save Vp' int2str(Vp2) '.mat']
   eval(name);
end

axis([1 2 3 4]); axis; plot(lmin:lstep:lmax,VRayleigh,'x');
title('Rayleigh Waves Dispersion Curves (Vs1=1700m/s)');

 xlabel('Wavelength (m)');ylabel('Wave Velocity');

axis([0.05,0.3,1000,2000]); plot(lmin:lstep:lmax,VRayleigh,'x');
title('Rayleigh Wave Dispersion Curves');
xlabel('Wavelength (m)');ylabel('Wave velocity (m/s)');
```

% two_layer.m

```
lmin=0.05;
lstep=0.005;
lmax=0.30;

%Vp1=2400;
%Vs1=1200;
%h1=0.05;
%ro1=2100;

%Vp2=4000;
%Vs2=2450;
h2=0.25;
ro2=2200;

Vs=max(Vs1,Vs2);

axis([1 2 3 4]);axis;clg;hold off;subplot;
L=[];
F=[];
axis([0,Vs/lmin/1000,-0.005,0.01]);
Vr=zeros(lmin:lstep:lmax);
for l=lmin:lstep:lmax;
%      disp(['lambda= ' num2str(l) ' m']);
       k=2*pi/l;
       fmax=Vs/l*0.99;
       Nb_freq=200;
       fmin=fmax/Nb_freq;
       y=zeros(1:Nb_freq);
```

```
        for m=1:Nb_freq
            f=m*fmin;
            w=2*pi*f;
            y(m)=real(det((total_stiff(k,w,h1,ro1,Vp1,Vs1,h2,ro2,Vp2,Vs2))));
        end
        plot([1:Nb_freq]*fmin/1000,y);
        if (l==lmin)
            hold on;
        end
        signe=sign(y);
        racine=0.5*abs(diff(signe));
        FF=[];
        for m=1:(Nb_freq-1);
            if (racine(m)>0)
                FF=[FF ((m+0.5)*fmin)];
            end
        end
        if (length(FF)>0)
            F=[F FF];
            L=[L l*ones(1:length(FF))];
            Vr((l-lmin)/lstep+1)=min(FF)*l;
        end;
end
grid;
xlabel('Frequency (kHz)');title('det(K)');
%print('electra');
hold off;
clg;
subplot;
Velocity=F.*L;
axis([0.05,0.3,1000,2400]);
plot(L,Velocity,'o');xlabel('Wavelength (m)');ylabel('Wave Velocity'); hold on;
plot(lmin:lstep:lmax,Vr,'x');hold off;axis;
titre=['Surface Wave propagation modes,  Vp2=' int2str(Vp2) ' m/s, Vs2=' int2str(Vs2) ' m/s']; title(titre);
%print('electra');
Vr=Vr';


function K_tot=total_stiff(k,w,h1,ro1,Vp1,Vs1,h2,ro2,Vp2,Vs2);

G1=ro1*Vs1^2;
G2=ro2*Vs2^2;

Zero_mat=[0 0;0 0];
K1=[Zero_mat Zero_mat Zero_mat;
    Zero_mat Zero_mat Zero_mat;
    Zero_mat Zero_mat Zero_mat];
K2=K1;
K1(1:4,1:4)=stiff(k,w,Vp1,Vs1,h1)*G1/(G1+G2);
K2(3:6,3:6)=stiff(k,w,Vp2,Vs2,h2)*G2/(G1+G2);
K_tot=K1+K2;
```

```
function K=stiff(k,w,Vp,Vs,h);

r=(1-(w/k/Vp)^2)^(0.5); s=(1-(w/k/Vs)^2)^(0.5); Cr=cosh(k*r*h);
Cs=cosh(k*s*h);
Sr=sinh(k*r*h);
Ss=sinh(k*s*h);

D=2*(1-Cr*Cs)+(1/(r*s)+r*s)*Sr*Ss; a11=1/s*(Cr*Ss-r*s*Cs*Sr); a12=-(1-
Cr*Cs+r*s*Sr*Ss);
a21=a12;
a22=1/r*(Cs*Sr-r*s*Cr*Ss);

A11=[a11 a12; a21 a22];
B11=[0 1; 1 0]; K11=(1-s^2)/2/D*A11-(1+s^2)/2*B11;

A22=[a11 -a12; -a21 a22];
B22=[0 -1; -1 0];

K22=(1-s^2)/(2*D)*A22-(1+s^2)/2*B22;

c11=1/s*(r*s*Sr-Ss);
c12=-(Cr-Cs);
c21=-c12;
c22=1/r*(r*s*Ss-Sr);


K12=(1-s^2)/2/D*[c11 c12;c21 c22]; K21=K12';

K=[K11 K12; K21 K22];
```

```
%    WAVELET.M
%    local Fourier analysis with varying window
%    X is the main variable
%    dt is the sample period

[m,n]=size(X);
if (n==1)
   X=X';
end

time_step=0.01e-03; % the Fourier analysis is conducted every time_step
time_step=floor(time_step/dt)*dt;
trace_length=length(X);
t=[0:trace_length-1]*dt;
Nb_Windows=trace_length/time_step; % number of time windows per frequency
fft_length=max(1024,2^(ceil(log(trace_length)/log(2))));

Frequency_min=1000;
Frequency_max=25000;
Frequency_step=500;

if (Frequency_max>1/dt/2)
   Frequency_max=1/dt/2
end

Kmin=floor(Frequency_min*dt*fft_length); Kmax=ceil(Frequency_max*dt*fft_length);
Kstep=max(floor(Frequency_step*dt*fft_length),1); FourierTransform=zeros(1:trace_length);
for n=1:trace_length
   FourierTransform(n)=exp(-i*2*pi*(n-1)/fft_length);
end
GFW=[];

for k=Kmin:Kstep:Kmax
   frequency=k/fft_length/dt;
   disp(['Frequency = ' int2str(frequency) ' Hz']);
   f0=frequency/3;
   t0=0.51/f0;
   Low0=floor(-1/2/f0/dt);
   High0=ceil(1/2/f0/dt);
   Interval0=[Low0*dt:dt:High0*dt];
   g0=my_win(t0,f0,Interval0);
   FT=FourierTransform.^k;
   F=[];
   for TT_shift=0:floor((trace_length-1)*dt/time_step)
   % beginning of the main loop
      % CONSTRUTION OF THE SHIFTED WINDOW
      t_shift=TT_shift*time_step;
      n_shift=floor(t_shift/dt)+1;
      g=zeros(t);
      for k=1:trace_length
```

```
            if ((Low0+n_shift<=k) & (k<=n_shift+High0) ) g(k)=g0(k-n_shift-Low0+1);
            end
        end
        % MULTIPLICATION AND 'FOURIER' TRANSFORM
        % computation of the average value of X on the support of g max_g=max(g);
        one_g=g ./ (g+max_g/10000);
        % approximately 1 for non zero values of g, zero elsewhere mean_X=sum(X .*
        one_g)/sum(one_g);
        WX=(X-mean_X) .* g;
%       plot(t*1e03,WX/max_g);title('Windowed Trace');
        F_kt=sum(WX.*FT);
        F=[abs(F_kt) F ];
    end % OF MAIN LOOP
GFW=[GFW ; F ];
end
GFW=GFW';

hold off;
axis([1 2 3 4]);axis;
mesh(GFW);
title(titre);
print('electra');
%     pause;

contour(GFW,10,[Kmin:Kstep:Kmax]/fft_length/dt/1000,[0:floor((trace_length-
1)*dt/time_step)]*time_step*1000); title(titre);
xlabel('Frequency in kHz');
ylabel('time in milliseconds (window center)');
print('electra');


function g=my_win(t0,f0,x);

w0=2*pi*f0;
%     t0*w0>=pi and t0*w0<=2*pi

[m,n]=size(x);
if (m==1)
    x=x';
end;
[m,n]=size(x);
%     x is now a column vector of size m

if (t0*w0<pi)
disp('Warning t0*f0 must be larger than 1/2');
elseif (t0*w0>2*pi)
    disp('Warning t0*f0 must be smaller than 1'); elseif ( (t0*w0>=pi) & (t0*w0<=2*pi))
    g=zeros(x);
    for k=1:m
        if ( (-pi/w0<=x(k)) & (x(k)<=pi/w0-t0) )
g(k)=sin(pi/2*nu((pi+w0*x(k))/(2*pi-w0*t0)));
elseif ( (pi/w0-t0<=x(k)) & (x(k)<=-pi/w0+t0))
            g(k)=1;
```

```
        elseif ( (-pi/w0+t0<=x(k)) & (x(k)<=pi/w0) ) g(k)=sin( pi/2*nu( (pi-w0*x(k)) /
                (2*pi-w0*t0) ) );
        elseif (x(k)<-pi/w0)
                g(k)=0;
        elseif (pi/w0<x(k))
                g(k)=0;
        end
    end
    g=t0^(-0.5) * g;
end

function n=nu(x);

if (x<=0)
    n=0;
elseif ((x>0) & (x<1)) n=sin(pi/2*x)^2;
elseif (x>=1)
    n=1;
end
```

REFERENCES

[1] J.D. ACHENBACH, "Wave Propagation in Elastic Solids", 1975, North-Holland Publishing Company.

[2] I. DAUBECHIES, "Ten Lectures on Wavelets", 1992, CBMS-NSF, Regional Conference Series in Applied Mathematics.

[3] J.F. DOYLE, "Wave Propagation in Structures: An FFT-Based Spectral Analysis Methodology", (1989), Springer-Verlag New-York, N.Y.

[4] K.F. GRAFF, "Wave Motion in Elastic Solids", 1975, Ohio State University Press.

[5] HASKELL, N.A. "The Dispersion of Surface Waves on Multilayered Media", Bulletin of the Seismological Society of America, 73, pp 17-34, 1953.

[6] M. C. KAHAN, personal communication

[7] E. KAUSEL, J.M. ROESSET, "Stiffness Matrices for Layered Soils", Bulletin of the Seismological Society of America, Vol. 71, No. 6, pp 1743-1761, December 1981

[8] G.F. MILLER, H. PURSEY, "On the Partition of Energy Between Elastic Waves in a Semi-Infinite Solid", Proc. Royal Society, London, A, Vol 233, 1955, pp. 55-69.

[9] S. NAZARIAN and K. H. STOKOE, II, "In Situ Determination of Elastic Moduli of pavement systems by Spectral-Analysis-of-Surface-Waves Method (Theoretical Aspects)", (November 1986), Research REPORT Number 437-2, Center for Transportation Research, Bureau of Engineering Research, The University of Texas at Austin.

[10] S. NAZARIAN and K. H. STOKOE, II, "In Situ Determination of Elastic Moduli of pavement systems by Spectral-Analysis-of-Surface-Waves Method (Practical Aspects)", (August 1985), Research REPORT Number 368-1F, Center for Transportation Research, Bureau of Engineering Research, The University of Texas at Austin.

[11] D.E. NEWLAND, "An Introduction to Random Vibration and Spectral Analysis", 1984, Longman Scientific & Technical

[12] A.V. OPPENHEIM, R.W. SCHAFER, "Discrete-Time Signal Processing", 1989, Prentice-Hall, Englewood Cliffs, N.J.

[13] A. PAIS, E. KAUSEL, "Approximate formulas for dynamic stiffnesses of rigid foundations", Soil Dynamics and Earthquake Engineering, 1988, Vol.7, No. 4

[14] G.J. RIX, "Experimental Study of Factors Affecting the Spectral-Analysis-of-Surface-Waves Method", PhD Thesis, (December 1988), University of Texas at Austin.

[15] E.A. ROBINSON, S. TREITEL, *Geophysical Signal Analysis,* (1980) Prentice-Hall, Englewood Cliffs, N.J.

[16] J.M. ROESSET, D-W CHANG, K.H. STOKOE, M. AOUAD, "Modulus and Thickness of the Pavement Surface Layer from SASW Tests", 1990 Transportation Research Board Meeting.

[17] M. SANSALONE, N.J. CARINO, N.N.HSU, "A Finite Element Study Of Transient Wave Propagation in Plates", Journal of Research of The National Bureau of Standards, vol.92, Number 4, July-August 1987.

[18] M. SANSALONE, N.J. CARINO, N.N.HSU, "A Finite Element Study of the Interaction of Transient Stress Waves with Planar Flaws", Journal of Research of The National Bureau of Standards, vol.92, Number 4, July-August 1987.

[19] M. SANSALONE, N.J. CARINO, "Transient Impact Response of Thick Circular Plates", Journal of Research of The National Bureau of Standards, vol.92, Number 6, November-December 1987.

[20] M. SANSALONE, N.J. CARINO, "Transient Impact Response of Plates Containing Flaws", Journal of Research of The National Bureau of Standards, vol.92, Number 6, November-December 1987.

[21] M. SANSALONE, N.J. CARINO, "Finite Element Studies of the Impact-Echo Response of Layered Plates Containing Flaws", International Advances in Non destructive Testing, 1990, Vol. 15, pp 313-336, Gordon and Breach Science Publishers, S.A.

[22] M. SANSALONE, N.J. CARINO, "Flaw Detection in Concrete by Frequency Spectrum Analysis of Impact-Echo Waveforms", International Advances in Non destructive Testing, 1986, Vol.12, pp117-146, Gordon and Breach Science Publishers, S.A.

[23] M. SANSALONE, N.J. CARINO, "Impact-Echo: A New Method for Inspecting Construction Materials", Non Destructive Testing and Evaluation for Manufacturing and Construction, 1990, pp 209-223, Hemisphere Publishing Corporation, N.Y.

[24] W. SHAKESPEARE, "Julius Caesar"

[25] J.c1. SHEU, K.H. STOKOE, II, J.M. ROESSET, W.R. HUDSON, "Applications and Limitations of the Spectral-Analysis-of-Surface-Waves Method, (November 1986)", Research Report 437-3F, Center for Transportation Research, Bureau of Engineering Research, The University of Texas at Austin.

[26] S. TIMOSHENKO, J.N. GOODIER, "Theory of Elasticity", 1970, McGraw-Hill, New-York